

Dissertation

zur Erlangung des Doktorgrades
der Fakultät für Chemie und Pharmazie der
Ludwig-Maximilians-Universität München

PREPARATION OF NANODISPERSIONS BY ANTISOLVENT PRECIPITATION

A new formulation approach



vorgelegt von

Klaus Freitag
aus Frankenberg (Eder)

2010

Erklärung

Diese Dissertation wurde im Sinne von § 13 Abs. 3 der Promotionsordnung vom 29. Januar 1998 von Herrn Prof. Dr. Gerhard Winter betreut.

Ehrenwörtliche Versicherung

Diese Dissertation wurde selbständig, ohne unerlaubte Hilfe erarbeitet.

München, am 23.11.2010

.....
(Klaus Freitag)

Dissertation eingereicht am:	01.12.2010
1. Gutachter:	Prof. Dr. Gerhard Winter
2. Gutachter:	Prof. Dr. Wolfgang Frieß
Mündliche Prüfung am:	21.12.2010

Für meine Eltern
Inge & Kurt Freitag

Abstract

Since the 1970s nanostructures were concertedly developed in the pharmaceutical field as drug carriers [1, 2]. Since then, the advantage of reducing potential side effects and to stimulate specific responses by modulating drug release and body distribution reverberates in a substantial number of approved products.

The growing amount of poorly soluble drugs recently approaching the market led to an increased attention to nanoparticulate drug delivery systems almost exclusively consisting of pure active pharmaceutical ingredients. In this context, antisolvent precipitation as enabling technology offers an immense potential for improving drug bioavailability. With this technique particles in the submicrometer range can be easily and reproducibly prepared. In addition to the particle size dependent solubilization of the drugs [3, 4], the rapid precipitation kinetics within the antisolvent processes often result in thermodynamically metastable products, assuring for further solubilizing effects [5]. While precipitation reactions find application e.g. in a wide range of industrial processes [6], antisolvent precipitation so far rarely evolved towards a marketable level in the pharmaceutical field. One reason therefore is, that the mechanisms governing phase separation processes are still poorly understood [7, 8]. Furthermore, the transfer of the often metastable products to a stable, storable pharmaceutical dosage form is critical. Transformations from the amorphous to the crystalline state or between different polymorphs can already start within the precipitation process and proceed within fabrication of the final dosage form.

Both issues are addressed within this work. A mathematical model was developed for simulating the particle formation process of a poorly soluble model compound, fenofibrate. The results are compared to experimental data and conclusions are drawn about the particle formation process and critical process parameters. Surprisingly, it was not solid particles that formed within the precipitation process, as is commonly anticipated in the literature [9], but a liquid, solute rich phase. This liquid intermediate was extremely instable and rapidly crystallized. It was found that liquid-liquid phase is not an exceptional phenomenon for fenofibrate, but can be widely observed in different morphological varieties. Upon detailed analysis of the precipitates of a series of poorly soluble compounds, a new approach was developed for stabilization of the liquid precipitate. Crystallization could be tremendously postponed by coprecipitation of a second poorly soluble compound and the use

of surface active reagents. Thereby not only sufficient time for downstream processing could be gained, a door was opened towards a new formulation approach for poorly soluble drugs. The robustness of this innovative process as well as the ability of preparing drug dispersions without the need of sophisticated and expensive equipment enlarge the available formulation space, and suggests the application of the liquid precipitates as in-situ forming drug delivery system.

Acknowledgments

First of all, I like to cordially thank my supervisor, Professor Dr. Gerhard Winter, for giving me the chance to join his research group and to explore this interesting field of science. The intense and inspiring discussions and his openness in sharing his extensive experience in science and with respect to the pharmaceutical industry provided an amazing opportunity to learn. Always open minded for adjusting the course of the research plan, he vitally contributed to the successful completion of this work.

The scientific data presented are the output of a shared cooperation project with the research group of Prof. Dr. Wolfgang Peukert from the Chair of Particle Technology at the Friedrich-Alexander-University Erlangen-Nuremberg, as well as Abbott Laboratories in Ludwigshafen. Within Abbott, it were namely Dr. Hans-Jürgen Krause and Dr. Michael Neu who were supervising the project, but also Dr. Anette Königsdorfer, who joined the first part of the project. The support offered by these three was at the positive edge of the feasible concerning financial and political requirements. Their extraordinary input to scientific questions enriched the discussions and very productively brought the project forward. I thank Abbott for offering this interesting project and for the guidance and inspiring discussions.

The process-oriented background of the work was to a large extent provided by Prof. Peukert and his group from Erlangen. Working with such experienced and highly skilled engineers really made the project an interdisciplinary come together, were all sides benefitted from the positive atmosphere and the fruitful exchange of ideas. Besides Prof. Peukert, special thanks go to Dr. Johannes Gradl, for his outstanding work on the simulation model for particle precipitation as well as his practical work in diverse projects, which could not be accounted for in this manuscript.

Another cooperation project derived due to the dedication of Prof. Dr. Thomas Joseph Anchordoquy from the University of Colorado, who invited me to join his research group and introduced me to the secrets of the American way of life and research. The time in Denver was financially supported by the Bayerische Apothekerstiftung, which is kindly acknowledge for giving me the opportunity for the scientific exchange abroad. A special gratitude belongs to the members of Prof. Anchordoquy's group, especially Dr. Michelle Zeles-Hahn, Dr. Long Xu and Dr. Jinxiang Yu, who made the stay an extraordinary experience. Dr. Yu kindly taught me

Acknowledgements

how to use an atomic force microscope, and, by the same time, offered me his car for fleeing the country in case I broke it.

Further background information on AFM measurements was provided from Veeco Instruments GmbH as well as members of different research groups in Germany. Therefore I would like to express my greatest thanks to Dr. Martin Benoit from the Ludwig-Maximilians-University in Munich as well as to Johannes Sitterberg from the Philipps-University in Marburg.

Wide-field fluorescence microscopy as well as confocal fluorescence spectroscopy measurements were accomplished in close cooperation with Dr. Timo Lebold from the research group of Prof. Dr. Bräuchle, Ludwig-Maximilians-University. Being much more than just a cooperation partner, it was always a pleasure coming over for working with Timo and taking benefit from his always immediate and uncomplicated help.

Very warm thanks also go to Prof. Dr. Wolfgang Frieß as well as to Dr. Conrad Coester from the Department of Pharmaceutical Technology and Biopharmaceutics at the Ludwig-Maximilians-University in Munich for providing a familiar and positive work environment. The lively discussions with you and your group members will be remembered. I also thank Prof. Frieß very much for his personal support and for offering his expert opinion on this manuscript.

Vivid support during lab routing was also provided by the students working under my supervision and substantially contributing with their work to the positive outcome of this thesis. Julia Schwarzberg, Peter Schweiberger and Veronika Schmitt, Eileen Engel and Eva Kirmaier are greatly acknowledged for their dedication, their refreshing humor and the numerous cakes provided during their internships.

However, without the trust, friendship and mutual support of the best lab in the world, the Bubble Lab, the accomplishment of this work would never have been as funny, productive or feasible at all. Therefore my respect and deepest appreciation are addressed to Dr. Sebastian Fuchs, Dr. Stephan Johannes Baptist Schultes, Dr. Steliyan Stanimirov Tinkov as well as our mentor and distinguished scientist, Pat.

Throughout the years of the accomplishment of this thesis, my family was my greatest support. Although the scientific work was very different from their everyday business, their

enduring interest and surprisingly far-reaching understanding of the matter bolstered the way from the beginning. I thank you a lot for your support, incitation and constant reliability.

I can hardly express my appreciation to Karina, my most honest critic, loving supporter and unfailing source of motivation. I gladly remember the many weekends you spent painting during the preparation of this manuscript, and am sure your artwork will be a steady reminder on the importance of **lasting overwhelmingly victorious engagements**.

Table of Contents

ABSTRACT	VII
ACKNOWLEDGMENTS	IX
TABLE OF CONTENTS	XIII
LIST OF FIGURES	XVII
LIST OF TABLES	XXI
DEFINITIONS	XXII
NOTATIONS	XXIII
1.1. LATIN LETTERS	XXIII
1.2. GREEK LETTERS	XXV
CHAPTER 1. INTRODUCTION	27
1.1. BACKGROUND	27
1.2. DEPENDENCE OF DRUG SOLUBILITY ON PARTICLE SIZE	28
1.3. THE PHYSICAL STATE AND DRUG SOLUBILITY	30
1.4. PREPARATION OF NANODISPERSIONS	31
1.5. OBJECTIVES OF THE THESIS	35
CHAPTER 2. SIMULATION OF THE PRECIPITATION PROCESS	37
2.1. ABSTRACT.....	37
2.2. INTRODUCTION.....	38
2.3. MATERIAL AND METHODS	41
2.3.1 EQUIPMENT AND SAMPLE CHARACTERIZATION	41
2.3.2 SOLUBILITY CHANGES WITHIN THE MIXING PROCESS	44
2.3.3 ACCOMPLISHMENT OF THE SIMULATIONS	45
2.3.4 MIXING CONDITIONS.....	46
2.3.5 PARTICLE FORMATION	48
2.4. RESULTS AND DISCUSSION.....	52
2.4.1 DETERMINATION OF EXPERIMENTAL DATA FOR THE SIMULATION MODEL.....	52
2.4.1.1. PARTICLE SIZE AND INTERFACIAL ENERGY.....	52
2.4.1.2. DRUG SOLUBILITY	55
2.4.2 DRUG DENSITY	57
2.4.3 OUTCOME OF THE SIMULATIONS	57
2.4.4 INTERPRETATION OF THE EXPERIMENTAL RESULTS IN THE CONTEXT OF THE MODEL BASED EXPECTATIONS.....	58
2.4.4.1. EFFECTIVENESS OF THE MIXING PROCESS.....	59
2.4.4.2. SOLUBILIZING EFFECTS OF THE DISPERSIONS.....	61
2.5. CONCLUSIONS	62
CHAPTER 3. EXPERIMENTAL EVALUATION OF CERTAIN PROCESS PARAMETERS	63
3.1. ABSTRACT.....	63
3.2. INTRODUCTION.....	64
3.3. MATERIAL AND METHODS	68
3.3.1 NON-MIXING RELATED PROCESS VARIATIONS	68
3.3.1.1. SOLVENT COMPOSITION	68
3.3.1.2. INTERFACIAL TENSION	68
3.3.1.3. TEMPERATURE CONTROLLED EXPERIMENTS.....	69
3.3.1.4. DRUG CONCENTRATION	69
3.3.2 THE IMPACT OF MIXING	70
3.4. RESULTS AND DISCUSSION.....	73
3.4.1 INFLUENCE OF THE SOLVENT COMPOSITION.....	73
3.4.2 THE IMPACT OF INTERFACIAL TENSION.....	74
3.4.3 INFLUENCE OF TEMPERATURE.....	76

Table of Contents

3.4.4 INFLUENCE OF DRUG CONCENTRATION.....	77
3.4.5 IMPACT OF DIFFERENT MIXING DEVICES	78
3.4.6 INTERPRETATION OF THE EXPERIMENTAL DATA	80
3.5. CONCLUSIONS	83
CHAPTER 4. STRUCTURAL CHARACTERIZATION OF THE PRECIPITATE.....	85
4.1. ABSTRACT.....	85
4.2. INTRODUCTION.....	86
4.3. MATERIAL AND METHODS	90
4.3.1 REAGENTS USED	90
4.3.2 SCANNING ELECTRON MICROSCOPY	91
4.3.3 ATOMIC FORCE MICROSCOPY	91
4.3.4 WIDE-FIELD FLUORESCENCE MICROSCOPY	93
4.3.5 CONFOCAL FLUORESCENCE SPECTROSCOPY	93
4.3.6 LIGHT MICROSCOPY.....	94
4.4. RESULTS AND DISCUSSION.....	95
4.4.1 SCANNING ELECTRON MICROSCOPY	95
4.4.2 ATOMIC FORCE MICROSCOPY	97
4.4.3 WIDE-FILED FLUORESCENCE MICROSCOPY	102
4.4.4 CONFOCAL FLUORESCENCE SPECTROSCOPY	105
4.4.5 LIGHT MICROSCOPY	107
4.4.6 NEW INSIGHTS ON THE IMPACT OF THE PROCESS CONDITIONS ON PARTICLE FORMATION.....	111
4.5. CONCLUSIONS	114
CHAPTER 5. STABILIZATION OF THE DISPERSIONS.....	117
5.1. ABSTRACT.....	117
5.2. INTRODUCTION.....	118
5.2.1 CRYSTALLIZATION	119
5.2.2 OSTWALD RIPENING.....	124
5.2.3 OSTWALD RIPENING IN SAMPLES CONTAINING DIFFERENT POLYMORPHS.....	126
5.2.4 AGGLOMERATION, COALESCENCE AND MECHANICAL PARTICLE DISRUPTION	127
5.2.5 SEDIMENTATION AND FLOCCULATION	129
5.2.6 DOWNSTREAM PROCESSING	130
5.3. MATERIAL AND METHODS	132
5.3.1 EXCIPIENT SCREENING	132
5.3.1.1. LITERATURE BASED STABILIZATION APPROACHES	132
5.3.1.2. BHT AS CRYSTALLIZATION INHIBITOR	134
5.3.1.3. SAMPLE ANALYSIS	137
5.3.2 LYOPHILIZATION	138
5.3.2.1. SAMPLE PREPARATION.....	138
5.3.2.2. HPLC ANALYSIS	143
5.3.2.3. SCANNING ELECTRON MICROSCOPY	143
5.3.2.4. RESIDUAL ETHANOL CONTENT	143
5.3.2.5. RESIDUAL WATER CONTENT.....	144
5.3.2.6. X-RAY POWDER DIFFRACTION	144
5.3.2.7. DIFFERENTIAL SCANNING CALORIMETRY	145
5.4. RESULTS AND DISCUSSION.....	146
5.4.1 EXCIPIENT SCREENING	146
5.4.1.1. CLASSICAL STABILIZATION APPROACHES.....	146
5.4.1.2. INFLUENCE OF BHT ON DISPERSION MORPHOLOGY AND STABILITY	150
5.4.1.3. APPLICATION OF THE STABILIZING MEASURES TO THE PREPARATION OF DISPERSIONS WITH THE PUMPING SETUP	157
5.4.2 LYOPHILIZATION	166
5.4.2.1. COMPOSITION OF THE LYOPHILIZATES	166
5.4.2.2. CAKE STRUCTURE OF THE LYOPHILIZATES	167
5.4.2.3. THE INFLUENCE OF FREEZE DRYING ON THE PHYSICAL STATE OF FENOFIBRATE	171
5.5. CONCLUSIONS	174
CHAPTER 6. GENERAL SUMMARY OF THE THESIS	177
6.1. UNDERSTANDING PARTICLE FORMATION.....	177
6.2. DISPERSION STABILITY	180

6.2.1 STRUCTURE BASED STABILIZATION APPROACHES	181
6.2.1.1. CONTROLLING FENOFIBRATE CRYSTALLIZATION.....	181
6.2.1.2. COPRECIPITATION AS A TOOL TO MODIFY THE MOLECULAR INTERACTION	182
6.2.1.3. DOWNSTREAM PROCESSING	183
6.3. OUTLOOK	184
6.3.1 THE SIMULATION AND THE ACCOMPLISHMENT OF ANTISOLVENT PRECIPITATION.....	184
6.3.2 THE POTENTIAL USE OF GENERATING AND APPLYING LIQUID-LIQUID PHASE SEPARATION	185
REFERENCES.....	189
CURRICULUM VITAE.....	201

List of Figures

Figure 1: Classification of marketed drugs (left) and NCE (right) according to the Biopharmaceutical Classification System [15].....	28
Figure 2: Potential energies of different polymorphic forms of a substance (modified from [38]).....	31
Figure 3: The influence of mixing on particle formation [6].....	33
Figure 4: Different kinds of mixing devices used in antisolvent precipitation. Left: static mixer [9], middle: batch reactor [55], right: impinging jet reactor.....	33
Figure 5: Phase diagram of a mixture showing upper and lower critical solution temperatures (adopted from [62, 64])	38
Figure 6: Dependency of the phase separation mechanism on the degree of supersaturation	39
Figure 7: Chemical structure of fenofibrate.....	41
Figure 8: Setup of the impinging jet reactors equipped with a t-shaped mixing chamber for preparation of the drug dispersions (image modified from www.isco.com)	42
Figure 9: Particle size distributions of fenofibrate dispersions prepared at flow rates ranging from 12 ml/min to 60 ml/min (mean values of 3 runs per flow rate)	52
Figure 10: Left: Observation of μm -sized drug particles by microscopical observation. Right: Comparison of PCS and laser diffraction data from filtered and unfiltered dispersions prepared at a total flow rate of 60 ml/min	53
Figure 11: Model based evaluation of interfacial energy.....	54
Figure 12: Zeta-potential of fenofibrate dispersions prepared at a total flow rate of 60 ml/min	54
Figure 13: Supersaturation effect in freshly prepared fenofibrate dispersions. After removal of the precipitate, secondary phase separation occurred as indicated by a decreasing absorption of dissolved drug (280 nm) and an increasing amount of precipitate (500 nm)	55
Figure 14: Solubility changes of fenofibrate in freshly prepared dispersions containing 10, 25, 40, 60, 70, 80, 85, 90 and 99.98 % of ethanol.....	56
Figure 15: Solubility profile of fenofibrate at time point 0 min. The profile mimics the solvent gradient passed within the precipitation process	57
Figure 16: Simulation of the particle formation process. Arising supersaturation is closely followed by nucleation and growth of the primary particles	58
Figure 17: Pressure drop recorded upon mixing of water and ethanol [■] or with an ethanolic fenofibrate solution [◆]. It is a measure for the energy dissipated for the mixing process	59
Figure 18: Comparison of the experimentally determined specific power input for the mixing process (●) and the specific input predicted by simulating the mixing conditions (∇).....	60
Figure 19: Solubility advantage of the precipitate compared to crystalline fenofibrate	61
Figure 20: Proposed impact of heterogeneous flow patterns (blue = water, red = ethanolic drug solution).....	65
Figure 21: Surface tensions in ethanol water mixtures (modified from [93]).....	66
Figure 22: Particle size as a function of temperature [59]	67

List of Figures

Figure 23: Mechanical drawing of the cross shaped mixing chambers used for nanodispersion preparation.....	70
Figure 24: Sample preparation with cross shaped mixing chambers. The aqueous phase is homogeneously split by insertion of a t-piece	71
Figure 25: Influence of the solvent composition on the resulting particle size (simulation)	73
Figure 26: Experimental verification of the impact of the solvent composition on particle size.....	74
Figure 27: Influence of supersaturation and interfacial energy on the calculated nucleation rate	75
Figure 28: Effect of Tween 80 on fenofibrate particle size	76
Figure 29: Dependency of particle size and polydispersity (span) on temperature	77
Figure 30: Dependency of particle size and polydispersity (span) on drug concentration	78
Figure 31: Preparation of fenofibrate nanodispersion with differently sized t-shaped mixing devices	79
Figure 32: Standard particle characterization techniques	88
Figure 33: Chemical structures of lopinavir and loratadine and fenofibrate.....	90
Figure 34: Schematic illustration of AFM force-distance measurements.....	92
Figure 35: SEM sample prepared from an undiluted fenofibrate dispersion containing 16.7% (V/V) ethanol, mixed by hand, unsputtered sample	95
Figure 36: Melting of amorphous (left) and crystalline (right) particles in the electron beam. The samples were prepared with the pumping setup at a total flow rate of 24 ml/min. The ethanol concentrations in the dispersions were 50% (V/V) (left) and 16.7% (V/V) (right)	96
Figure 37: Fenofibrate particles embedded in layers of solvent debris. Particles appear homogeneous without an internal structure. The samples were prepared at total flow rates of 12 ml/min (left) and 24 ml/min (right). The ethanol concentrations in the dispersion were 16.7% and 50% (V/V).....	97
Figure 38: Elasticity of the precipitate vs. particle size. Smaller fenofibrate particles were found to have higher spring constants, meaning they appear to be harder to their environment than bigger particles	98
Figure 39: Lopinavir particles exhibiting mechanically robust, solidified structures, indicating a transient liquid state of the precipitate during phase separation.....	99
Figure 40: Video snapshots of the mechanical straining of a loratadine particle. Center left: loratadine particle attached to the cantilever. Right: long, viscoelastically deforming filaments can be pulled out of the particle.....	100
Figure 41: Lopinavir particle under application of mechanical stress from the cantilever. The particles remain stiff and undeformable, while the cantilever (middle of the right image) bends tremendously	100
Figure 42: Fenofibrate particle pierced with a cantilever. The precipitates behave as a liquid with relatively low viscosity	101
Figure 43: Light microscopical image of a fenofibrate dispersion. The particles have a homogeneous appearance	103
Figure 44: Snapshot of the wide-field fluorescence microscopy movie shown in Figure 43. Subparticles are rapidly moving inside bigger precipitate particles	103

Figure 45: Video snapshot of an undiluted fenofibrate dispersion. The interior of the particles remains rather liquid; particles are prone to Ostwald ripening and coalescence. The particle in the middle (image a) bursts, its content pours out.....	105
Figure 46: Fluorescence spectra of a 5% (w/w) ethanolic fenofibrate solution. Only weak signals are obtained for the dissolved drug	106
Figure 47: Fluorescence spectra of a freshly prepared dispersion containing 7 mg fenofibrate/g dispersion. Depending on local concentration fluctuations, differently strong signals for the dispersed phase as well as dissolved drug were observed	106
Figure 48: Fluorescence spectra acquired from a crystallized fenofibrate dispersion. Signals are comparable to those of the liquid precipitate were obtained	107
Figure 49: Fenofibrate dispersions prepared under normal (left) and very gentle (right) mixing conditions. Even particles up to 10 μm have an optically homogeneous appearance.....	108
Figure 50: Lopinavir dispersion prepared under weak mixing conditions. The process of decomposition and shaping of individual sample particles can be observed	110
Figure 51: Dispersion of lopinavir prepared under weak mixing conditions. Formation of an interconnected gel like network of which subparticles constrict.....	110
Figure 52: Dispersion of loratadine prepared under weak mixing conditions. As for the other drugs, droplets of organic solvent entrapped in the precipitate (centre) could be observed.....	111
Figure 53: Crystallization in a supersaturated solution.....	120
Figure 54: Schematic description of the enthalpy variation with temperature (adopted from [131]).....	121
Figure 55: Schematic illustration of the parameters controlling crystallization from the amorphous state (adopted from [115])	122
Figure 56: Ostwald ripening	125
Figure 57: Solubility pressure and mass transfer of different particles in dispersion. Mass transfer takes place from small particles to bigger ones and from liquid/amorphous material to crystals.....	126
Figure 58: Ageing of a dispersed phase by Ostwald ripening and crystallization	127
Figure 59: Agglomeration and sedimentation.....	128
Figure 60: Coalescence of a liquid dispersed phase.....	129
Figure 61: Particle size reduction within mixing processes.....	129
Figure 62: Butylated hydroxytoluene	134
Figure 63: Setup for flash freezing the fenofibrate dispersions	141
Figure 64: White junks of agglomerated fenofibrate crystals partly adhere to the sample container upon crystallization of the dispersions.....	147
Figure 65: Agglomeration of a dispersion containing excessive amounts of Phospholipon 100H.....	149
Figure 66: Dispersion obtained from an ethanolic BHT solution upon addition of water.....	150
Figure 67: Coprecipitates of BHT and fenofibrate in a 5:5 ratio (w/w) coloured with methylene blue (left) and sudan red (right).....	151
Figure 68: Elasticity of the coprecipitates of 3:5 mixtures of BHT with fenofibrate, lopinavir and loratadine. For comparison, also the force-distance curves for precipitates of the individual substances are shown.....	152

List of Figures

Figure 69: Mechanical stress applied on the coprecipitates of BHT with loratadine (left) and lopinavir (right). Viscoelastic, chewing gum like filaments form from the lopinavir coprecipitates, while the BHT: loratadine particles showed predominantly elastic behavior	153
Figure 70: Coalescence of highly viscous precipitate particles as a result of the presence of citric acid in the continuous phase (sample composition: BHT:fenofibrate ratio 0.05:5, Phospholipon 100H, and Tween 80, citric acid)	155
Figure 71: Fenofibrate dispersion prepared without the use of any additional excipients. Crystallization started directly after sample preparation and rapidly comprised the whole dispersed phase	158
Figure 72: Stabilization of a dispersion containing BHT and fenofibrate in a 3:5 ratio, stabilized with Phospholipon 100H and Tween 80.....	159
Figure 73: Stabilizing effect observed by the combinatorial stabilization of fenofibrate dispersions with BHT and the surfactants DPPC and DPPG	160
Figure 74: Fenofibrate dispersion stabilized with the phospholipids DPPC and DPPG, without the additional use of BHT.....	161
Figure 75: Dispersion of fenofibrate, BHT and the phospholipids DPPC and DPPG additionally stabilized by addition of 0.5% PVP to the aqueous phase.....	162
Figure 76: BHT content in the fenofibrate dispersions prior and after the lyophilization process. Data are shown in percent (w/w) of the solid formulation compounds (fenofibrate, BHT, surfactants, citric acid and trehalose).....	167
Figure 77: Lyophilization cakes from dispersions 4 (top) and 5 (bottom). Dispersions containing no or low amounts of BHT prior to lyophilization (dispersion 4) showed nice and stable cake structures, while those originally containing high amounts of BHT partly collapsed upon removal of the antioxidant (dispersions 5).....	168
Figure 78: Scanning electron microscopy image of the lyophilized dispersion 2. Wide pores aligned by partly sintered particles can be identified at the surface of the lyophilizate	169
Figure 79: Particles from dispersion 8 being embedded into a trehalose matrix (top) and redispersed agglomerate complexes of dispersion 9 (bottom)	170
Figure 80: DSC diagram of the lyophilizate of dispersion 1, containing only fenofibrate as solute	171
Figure 81: Diffractogram of the fenofibrate bulk substance and the lyophilization products of dispersions 1 and 2	172
Figure 82: Schematic illustration of the processes affecting the particles size distribution in antisolvent precipitation (adopted from [88]).....	180

List of Tables

Table 1: Experimental matrix for investigating the impact of solvent composition on particle formation.....	68
Table 2: Layout of cross shaped mixing chambers used for nanodispersion preparation	71
Table 3: Comparison of mean particle size and energy dissipation of 4-jet impinging jet reactors and a 0.5 mm i.d. t-piece	80
Table 4: Vapor pressures of different solvents used for lyophilization as well as fenofibrate and citric acid and BHT	131
Table 5: Literature based formulation screening for fenofibrate dispersions	133
Table 6: Empirical investigation of stabilizing reagents	134
Table 7: Weight ratios of fenofibrate and BHT applied for investigating dispersion stability.....	135
Table 8: R2 values for the exponential fit from the elasticity data obtained from force-distance measurements.....	138
Table 9: Differently composed fenofibrate dispersions used for lyophilization (values represent the composition in the final dispersions prior to the lyophilization process).....	139
Table 10: Freeze drying protocol applied for the lyophilization of fenofibrate dispersion 1	142
Table 11: Freeze drying protocol applied for the lyophilization of fenofibrate dispersions 2	142
Table 12: Freeze drying protocol applied for the lyophilization of fenofibrate dispersions 3-7	142
Table 13: Freeze drying protocol applied for the lyophilization of fenofibrate dispersions 8-10	143
Table 14: Literature based excipient screening for fenofibrate dispersions. (+) improved stability compared to the excipient free drug formulation; (±) equivalent stability, (-) destabilizing effect	147
Table 15: Investigation of the stabilizing effects of individual excipients. (+) Improved stability compared to the excipient free drug formulation; (±) equivalent stability, (-) destabilizing effect	148
Table 16: Qualitative overview of the results on the stabilization of fenofibrate dispersions (the time span covered is 1 hour; +++ massive, immediate reaction/rapid proliferation; ++ moderate intensity/slow proliferation; + weak, very slow process)	163
Table 17: Particle sizes measured after redispersion of selected lyophilized dispersions, prior and after application of ultrasound.....	170

Definitions

Polymorphism

In this communication the term “polymorphism“ is used according to the Food and Drug Administration’s Abbreviated New Drug Applications Guidance (ANDA) [10]. Polymorphic forms in this context refer to crystalline and amorphous forms as well as solvate and hydrate forms.

- Crystalline forms have different arrangements and/or conformations of the molecules in a crystal lattice
- Amorphous forms consist of disordered arrangements of molecules that do not possess a distinguishable crystal lattice
- Solvates are crystal forms containing either stoichiometric or nonstoichiometric amounts of a solvent. If the incorporated solvent is water, the solvate is commonly known as a hydrate

Exceeding this definition, within the context of this work also amorphous forms showing more or less liquid behavior are comprised in the term polymorph. The liquid can be formed by molecular interaction with solvent and antisolvent molecules.

Nanoparticle

Currently an internationally accepted definition of nanoparticles is missing [11]. As specific size related medical effects are not strictly limited to a certain particle size cut off, within the context of this work nanoparticles are defined as particles with a mean volume weight size of at most 1000 nm. If not pointed out elsewhere, the term particle is used synonymously for droplets, crystals or solid particles in general.

Dispersion

The term dispersion includes formulations containing a dispersed solid phase, a dispersed liquid phase or mixtures of both.

Notations

1.1. LATIN LETTERS

A	interfacial surface area, m^2
ANDA	Abbreviated New Drug Applications Guideline
API	active pharmaceutical ingredient
BCS	Biopharmaceutical Classification System
B_{hom}	rate of homogeneous nucleation, $\text{m}^{-3} \text{s}^{-1}$
BHT	2,6-di-tert-butyl-4-methylphenol, butylated hydroxytoluene
C	concentration of the dissolved drug, mol m^{-3}
C^*	concentration of the drug in a saturated solution, mol m^{-3}
C_1, C_2	solubility of particles with diameter d_1 and d_2 , mol m^{-3}
CMC	critical micelle concentration, kg m^{-3}
C_s	saturation solubility/solute concentration in the diffusion layer, mol m^{-3}
C_x	concentration in the bulk dissolution medium at time x , mol m^{-3}
d_1, d_2	particle diameter, m
d_{10}, d_{50}, d_{90}	10 th , 50 th and the 90 th percentile of the particle size distribution
D_{AB}	diffusion coefficient, $\text{m}^2 \text{s}^{-1}$
d_w/d_t	dissolution rate, mol s^{-1}
DPPE	dipalmitoyl phosphatidyl choline
DPPG	dipalmitoyl phosphatidyl glycerol
DSC	differential scanning calorimetry
f-d	force-distance
FDA	Food and Drug Administration
G	Gibbs free energy, kJ
G_{lin}	linear growth rate, m s^{-1}
h	boundary layer thickness, m
H	enthalpy, K
HPMC	hydroxypropyl methyl cellulose
HTS	high throughput screening
i.d.	inner diameter
k	Boltzmann constant, $1.381 \cdot 10^{-23} \text{ J K}^{-1}$
K_{sp}	solubility product, kg m^{-3}
LogP	octanol-water partition coefficient

Notations

LCST	lower critical solution temperature, K
m	total particulate mass concentration, kg m^{-3}
M	molecular weight, kg kmol^{-1}
MPEG-2000-DSPE	1,2-Distearoyl-phosphatidylethanolamine-methyl-polyethyleneglycol conjugate-2000 (MPEG-2000-DSPE)
N	total number concentration of particles, m^{-3}
N_A	Avogadro number, $6.023 \cdot 10^{26} \text{ k mol}^{-1}$
NCE	new chemical entities
P	pressure, N m^{-2}
P_a	hydrostatic pressure outside a dispersed droplet, N m^{-2}
PBA	population balance approach
PC	pressure control
PCS	photon correlation spectroscopy
P_d	pressure inside a dispersed droplet, N m^{-2}
P_r	vapor or solubility pressure of a particle with radius r, N m^{-2}
PVP	polyvinylpyrrolidone; Povidone K-12
P_∞	solubility pressure of a particle with an infinitely big radius, N m^{-2}
Q	flow rate, $\text{m}^3 \text{ s}^{-1}$
r	particle radius, m
R	ideal gas constant, $8.314 \text{ J mol}^{-1} \text{ K}^{-1}$
R^2	coefficient of determination
s	detected light intensity distribution vector
S	entropy, J K^{-1}
s^*	estimated light intensity distribution vector
S^*	supersaturation
Sh	Sherwood number
SR	sample receptacle
STDEV	standard deviation
t	time, s
T	temperature, K
TC	temperature control
T_g	glass transition temperature, K
T_K	Kauzmann temperature, K
Tween 80	polyoxyethylen(20)sorbitan monooleate
U	internal energy, J
UCST	upper critical solution temperature, K

u_{mean}	mean velocity in the main tube of a mixer, m s^{-1}
V	volume, m^3
V_{DIS}	effective volume in which the main turbulent dissipation of energy occurs, m^3
V_{m}	molecular volume, m^3
XRD	X-ray powder diffraction

1.2. GREEK LETTERS

γ	interfacial tension or surface tension, $\text{J}\cdot\text{m}^{-2}$
γ_{CL}	interfacial energy, J m^{-2}
ε	rate of energy dissipation in the turbulent flow per unit mass of the fluid (specific power input), $\text{J kg}^{-1} \text{s}^{-1}$
ζ	pressure drop coefficient
η_{C}	dynamic viscosity of the continuous phase, Pa s
λ_0	size of the smallest turbulent eddies, m
μ	chemical potential difference of a dissolved substance compared to its chemical potential in a saturated solution
μ^*	chemical potential difference between a solid and the corresponding dissolved substance
ρ_{C}	density of the continuous phase, kg m^{-3}
ρ_{F}	density of the fluid, kg m^{-3}
ρ_{P}	density of the precipitate, kg m^{-3}
ρ_{S}	density of a particle, kg m^{-3}
τ	mixing time, s
$\tau_{\text{micro-mixing}}$	micro mixing time, s
ν	kinematic viscosity, $\text{m}^2 \text{s}^{-1}$
χ	volume-equivalent particle diameter, m
χ_{c}	critical nucleus size (at $\Delta G = 0$), m

Chapter 1. Introduction

1.1. BACKGROUND

Until the 1980s drug development was mainly based on the empirical screening of potential active pharmaceutical ingredients (API). Lead structures had often undergone considerable scientific investigation before being selected as a lead. Many of these substances derived from observed clinical side effects of already marketed drugs, by variation of natural products or based on a chemistry focusing on the preparation of small and structurally comparably simple compounds. In consequence, within the development process those candidates showing the most undesirable physico-chemical properties such as chemical instability or low aqueous solubility were eliminated.

With the rise of high throughput screening (HTS) and combinatorial chemistry in the pharmaceutical industry, the automated screening of thousands of substances in in vitro assays became possible. Drugs were no longer solubilized in aqueous media, but more often in organic solvents, offering an applicability of the required assays to drug candidates with a wide structural diversity. Outcome of this development is a continuously increasing amount of poorly soluble drugs in the pipelines of pharmaceutical companies, meeting the HTS requirements, but failing in the aqueous environment of real life applications [12-14]. While about 40% of the marketed drugs show poor solubility, 70-90% of the new chemical entities (NCE) in the pipelines of pharmaceutical companies are pertained [15, 16]. They are appointed to classes II and IV of the Biopharmaceutical Classification System (BCS), meaning that solubility is the crucial factor for restraining their bioavailability (**Figure 1**).

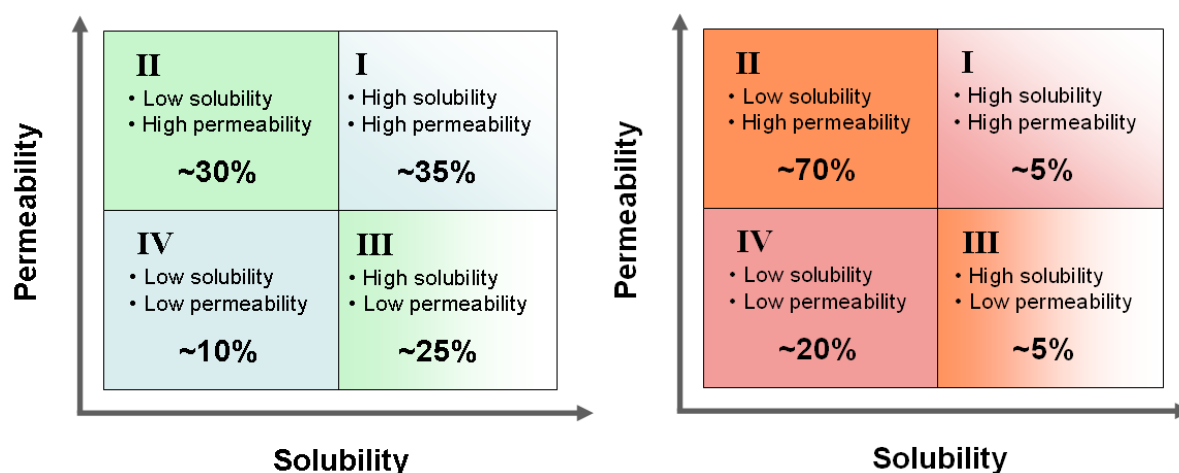


Figure 1: Classification of marketed drugs (left) and NCE (right) according to the Biopharmaceutical Classification System [15]

The need for new technological platforms to address these pipeline requirements led to the development of an array of formulation techniques and processes, including the use of cosolvents, nanosizing of the drug substance, complexing agents, surfactant-based methods, lipid-based approaches, solid dispersions and solutions, supersaturating drug delivery systems and the use of polymeric micelles [17-27]. Among these, nanosizing combines the advantage of an intrinsically high solubilization of the drug compounds with the applicability of very high drug loads, both for oral as well as parenteral applications. Its wide applicability makes it the mean of choice especially for neutral drug molecules.

1.2. DEPENDENCE OF DRUG SOLUBILITY ON PARTICLE SIZE

For many poorly soluble compounds, a high saturation solubility is the main factor assigning for the success or failure of a certain formulation approach. Saturation solubility is however not a constant, but depends on the kind and pH of the solvent, the temperature, the physical state and the particle size of the solute [28]. While in many cases not all of these factors can be controlled by the manufacturer, particle size is a mean that can be extensively influenced within the development of a given formulation. Based on fundamental physical principles, it has the potential to tremendously increase a drug's bioavailability without the need for the additional use of adjuvants.

The dependence of drug solubility on particle size is described by the Ostwald-Freundlich equation (**Equation 1**, [29]), where R represents the ideal gas constant, T is the temperature, M is the molecular weight of the solute, C_1 and C_2 are the corresponding solubilities of particles with the diameters d_1 and d_2 , γ_{CL} is the interfacial energy and ρ_s is the density of the particle. It states that the further particle size is decreased, the higher is the solubilization. While this effect is negligible in the μm -range, solubilization becomes most effective by application of nanoscopic material.

$$\frac{RT}{M} \ln \frac{C_1}{C_2} = \frac{4\gamma_{CL}}{\rho_s} \left(\frac{1}{d_2} - \frac{1}{d_1} \right)$$

Equation 1

According to Noyes and Whitney (**Equation 2**, [30, 31]), decreasing particle size also increases the dissolution rate, as it leads to a surface enlargement of the material. This is of advantage, as rapidly reaching the saturation solubility maximizes drug absorption and bioavailability. It has also been postulated, that in agitated systems a decrease in particle size lowers the thickness of the hydrodynamic layer surrounding the particles and thereby the diffusion distance for the dissolved material [32]. In the Noyes-Whitney equation d_w/d_t is the dissolution rate, D_{AB} is the diffusion coefficient, A is the interfacial surface area, h is the thickness of the boundary layer and C_s and C_x are the saturation solubility respectively the concentration of solute in the bulk dissolution medium time x.

$$\frac{d_w}{d_t} = \frac{D_{AB} A}{h} (C_s - C_x)$$

Equation 2

The accompanying increase in solubility pressure is described by the Kelvin equation (**Equation 3**, [33]), where P_r/P_∞ represents the ratio of the solubility pressure of a particle with a given radius r and a particle with an infinitely big radius; γ is the interfacial tension. Originally developed for evaluating the vapor pressure of a liquid, the Kelvin equation is

equally applied for both, liquid and solid dispersed phases [34]. However, it is not the size alone, also the interaction between particle and surrounding liquid plays a key role. Solubility pressure and saturation solubility depend on the interfacial tension between the dispersed and the surrounding continuous phase, providing additional formulation space for the developer.

$$\ln \frac{P_r}{P_\infty} = \frac{2\gamma M}{r R T}$$

Equation 3

1.3. THE PHYSICAL STATE AND DRUG SOLUBILITY

51% of small organic molecules show polymorphism [35]. Polymorphs have varying intermolecular interactions and in consequence can differ from each other by changed mechanical, thermal, electrical or optical properties. The crystalline state can be defined as the most stable and lowest energetic state for a solid. However, different energetic levels can be expected for each polymorph and amorphous form (**Figure 2**). The energetical state is represented by the Gibbs free energy function (**Equation 4**, [36]), where the internal energy U is the total of the kinetic energy (motion of molecules) and the potential energy (vibrational and electric energy of atoms within molecules or crystals) [37]. H represents the enthalpy of the system, T and S the temperature and the entropy, P the pressure and V the volume. It is the change in Gibbs free energy G within a solution process that determines a substance's solubility. Polymorphs with a high entropy and a low enthalpy change upon dissolution will hence show a general tendency towards higher solubilities (**Figure 2**).

$$G = H - TS = U + PV - TS$$

Equation 4

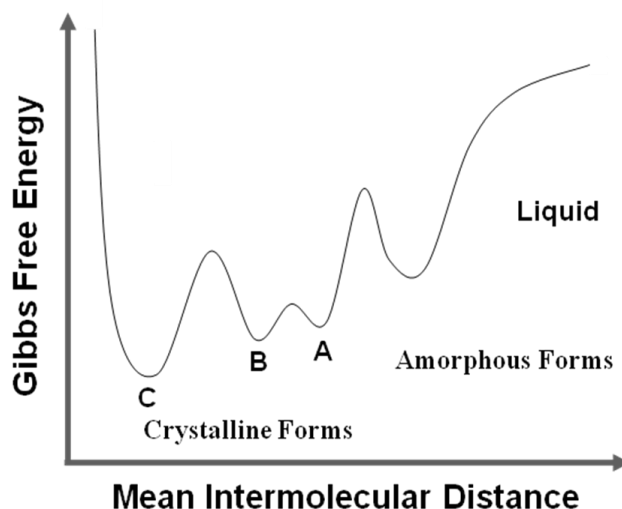


Figure 2: Potential energies of different polymorphic forms of a substance (modified from [38])

Beyond its liquid phase, it is the amorphous or the least stable crystalline form of a substance that provides the highest solubility. Hancock and Parks [39] found a 1.1 to 5 fold increase in solubility between different crystal forms of a drug, while a solubility improvement by factors of 4.4 to 24 between the amorphous phase and a corresponding crystalline phase were obtained. The solubility of a liquid derivate can be expected to be even higher. The preparation and, even more importantly, stabilization of maximally disordered condensed matter is hence critical in formulation development.

1.4. PREPARATION OF NANODISPERSIONS

Nanodispersions can be either prepared by “top-down” techniques, such as milling [40-44] or high pressure homogenization [45-47] or by bottom up approaches, where nanoparticles are prepared by self-assembly of their constituents. Bottom up approaches usually involve changes of a solute’s solubility based on physical or chemical triggers, e.g. due to changes in temperature [48], ionic strength [49] or the use of antisolvents [5, 9, 50], resulting in precipitation of the solute. As pointed out above (**Section 1.3**) most advantageous in terms of solubility improvement are nanodispersions containing a dispersed phase with high Gibbs free energy, e.g. an amorphous polymorph. While top-down techniques often require substantial energy for transforming a crystalline sample in its amorphous equivalent, this aim

can often be reached in an easier way by bottom up techniques. Within precipitation processes most substances intrinsically manifest in their least stable form [51]. Reasons therefore are mainly kinetical, when phase separation occurs so rapidly that the solute molecules have no time to assemble into an energetically favorable crystal lattice. The faster phase separation occurs, the more likely is the chance that a highly energetic precipitate is obtained.

Among the bottom up techniques antisolvent precipitation represents a highly effective, low priced and scalable approach. Briefly, a poorly soluble compound is dissolved in a solvent which is subsequently quenched with an antisolvent, resulting in the precipitation of the solute. Solvent and antisolvent need to be completely miscible, so that upon addition of the antisolvent the solubility limit of the dissolved compound is exceeded and phase separation occurs. A bulk liquid phase is obtained in which the precipitated compound is dispersed. In such processes phase separation typically occurs within a time frame of μs to ms [5, 6, 52], so that with a very high likelihood amorphous precipitates can be obtained [9, 34, 53, 54].

The mixing process of solvent and antisolvent occurs by forming vortices that fractally decrease in size down to a minimum scale [6]. Beyond this micromixing scale, mixing occurs due to diffusion controlled interpenetration of the solvents and solute. Phase separation occurs at the interface or inside the solvent/antisolvent layers formed by the mixing process (**Figure 3**). The particle formation process can be directly triggered by varying the mixing speed until blending occurs on a time scale approaching that of the diffusion controlled phase separation process. It is hence a key parameter for controlling the particle formation process in a well directed manner. The faster the mixing process is, the smaller the particles sizes obtained typically are.

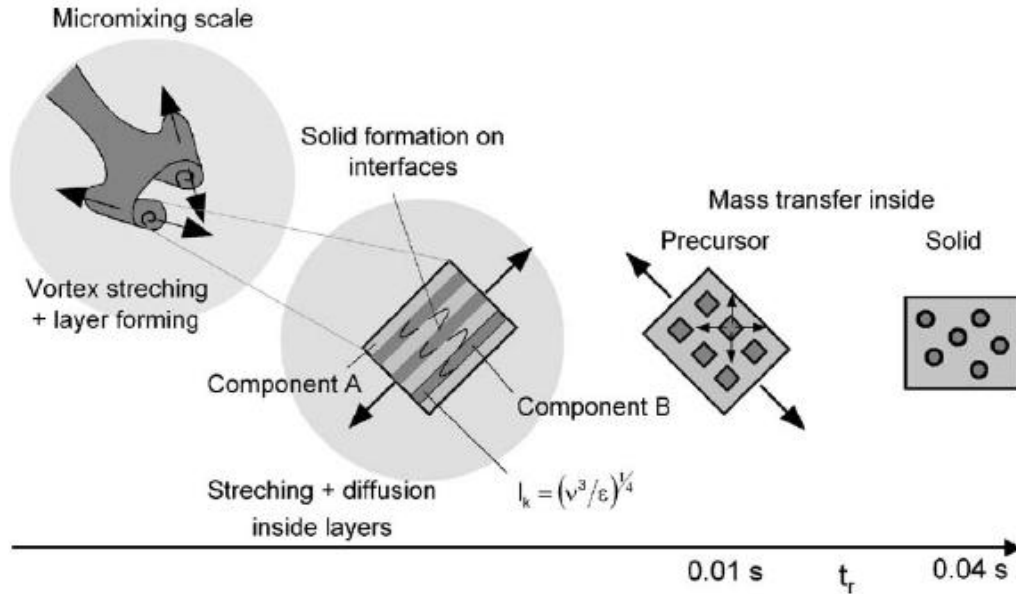


Figure 3: The influence of mixing on particle formation [6]

A wide variety of mixing devices is used within precipitation processes, such as static mixers [9] or different kinds of batch reactor vessels which can be equipped with multiple sample and sensor ports [55] (Figure 4). Most reproducible results and defined mixing conditions are provided by rather simple structured setups, such as y- or t-shaped impinging jet reactors [56]. Especially the latter are well known and mathematical models exist coupling the mixing process to the precipitation event, thereby allowing for a better understanding of the impact of certain process parameters [57, 58].

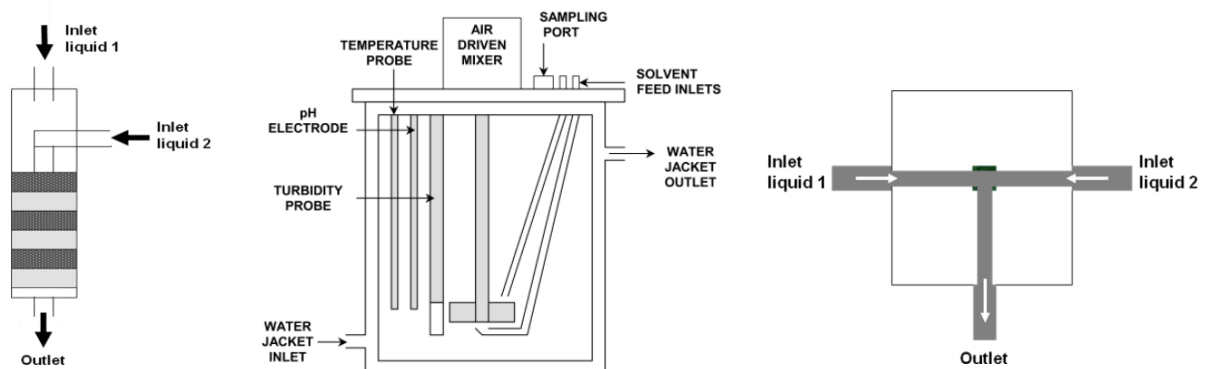


Figure 4: Different kinds of mixing devices used in antisolvent precipitation. Left: static mixer [9], middle: batch reactor [55], right: impinging jet reactor

Although the flow patterns in structurally simple mixers are known, the particle formation process itself generally lacks detailed understanding. The mechanisms for particle formation are often unclear, especially in cases where structurally complex organic molecules are involved. Gaining control of the process is therefore often difficult and a matter of try and error in terms of process optimization. Besides mixing also the solvent composition, solute concentration and temperature are known to have certain effects [59, 60], but it often remains unclear and unpredictable to what extent changes in these parameters affect the final particle size distribution.

Independent from the phase separation process, the stability of the obtained dispersions plays a key role. An antagonism exists between the need of increasing drug solubility and the stabilization of the dispersions. Aqueous dispersions prepared by antisolvent precipitation in most cases contain about 1-10% solvent. In combination with the high solubility of the metastable precipitate, this leads to tremendous stabilization issues due to Ostwald ripening, agglomeration and crystallization of the particles [5, 34]. Ostwald ripening means the mass transfer from smaller particles to bigger ones of the same kind due to an increased surface energy of the smaller particles. Crystallization on the other hand means the formation and propagation of a purely crystalline solid phase by conversion from either a solution or from an amorphous substrate with a high degree of disorder. Especially for pharmaceutical applications the clearly defined physical state of the drugs and excipients is a precondition for permanently assuring high performance of a product. It is hence stringent to find means to assure the morphological stability of the dispersions in order to gain the freedom for downstream processing of the formulations, e.g. solvent removal, concentration steps or drying.

1.5. OBJECTIVES OF THE THESIS

The present work was accomplished as part of a cooperation project between the Department of Pharmacy, Pharmaceutical Technology and Biopharmaceutics, Ludwig-Maximilians-University Munich, the Chair of Particle Technology, Friedrich-Alexander-University Erlangen-Nuremberg as well as the industrial partner Abbott GmbH & Co. KG, Ludwigshafen. Objectives of the thesis were

- 1) the preparation of nanosuspensions of poorly soluble drugs by means of antisolvent precipitation. For obtaining the highest possible solubilizing effects the experiments aimed on obtaining dispersions containing amorphous drug.

- 2) to systematically investigate the process parameters influencing the particle formation process for gaining a deeper understanding of the mechanisms influencing the particle formation process.

- 3) the application and refinement of a mathematical model for the simulation of nucleation based particle formation processes. The model was thought to allow to estimate and to predict the impact of certain process parameters. Comparison of the model with experimental data was intended to be used to identify critical process parameters and to direct the product characteristics. In a best case scenario the model was thought of being capable to predict the suitability of certain drugs/solvents for antisolvent precipitation.

- 4) to stabilize the drug dispersions in size and under maintaining their morphology. Short term stabilization was thought to be accomplished to allow for further downstream processing and the implementation of additional means necessary for a permanent stabilization of the dispersions. The excipients used were selected for enabling parenteral as well as peroral applicability.

Depending on the specific expertise of the cooperation parameters, experiments were partly accomplished at Abbott GmbH & Co. KG, at the University Erlangen-Nuremberg or at the Ludwig-Maximilians-University in Munich. In cases where a transfer of equipment between the research sites was not possible, experiments were accomplished using equivalent equipment and measurement conditions at both sites. Each individual set of measurements was accomplished using the same instrumentation, for assuring innerexperimental comparability of the results.

Chapter 2. Simulation of the Precipitation Process

2.1. ABSTRACT

Antisolvent precipitation has been widely investigated in the pharmaceutical industry [9, 34, 59, 61]. However, although technologically closely related to the widely applied crystallization techniques, antisolvent precipitation rarely succeeded to reach a commercial stage in the field of amorphous drug delivery systems. Critical in this context are poorly understood processes as well as the need for producing stable polymorphs with sufficiently long shelf lives.

Using antisolvent precipitation for the preparation of nanodispersions, the focus of this work was put on gaining detailed insight into the mechanism governing particle formation. It should enable us to further optimize this technology towards a tailor made drug delivery system. A simulation model was developed based on the density, the interfacial properties and the solubility profile of the lipophilic model drug fenofibrate. This mathematical approach allows for a theoretical, time resolved analysis of the particle formation process including rise and fade of supersaturation, nucleation and growth of the particles. In agreement with the simulations, particle size was found to decrease under intense mixing conditions, allowing for the preparation of particles with a specific mean particle size under defined flow rates. The efficiency of the mixing process of solvent and antisolvent was judged based on pressure drop measurements and compared to the simulation results. Mixing was found to be surprisingly energy consuming, implementing a relative ineffectiveness of the mixing process. The dispersions obtained by antisolvent precipitation showed a tremendously increased solubility compared to the crystalline drug. The precipitates were found to be noncrystalline, as indicated by an extreme instability and the onset of crystallization immediately after sample preparation. Based on the mathematical model developed, further investigations on the details of the phase separation process became possible.

2.2. INTRODUCTION

For liquid solutions both upper and lower critical solution temperatures and compositions can exist (**Figure 5**) [31, 62-64]. At the critical temperature/composition solute and solvent become completely miscible. Below an upper critical solution temperature (UCST) or above the lower critical solution temperature (LCST) a miscibility gap exists where phase separation can occur. The region in a phase diagram in which composition and temperature for a mixture leave the thermodynamically stable range is called metastable. It is enclosed by the binodal and spinodal curves. The binodal curve represents the border to thermodynamically stable conditions. When crossing the binodal from the thermodynamically stable site, local concentration density fluctuations such that one part of the system gets more concentrated on the expense of another lead to local supersaturation, which can be diminished by separation of the solute and subsequent growth of the dispersed phase.

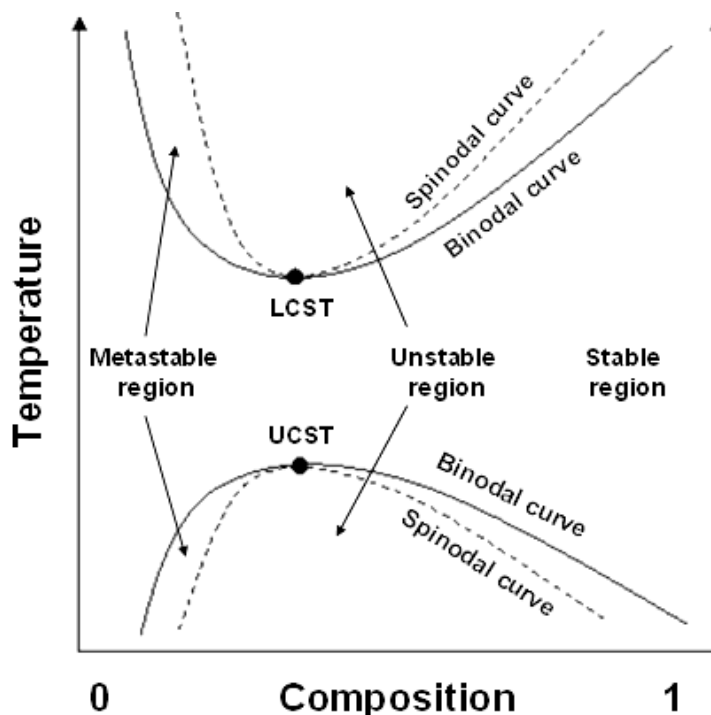


Figure 5: Phase diagram of a mixture showing upper and lower critical solution temperatures (adopted from [62, 64])

Phase separation can occur due to two mechanisms, nucleation and growth or spinodal decomposition. Nucleation is a phase transition where strong changes in composition take

place, but which has a small spatial range, typically resulting in the formation droplets/particles of well defined size. Shifting a sample further across the binodal curve leads to increased destabilization of the system; the likelihood of nucleation increases (**Figure 6**). At infinitely high likelihood, the spinodal curve is reached. At the spinodal curve no thermodynamical barrier for phase separation exists anymore. Precipitation does no longer occur due to nucleation, but due to spinodal decomposition. Small degrees of compositional changes result in extended spatial decomposition. The phase separation product is hence no longer well defined, but demulsification results in spontaneously forming large scale precipitates. The occurrence of spinodal decomposition from solutions of a solid in a liquid phase is considered unlikely, due to the commonly broad width of the metastable zone [65]. Nevertheless, although nucleation remains the predominant phase separation mechanism, recent research lead to the conclusion that the transition between spinodal and binodal demixing is gradual and that short lived spinodal stages can occur prior to particle formation [6].

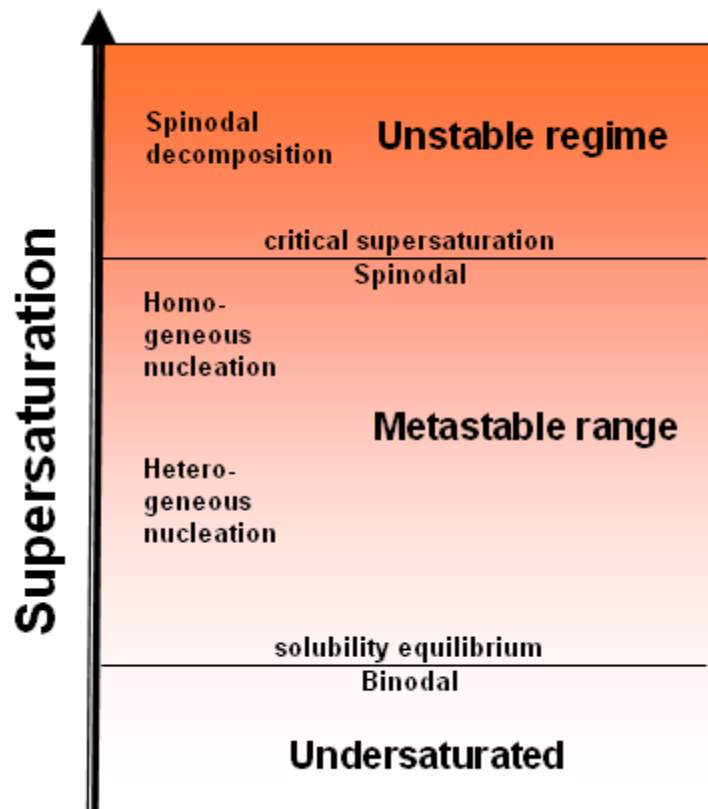


Figure 6: Dependency of the phase separation mechanism on the degree of supersaturation

By comparison of experimental data and model based evaluation, the mathematical description of precipitation processes can be of extensive use in understanding phase separation processes in more detail, allowing for the differentiation between the individual phase separation mechanisms.

Generally, for inorganic materials the mechanisms controlling precipitation processes are well known and mathematical models exist describing these processes. State-of-the art are simulations using the population balance approach, which is capable to simulate the particle formation kinetics and to predict particle size distributions. For some inorganic compounds where the necessary physico-chemical parameters are known, even quantitative predictions of the expected particle sizes can be made [66, 67]. Simulations of the underlying hydrodynamics and the impact of mixing effects are well established.

The development of such models of precipitation processes where organic molecules and solvents are involved is however complicated, and requires distinct additional skills. Crystallization processes may be impaired by the time-determining step of surface integration of the more complex molecules into an oriented crystalline polymorph of the organic compound. Tremendous changes in solvent composition and interfacial energy occur upon blending solvent and antisolvent. Especially variations in the interfacial energy are expected to have a main impact on nanoparticle formation processes as it affects the mass transfer to and from a particle as well as its wetting behavior.

Maybe due to these reasons, only a limited amount of publications exist describing such experimental setups [68-70]. After all, the authors by implication agree that the general principles of particle formation are the same between organic and inorganic compounds as well as aqueous and organic solvent systems. One purpose of this work was to develop a mathematical model describing precipitation processes based on experimental data and known physicochemical characteristics of solvent, antisolvent and solute. The model was based on the experiences previously gained on the homogeneous nucleation of inorganic compounds and further developed to meet the special requirements for the fenofibrate system under investigation. With this model we aim to critically investigate key process conditions and to determine by what means particle formation can be influenced in antisolvent precipitation. Also the hydrodynamic effects within the mixing process were evaluated and conclusions were drawn about the efficiency of the mixing process.

2.3. MATERIAL AND METHODS

2.3.1 EQUIPMENT AND SAMPLE CHARACTERIZATION

Fenofibrate was used as a model compound for the investigation of the mechanisms governing antisolvent precipitation. It is a generic antihypercholesterolemic and antihypertriglyceridemic drug; its chemical structure is shown in **Figure 7** [71]. Based on a literature research of compounds successfully used in antisolvent precipitation, fenofibrate was selected due to its physicochemical properties (melting point 80°C), molecular weight 360.83 g/mol, aromatic structure, LogP 4.8), as well as its solubility in the ethanolic phase (“soluble” according to Pharm. Eur.) and aqueous phase 2.3 mg/l (calculated value according to [71]). Fenofibrate was a generous gift from Abbott GmbH & Co. KG Ludwigshafen, Germany. It was used in Pharm. Eur. quality.

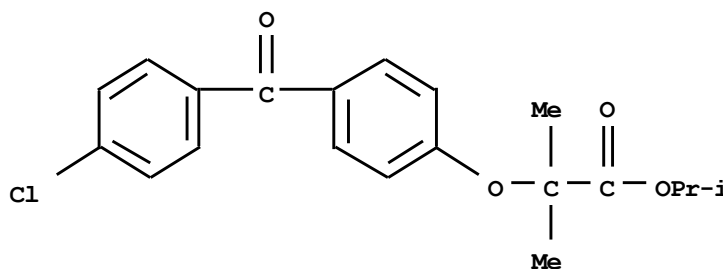


Figure 7: Chemical structure of fenofibrate

For the experiments fenofibrate was dissolved in analytical grade, undenatured ethanol absolute. The ethanol was filtered using 0.2 µm cellulose acetate membrane filters (Macherey-Nagel, Düren, Germany) for reducing potentially contained particulate impurities. The water used as antisolvent for the preparation of the dispersions was highly purified water prepared with a Purelab Plus laboratory water purification system (conductivity < 0.056 µS/cm; ELGA LabWater, Celle, Germany). Dispersions were prepared by quenching a 5% (w/w) ethanolic fenofibrate solution with water in a 1+5 ratio. The two solutions were either mixed by pipetting one to the other or by using an impinging jet reactor consisting of a mixing chamber fed by two syringe pumps (100DX Syringe Pump, Teledyne Technologies Incorporated, Thousand Oaks, USA).

A t-shaped mixing chamber with an inner diameter of 0.5 mm (Klaus Ziemer GmbH, Langerwehe, Germany) was used for preparations with the syringe pumps. The outlet of the mixing chamber as well as the connections to the pumps consisted of PEEK tubing with the same inner diameter (**Figure 8**). For obtaining a complete flow rate dependent particle size distribution profile, fenofibrate dispersions were prepared at total flow rates of 12, 24, 36, 48 and 60 ml/min (combined flow from both pumps). All dispersions were prepared without the use of excipients for not altering the structure of the dispersed phase or influencing the particle formation process.

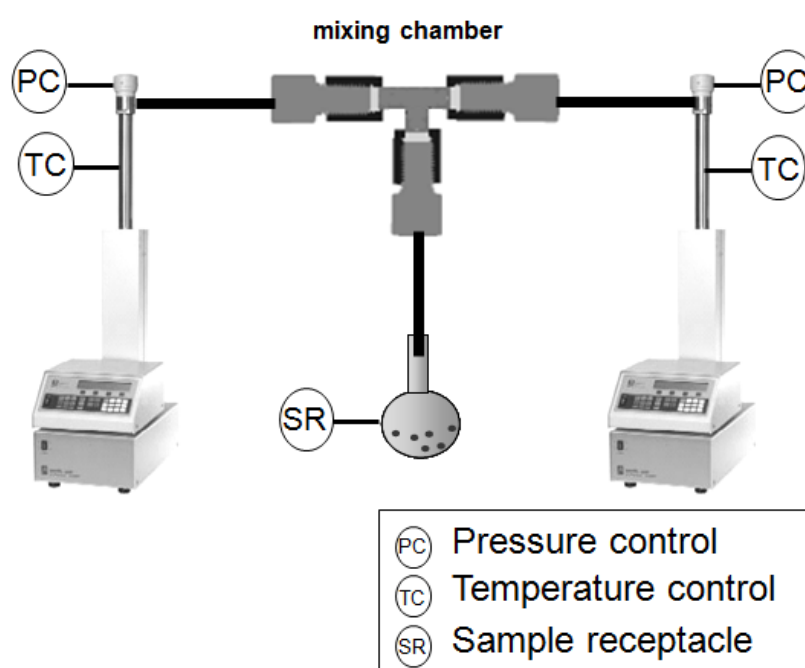


Figure 8: Setup of the impinging jet reactors equipped with a t-shaped mixing chamber for preparation of the drug dispersions (image modified from www.isco.com)

After dilution of the samples with deionized water, particle size was determined by static light scattering using a Horiba LA-950 (Retsch Technology, Haan, Germany) or a Mastersizer 2000 (Malvern Instruments, Herrenberg, Germany). An appropriate optical model was established according to Kinoshita et al. [72]. Thereby the detected intensity of scattered light s is mathematically transformed according to the Fraunhofer and Mie theory into a particle size distribution and back again into the estimated light intensity distribution s^* . The conformity of s and s^* as a function of the refractive index was calculated with the

built-in software of the Horiba instrument and the optimum refractive index was converged towards s^* being very close to s . The optical model thus obtained used a refractive index of 1.56 and an absorption coefficient of 0.012. The Span value as a measure for the particle size distribution was calculated according to **Equation 5**. The d_{10} , d_{50} and d_{90} represent the 10th, 50th and the 90th percentile of the particle size distribution, respectively, as measured by volume distribution.

$$Span = \frac{d_{90} - d_{10}}{d_{50}}$$

Equation 5

The results were verified by photon correlation spectroscopy (PCS) with a Zetasizer Nano ZS (Malvern Instruments, Herrenberg, Germany). Therefore samples were partly filtered using Minisart syringe filters (Sartorius AG, Göttingen, Germany) with a pore size of 1.2 μm to remove coarse contaminations which might disturb the PCS measurements. Although the particle sizes were measured directly after preparation of the dispersions, the particles were expected to have already undergone ripening due to growth and agglomeration. Such ripening effects typically start already within the precipitation process, even before the phase separation stops. The measured particle size distributions do hence not accurately represent the size of the primary particles formed. For estimating the extent of agglomeration, zeta-potential measurements were accomplished by electrophoretic light scattering using a Zetasizer Nano ZS (Malvern Instruments, Herrenberg, Germany). The dispersions used for the zeta-potential measurements were prepared at total flow rates of 60 ml/min, using a t-piece with 0.5 mm i.d. (Klaus Ziemer GmbH, Langerwehe, Germany). The diluted dispersions were investigated directly after sample preparation. The pH of the dispersions was automatically adjusted with 0.1 N NaOH and HCl, using the MPT2 multipurpose titrator (Malvern Instruments, Herrenberg, Germany). The voltage of the Zetasizer Nano ZS was set to 40 V; the number of runs was set to 30. After each run the system was rinsed with ethanol and desalted water.

Additionally, samples were monitored with a Nikon Labophot light microscope equipped with a JVC digital camera Model JVC TKC 1380E. Crystallization of the samples was monitored by using crossed polarized filters.

The true density of fenofibrate was determined using an AccuPyc 1330 helium gas pycnometer (Micromeritics, Norcross, USA).

Parsival software (CiT-Computing in Technology GmbH, Rastede, Germany) was used for simulating the particle formation process.

2.3.2 SOLUBILITY CHANGES WITHIN THE MIXING PROCESS

Upon mixing ethanolic and aqueous phase, the drug molecules pass a transient solvent gradient, starting from 100% ethanol and ending at approximately 16.7% (V/V) ethanol, which is the ethanol concentration in the final dispersion. For simulating the precipitation process, a solubility profile of fenofibrate in ethanol-water mixtures was accomplished by adding different amounts of water to a saturated ethanolic fenofibrate solution. Thereby the dispersions were adjusted to a defined ethanol concentration. Samples were drawn 0.75, 3, 10, 20 and 40 min after preparation of the dispersion. They were sterile filtered using Minisart RC 15 filters with a pore size of 0.2 μm (Sartorius AG, Göttingen, Germany) before the drug concentration in the supernatant was determined spectrophotometrically using a Shimadzu densitometer CS-9301PC (Shimadzu Deutschland GmbH, Duisburg, Germany). The data set for each ethanol concentration was fitted to an exponential function and extrapolated to the time point of the preparation of the dispersion (0 min). Based on the so obtained solubility profile, the solubility of fenofibrate in a given solvent composition within the precipitation process was calculated. As dissolved fenofibrate showed absorption at wavelengths between 200 and 380 nm, secondary phase separation of the supernatant could additionally be recorded at a wavelength of 500 nm for differentiating dissolved drug from dispersed material.

2.3.3 ACCOMPLISHMENT OF THE SIMULATIONS

A numerical model previously developed and successfully used by the Chair of Particle Technology, Friedrich-Alexander University Erlangen-Nuremberg, was used as basis for simulating the mixing and phase separation process of fenofibrate. Previously exclusively used for the simulation of phase separation processes of inorganic compounds, the model was refined to meet the specific needs required for describing the phase separation of complex organic molecules. The model was based on homogeneous nucleation, as this phase separation mechanism is known to predominantly occur in systems involving high supersaturations [73] and to be widely independent from the physical state and structural nature of the compound used. Secondary processes as aggregation or ripening were neglected in the model due to the short time span between sample preparation and characterization (< 2 min) and the relatively high zeta-potential of the drug particles.

Current state-of-the-art modeling of polydisperse particulate processes is based on the population balance approach (PBA). In this case, the complete PBA is simplified to a monomodal method of moment model, calculating the 0th and the 3rd moment. Consequently the total number and mass concentrations of the particles are computed according to **Equation 6** and **Equation 7** [74], a corresponding mean particle size is calculated according to **Equation 8** [74].

$$\frac{dN}{dt} = B_{\text{hom}}$$

Equation 6

$$\frac{dm}{dt} = B_{\text{hom}} \cdot \rho_p \cdot \frac{\pi}{6} \cdot x_c^3 + N \cdot \rho_p \cdot \frac{\pi}{2} \cdot x^2 \cdot G_{\text{lin}}$$

Equation 7

$$x = \sqrt[3]{\frac{m}{N}} \cdot \frac{6}{\pi \cdot \rho_p}$$

Equation 8

Here N is the total number concentration of the particles, t is the time, B_{hom} is the rate of homogeneous nucleation, m is the total particulate mass concentration, ρ_p is the density of the precipitate, χ_c is the critical nucleus size, χ is the volume equivalent particle diameter and G_{lin} in the linear growth rate.

As growth of the obtained particles was expected to be diffusion limited rather than depending on surface integration of adsorbing molecules, the growth rate is particle size dependent and can be written as shown in **Equation 9** [74], where Sh is the Sherwood number, K_{SP} is the solubility product ρ_c is the density of the continuous phase and S^* is the supersaturation.

$$G_{\text{lin}} = \frac{d\chi}{dt} = 2 \frac{Sh \cdot D_{AB} \cdot \sqrt{K_{SP}} \cdot M \cdot S^* - 1}{\rho_c \chi}$$

Equation 9

Additionally to the precipitation process, the fluid dynamics in the mixer were described by a simple mixing model, estimating the mixing time via the pressure drop measured [58].

2.3.4 MIXING CONDITIONS

In the mixing process described here, two phases are combined in a t-shaped mixing chamber. One of these phases is an ethanolic drug solution, the other one is water which is used as antisolvent. Within the mixing process vortices of the blended phases are formed, which decrease in size through energy dissipation until a minimum vortex size is reached, the so called Kolmogorov eddies. Below this size mixing occurs on a molecular level by diffusion controlled interpenetration of the two phases. The energy introduced to the system is transported from bigger to smaller vortices (energy cascade) until it is converted into heat by viscous dissipation. The global energy dissipation of the mixing process can be calculated according to **Equation 10** [75], where ε is the rate of energy dissipation in the turbulent flow

per unit mass of the fluid (specific power input), p is the pressure, Q is the flow rate and V_{DIS} is the effective volume in which the main turbulent energy dissipation occurs.

$$\varepsilon = \frac{\Delta p Q}{\rho_C V_{DIS}}$$

Equation 10

Knowing the energy dissipation, the theoretical size of the Kolmogorov eddies can be determined according to **Equation 11** [75], where λ_0 is the size of the smallest turbulent eddies and η_C is the dynamic viscosity of the continuous phase. η_C and the density of the continuous phase ρ_C were obtained from [76].

$$\lambda_0 \approx \varepsilon^{-3/4} \eta_C^{3/4} \rho_C^{-3/4}$$

Equation 11

In the setup used within this work, the intensity of mixing is experimentally accessible by measuring the pressure drop. The pressure drop describes the pressure difference measured between simultaneously perfusing ethanolic and aqueous phase through the mixing setup and doing so with the liquids individually, without having the actual mixing effect. It is known that in t-mixers the pressure drop arises almost completely from the impinging jets of the two feed streams [77] and hence represents the major amount of viscous dissipation and friction in the mixing process. The higher the pressure drop of a system is, the more energy is consumed for the mixing process and the more intense will be the interpenetration of the phases. The pressure drop typically depends on the square of the mean velocity as shown by **Equation 12** [52], where ρ_F is the density of fluid, ζ is the pressure drop coefficient and u_{mean} is the mean velocity in the main tube of mixer.

$$\Delta p = \frac{1}{2} \rho_F \cdot \xi \cdot u_{mean}^2$$

Equation 12

The pressure was recorded with built in sensors of the syringe pumps at total flow rates of 12, 24, 36, 48 and 60 ml/min, using the t-shaped 0.5 mm i.d. mixing chamber. The results were compared to a mathematical model estimating the energy dissipation for the given setup. Therefore, for Schmidt-numbers smaller than 4000 the characteristic micro mixing time is estimated as a function of the kinematic viscosity ν and the specific power input ϵ , and was calculated according to **Equation 13** [78].

$$\tau_{\text{micro-mixing}} = 17.2 \cdot \sqrt{\frac{\nu}{\epsilon}}$$

Equation 13

In order to model the influence of mixing on the phase separation process, the simulation approach chosen starts with a purely ethanolic solution of fenofibrate and continues with the constant addition of water. After a mixing time τ the final experimental conditions of 16.7% (V/V) ethanol are reached; consequently the solubility is reduced and a supersaturated solution is generated. For comparing the simulation with the experimental data, the theoretical micro-mixing time $\tau_{\text{micro-mixing}}$, which characterizes the mixing time at small length scales, is estimated as a tenth of the mixing time τ [79].

2.3.5 PARTICLE FORMATION

The amount and size of precipitate formed depends strongly on the degree of supersaturation. The more intense mixing is, and the stronger the reduction of the solutes' solubility is, the higher will be the resulting supersaturation. The supersaturation S^* is defined by the difference of the chemical potential μ of the dissolved substance compared to a saturated solution **Equation 14** [80].

$$\frac{d\mu}{R T} = \ln S^*$$

Equation 14

For our purpose, supersaturation can be expressed as the concentration of a substance in solution C divided by its saturation concentration C^* (**Equation 15**) [81].

$$S^* = \frac{C}{C^*}$$

Equation 15

Precipitation can occur due to local concentration fluctuations by homogeneous or heterogeneous nucleation or by spinodal decomposition. While spinodal phase separation occurs spontaneously, for nucleation based decomposition an energy barrier has to be overcome in order to form thermodynamically stable nuclei. Whether phase separation of small molecules occurs due to nucleation or spinodal decomposition is, however, controversially discussed, as it is not always possible to clearly distinguish between both phenomena [5].

Assuming that phase separation occurs due to homogenous nucleation, this process can be described by the nucleation rate **Equation 16** [52]. Here D_{AB} is the diffusion coefficient, K_{SP} is the solubility product, S^* is the supersaturation, N_A is the Avogadro number, γ_{CL} is the interfacial energy, k is the Boltzmann constant, T is the temperature and V_m is the molecular volume.

$$B_{\text{hom}} = 1.5 D_{AB} \cdot (\sqrt{K_{SP}} \cdot S^* N_A)^{2/3} \cdot \sqrt{\frac{\gamma_{CL}}{kT}} \cdot V_m \exp\left(-\frac{16\pi}{3} \cdot \left(\frac{\gamma_{CL}}{kT}\right)^3 \cdot \frac{V_m^2}{(\ln S^*)^2}\right)$$

Equation 16

Homogeneous nucleation can occur when a certain amount of molecules collide in solution, forming clusters. The energy ΔG needed to form a nucleus with the radius r is given by

Equation 17 [82], with μ^* being the difference in chemical potential between a solid and the corresponding dissolved substance.

$$\Delta G = \frac{4\pi r^3 \rho_c d\mu^*}{3} + 4\pi r^2 \gamma_{CL}$$

Equation 17

Only for particles of a certain critical size the negative volume part of the function dominates the thermodynamically unfavorable positive surface part, the nucleus becomes stable and grows by incorporation of additional molecules to the existing particle. In accordance, homogeneous nucleation predominantly occurs at very high supersaturations as they are known to occur in antisolvent processes [65] and impinging jet reactors [55]. The critical nucleus size can be calculated by differentiating the free energy with respect to the nucleus radius r to determine the maximum of the free energy, where the critical nucleus size is given by **Equation 18** [52].

$$x_c = \frac{4 \cdot \gamma_{CL} \cdot V_m}{k \cdot T \cdot \ln S^*}$$

Equation 18

Besides supersaturation, the nucleation rate depends mainly on the interfacial energy γ_{CL} , which determines the interfacial behavior of a particle against the surrounding fluid. When the composition of the continuous phase changes within the precipitation process, also the interfacial energy is altered significantly.

γ_{CL} can be experimentally determined e.g. according to the Young equation [83, 84], but the parameters needed (e.g. surface energy of the solid) are hardly accessible and the results often differ in a range unacceptable for the simulations accomplished here [84, 85]. Therefore, the interfacial energy was determined by a model based evaluation. Based on simulations conducted under assuming perfect mixing conditions the interfacial energy in the model was

varied until the identical mean particle size was calculated as measured for the experiment with maximum mixing intensity.

The diffusion coefficient D_{AB} was estimated based on the Stokes-Einstein equation (**Equation 19**, [29]), the molecular volume V_m of fenofibrate was determined based on the molecular weight and the density of the drug (**Equation 20**).

$$D_{AB} = \frac{k \cdot T}{6 \cdot \pi \cdot \eta_C \cdot r}$$

Equation 19

$$V_m = \frac{M}{\rho_p \cdot N_A}$$

Equation 20

2.4. RESULTS AND DISCUSSION

2.4.1 DETERMINATION OF EXPERIMENTAL DATA FOR THE SIMULATION

MODEL

2.4.1.1. PARTICLE SIZE AND INTERFACIAL ENERGY

When preparing nanodispersions of fenofibrate at different flow rates, the mean particle size decreased from $\sim 4 \mu\text{m}$ at a total flow rate of 12 ml to about 250 nm at flow rates of 48-60 ml/min. Also the particle size distribution became narrower under more intense mixing (**Figure 9**). The flow rates applied correspond to Reynolds numbers between 256 and 1282, calculated based on the density and dynamic viscosity of the corresponding ethanol-water mixture in the final dispersion.

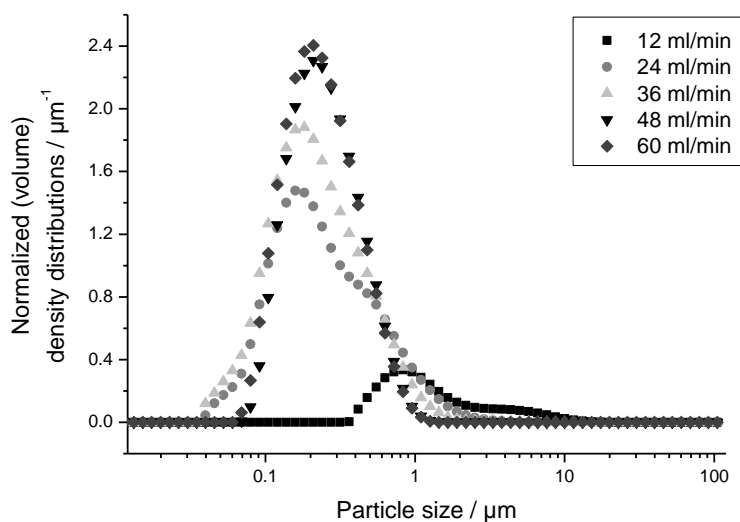


Figure 9: Particle size distributions of fenofibrate dispersions prepared at flow rates ranging from 12 ml/min to 60 ml/min (mean values of 3 runs per flow rate)

Even at the highest flow rate applied (60 ml/min) some particles up to $\sim 3 \mu\text{m}$ were observed by microscopical observation of the dispersions (**Figure 10, left**). Although their concentration was very low, distinct changes in mean particle size were observed when comparing filtered and unfiltered samples by laser diffraction and photon correlation

spectroscopy (**Figure 10, right**). Especially PCS was found to be very sensitive to the presence of big particles.

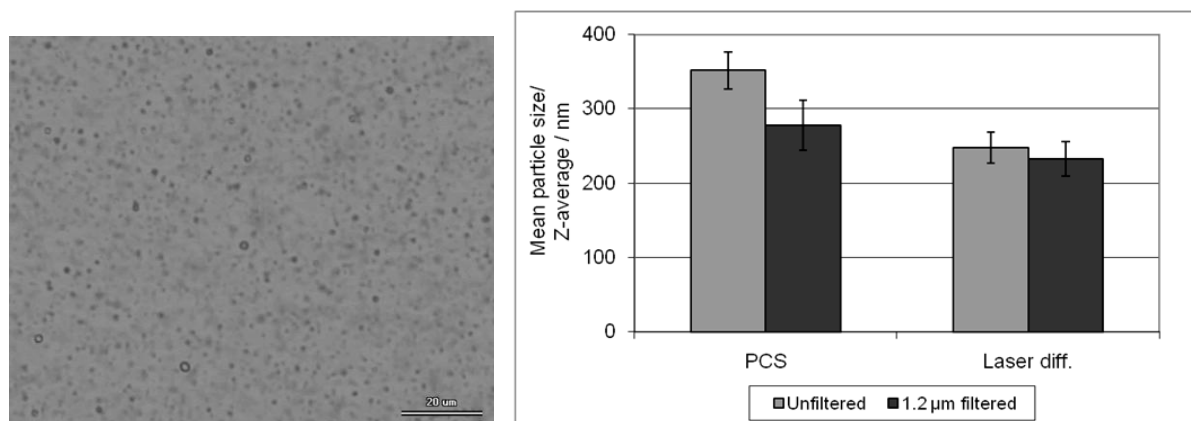


Figure 10: Left: Observation of μm -sized drug particles by microscopical observation. Right: Comparison of PCS and laser diffraction data from filtered and unfiltered dispersions prepared at a total flow rate of 60 ml/min

Based on the mean particle sizes obtained at different mixing intensities (refer also to **Figure 9**), an interfacial energy γ_{CL} of 29.8 mJ m^{-2} was determined for an ethanol concentration of 16.7% (V/V) (**Figure 11**). This value is in a comparable range as previously observed for other organic compounds [68, 86] and was subsequently used for the simulation of the precipitation process.

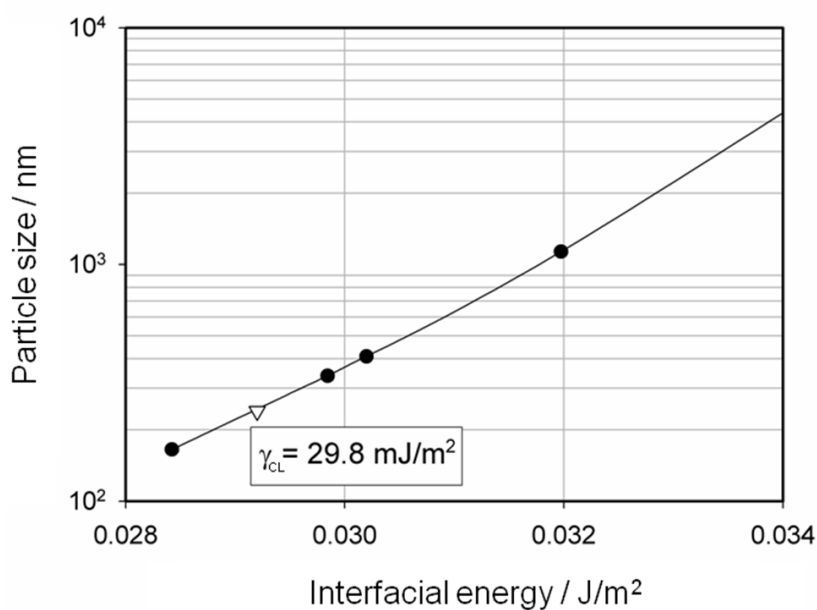


Figure 11: Model based evaluation of interfacial energy

The zeta-potential of the dispersed phase in the pH range relevant for the preparation of the suspensions (pH ~6) reached values of about -27 mV, and was hence considered sufficient for electrokinetical stabilization of the formulations (**Figure 12**). The relatively high negative magnitude of the zeta-potential might be attributed to the adsorption of hydroxide ions to the intrinsically nonpolar surfaces of the fenofibrate particles [87].

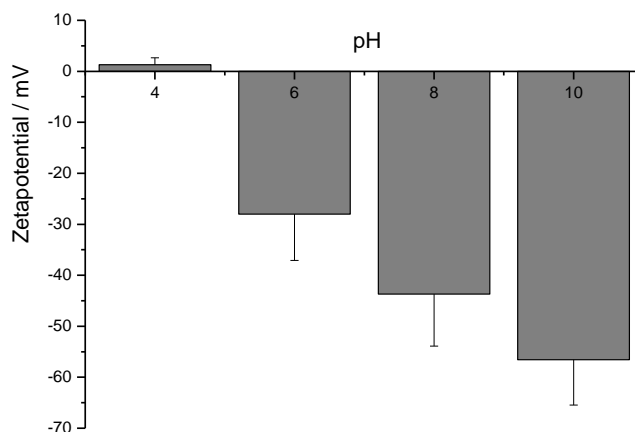


Figure 12: Zeta-potential of fenofibrate dispersions prepared at a total flow rate of 60 ml/min

2.4.1.2. DRUG SOLUBILITY

In the antisolvent precipitation process described here, the solubility of fenofibrate changes dynamically within the particle formation process. For process design and modeling the drug's solubility in the whole solvent gradient passed within the precipitation process needs to be known. Therefore fenofibrate dispersions were prepared by quenching saturated ethanolic drug solutions with different amounts of water. From these dispersions the solubility of the drug in the supernatant was determined. Samples were mixed by hand, as the low supersaturations generated under weak mixing conditions created particles big enough to be completely removed by filtration. The solubility measured hence exclusively derived from the dissolved drug and was governed by the amorphous state of the precipitate. As expected, the supernatant of the freshly prepared dispersions was indeed supersaturated compared to a crystalline dispersion. While the supernatants were clear directly after preparation, phase separation occurred within minutes upon storage (**Figure 13**).

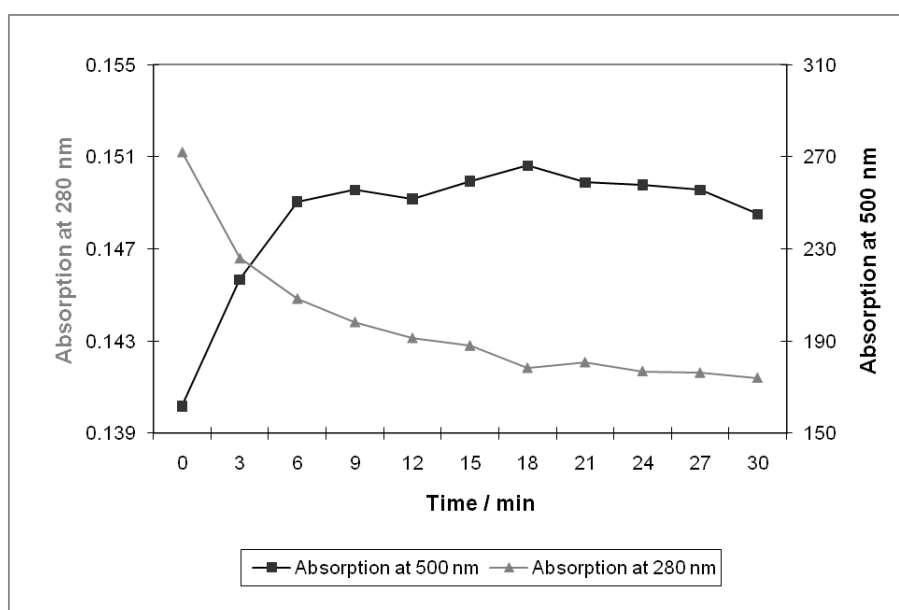


Figure 13: Supersaturation effect in freshly prepared fenofibrate dispersions. After removal of the precipitate, secondary phase separation occurred as indicated by a decreasing absorption of dissolved drug (280 nm) and an increasing amount of precipitate (500 nm)

The solubility of the drug in the presence of the precipitate continuously decreased over time. As it is known that the particle formation process commonly fades within less than 1 min [5, 6, 52], the described changes in drug solubility were hence attributed to Ostwald ripening and

crystallization. Both effects were confirmed by microscopical observation. The rapid decline in drug solubility faded about 40 min after preparation of the dispersions. By that time all drug had crystallized and an equilibrium solubility was approached (**Figure 14**).

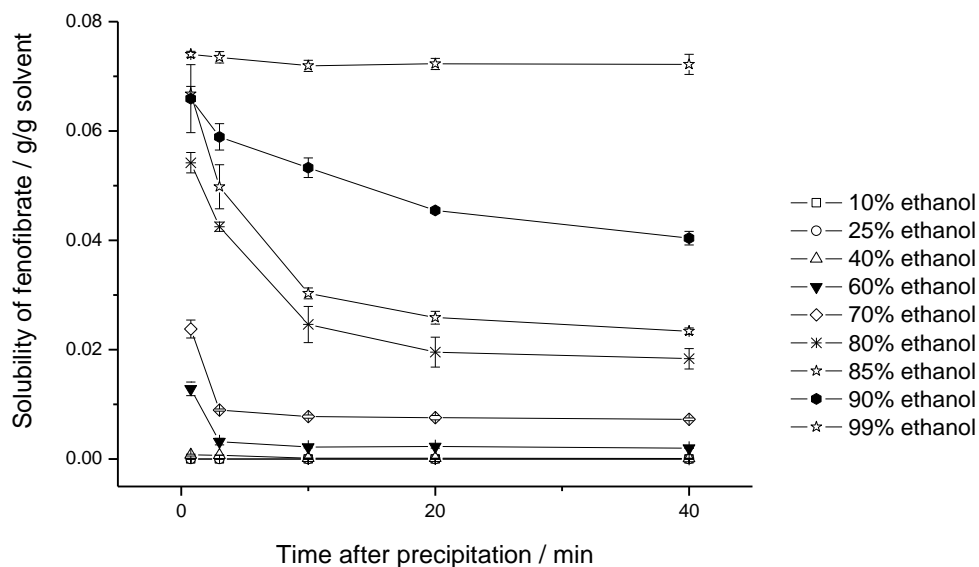


Figure 14: Solubility changes of fenofibrate in freshly prepared dispersions containing 10, 25, 40, 60, 70, 80, 85, 90 and 99.98 % of ethanol

The equivalent solubilities of fenofibrate at the time of precipitation (0 min) in the different dispersions are shown in **Figure 15**. These values were subsequently used for the mathematical modeling of the precipitations.

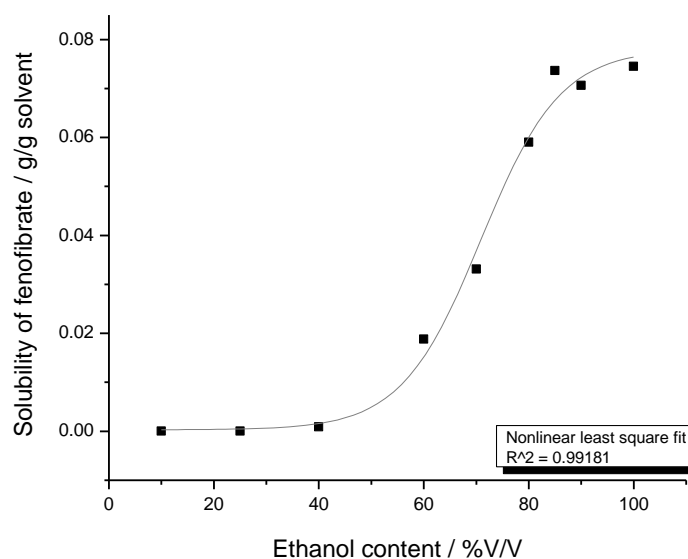


Figure 15: Solubility profile of fenofibrate at time point 0 min. The profile mimics the solvent gradient passed within the precipitation process

2.4.2 DRUG DENSITY

The true density of fenofibrate was determined to be 1.25 g/ml.

2.4.3 OUTCOME OF THE SIMULATIONS

Based on the experimental data computational simulations of the particle formation process were accomplished according to the correlations outlined under **Sections 2.3.3** and **2.3.5**. Assuming a mixing time of 1 ms the precipitation kinetics were studied. The results indicate that relevant supersaturation arises not until the ethanol concentration in the continuous phase drops below about 20% (V/V) (**Figure 16**). The occurrence of supersaturation is closely followed by the onset of nucleation. Particle formation fades after about 10 ms, while the supersaturation is further reduced by particle growth. These simulation results were in good agreement with data previously obtained for inorganic materials [6, 52, 74, 88], for which similar kinetical processes and time scales were observed.

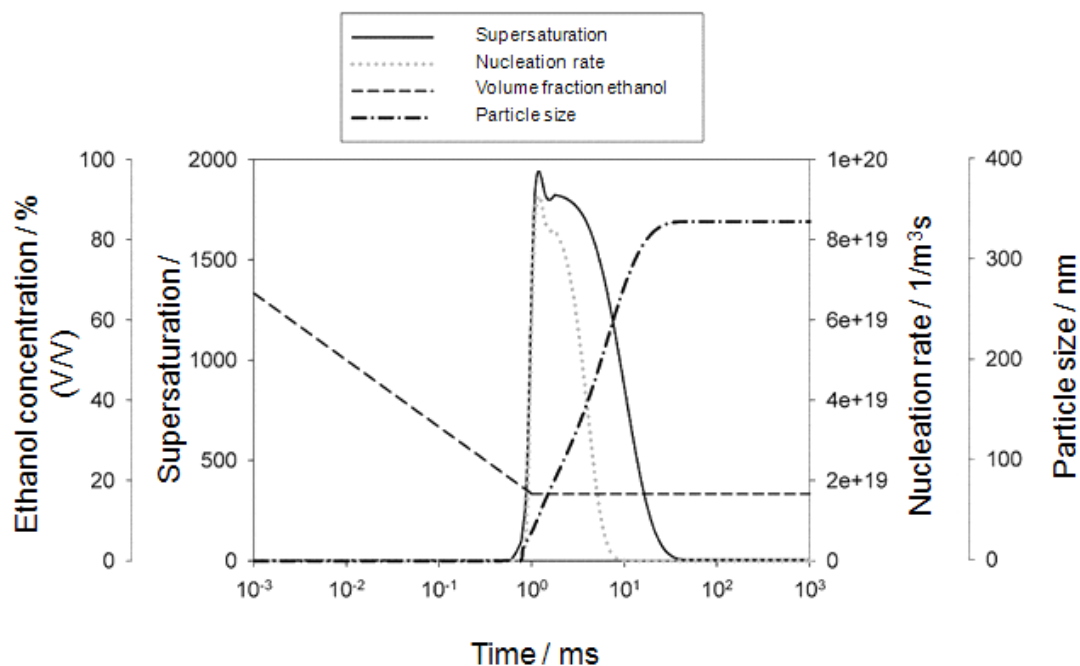


Figure 16: Simulation of the particle formation process. Arising supersaturation is closely followed by nucleation and growth of the primary particles

The mathematical model developed was intended to be used for a qualitative description of the phase separation process. So it provides feedback about whether and to what extent experimental results are in accordance with the presumptions of homogeneous nucleation and transport controlled growth.

2.4.4 INTERPRETATION OF THE EXPERIMENTAL RESULTS IN THE CONTEXT OF THE MODEL BASED EXPECTATIONS

A preliminary comparison between simulation and experimental data can already be made based on the particle sizes measured when investigating the impact of varying mixing intensities. According to classical nucleation theory, the particle size is expected to decrease under intensification of the mixing process. The reason therefore is a more rapid interpenetration of aqueous and organic phase. The hydrodynamic formation of ethanol-water layers leads to an immensely increased size of the interfacial area on the Kolmogorov scale at which diffusion controlled precipitation occurs. The fact that the particle size reaches a plateau already at total flow rates of 48 ml/min indicates that mixing is optimal for the given

setup. In consequence also the particle size distribution would be expected to be more homogeneous. However, the presence of particles in the μm -range under intense mixing conditions is not covered by the simulations.

2.4.4.1. EFFECTIVENESS OF THE MIXING PROCESS

The pressure drop for mixing ethanol and water at different flow rates (= blank) followed a square function as expected (**Figure 17**). In contrast, when preparing the dispersions from ethanolic fenofibrate solutions and water, the pressure drop surprisingly shows a linear dependency on the flow rate. Such a pressure drop profile would only be expected for a flow through packages at low Reynolds numbers, which, due to the comparably low particle concentrations, is not expected here.

The difference between blank and the preparation of the dispersion indicates that the mixing process is influenced by mechanisms involved in the particle formation process itself. At intermediate flow rates more energy is required for the mixing process, while less energy is necessary to mix the liquids at high speed.

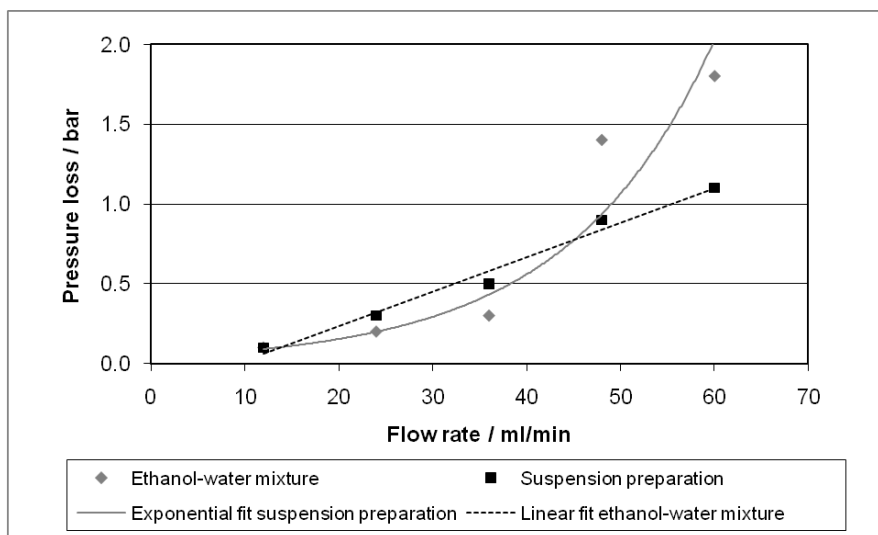


Figure 17: Pressure drop recorded upon mixing of water and ethanol [■] or with an ethanolic fenofibrate solution [◆]. It is a measure for the energy dissipated for the mixing process

Over all, the power input to the system was found to be about three orders of magnitudes higher than would have been expected based on the simulation of the mixing process (**Figure**

18). In consequence, particle sizes significantly smaller than the ones actually obtained could have been anticipated for optimal process conditions. In reality, mixing might be optimal for the given setup, but due to the high energy input required for the process still be ineffective, leaving a potential for further particle size reduction by changing size and shape of the mixing chamber. In addition to the potential impact of the dispersed phase which is formed within the mixing process, the higher energy dissipation might also be a result of noninstantaneous mixing of ethanolic and aqueous phase. Although ethanol and water are widely considered to mix completely, some evidence can be found in literature that mixing is neither necessarily instantaneous nor complete [89, 90].

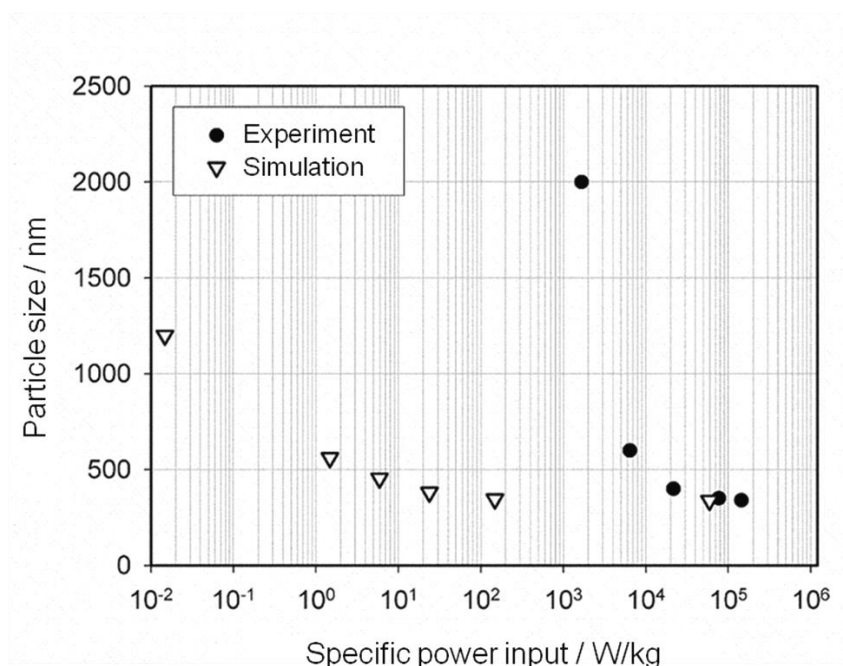


Figure 18: Comparison of the experimentally determined specific power input for the mixing process (●) and the specific input predicted by simulating the mixing conditions (▽)

The size of the Kolmogorov eddies calculated from the specific power input for the mixing process ranges from ~ 0.9 to $6.5 \mu\text{m}$ for both, the preparation of the dispersions as well as the mixing of the pure solvents. High values are obtained for low mixing intensities and, due an increased viscosity of the ethanol-water mixtures [76], for intermediate ethanol concentrations around 45% (w/w). The particle sizes obtained at low flow rates are hence well in the range of the Kolmogorov eddies.

2.4.4.2. SOLUBILIZING EFFECTS OF THE DISPERSIONS

The primary precipitate obtained was found to be non-crystalline, as was best shown by the fact that crystallization was observed shortly after preparation of the samples. In agreement with the remarkable thermodynamical instability of the primary dispersion, the precipitates showed a distinct solubility advantage compared to the fenofibrate's crystalline form. The difference between the drug solubility measured for the precipitate directly after preparation of the samples and the values obtained 40 min following sample preparation are shown in **Figure 19**. The solubility was compared to the crystallized drug up to almost 9 fold increased for the freshly prepared amorphous precipitate. This solubilizing effect is in good agreement with previous findings for amorphous materials [39] and represents an interesting challenge for the stabilization of the dispersed phase's size and physical state.

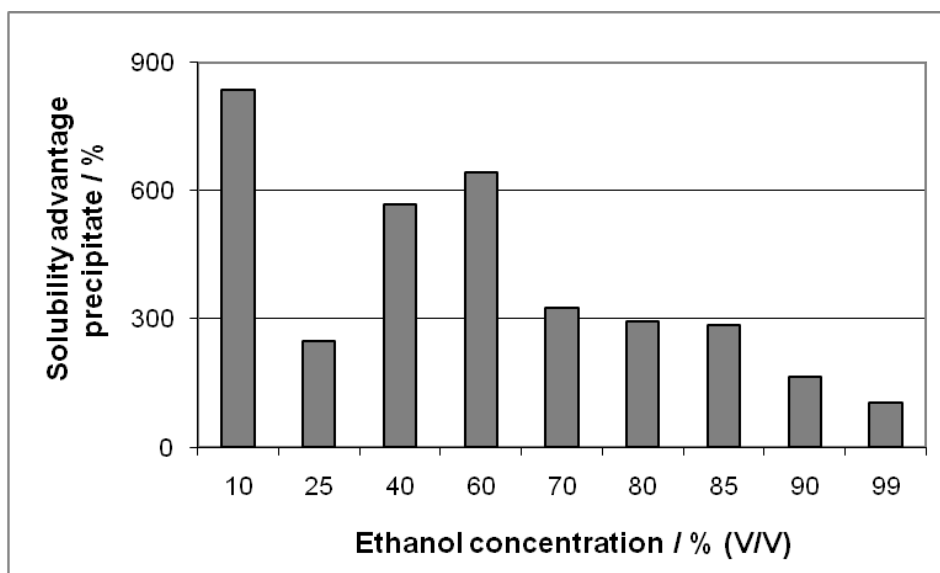


Figure 19: Solubility advantage of the precipitate compared to crystalline fenofibrate

2.5. CONCLUSIONS

A mathematical model was developed for simulating the antisolvent precipitation process of fenofibrate (**Sections 2.3.3** and **2.3.5**). The model assumes homogeneous nucleation and transport controlled growth of the particles. It allowed for a time resolved analysis of the impact of certain process parameters. By coupling the phase separation process to energy dissipation and mixing time (**Section 2.3.4**), also the impact of mixing conditions could be evaluated. Interfacial energy, solubility profile and density of the drug particles were determined based on experimental data. Based on these results first conclusions could be drawn about in how far the basic principles assumed in the simulations mirror the actual particle formation process. While the observed particle size reduction under intensified mixing is in good agreement with the simulations, the particle size obtained was significantly bigger than would have been expected. Correspondingly, the energy consumption required for the mixing process was found to be surprisingly high. The linear shape of the pressure drop profile and the presence of μm -sized particles even at optimal flow rates indicate that mixing might be ineffective and/or other mechanisms might be superimposed to the phase separation process. The hydrodynamical/mechanical impact of the forming precipitate, a noninstantaneous mixing of ethanol and water as well as the unequally applied flow rates applied for ethanolic and aqueous phase are potential explanations, as these were not implemented in the mathematical model applied.

Chapter 3. Experimental Evaluation of Certain Process Parameters

3.1. ABSTRACT

Based on the mathematical model developed for retracing the phase separation process, the experimental impact of a variety of process conditions was investigated for their influence on the resulting particle size distribution. By comparison of the experimental data with the results provided by the simulations, conclusions could be drawn about in how far the assumptions made for the model, homogeneous nucleation and transport controlled growth, apply to the model substance fenofibrate. Among the parameters investigated were the solvent to antisolvent ratio, the temperature of the educt solutions and the drug concentration. Tween 80 as surface active reagent was used for varying the interfacial properties of the continuous phase and the precipitate. Additionally a detailed review was conducted on the mixing process by applying differently sized and shaped mixing chambers. Homogeneous nucleation is generally considered to be the most likely phase separation mechanism for inorganic and organic substances in case of high supersaturation. It was also anticipated to occur for the fenofibrate system under investigation. Surprisingly, variations between the particle sizes obtained experimentally and those predicted by the simulations led to the conclusion that indeed spinodal decomposition must be the determining phase separation mechanism. While being in good agreement with most experimental data, a need for further investigations on the composition and the mechanical properties of the precipitates was uncovered, as also spinodal phase separation alone was incapable to explain all of the experimental results. Overall, the mathematical model in combination with the experimental investigations proved to be a powerful tool for investigating the kind and extend of the impact of the individual process parameters involved in the precipitation process. It allowed to draw conclusions about in how far the presumptions made for the model apply to a given experimental setup, or need to be refined.

3.2. INTRODUCTION

Process conditions can in many ways influence particle formation. Thereby differentiation between the individual parameters is complicated, as experimental modifications often unavoidably affect multiple criteria. The identification of critical factors in a manufacturing process is hence difficult.

The mathematical model developed in **Chapter 2** allows for better understanding the impact of individual process parameters by disintegrating their specific effects. The impact of changes in interfacial energy or drug concentration on supersaturation, nucleation and growth can be qualitatively assessed, indicating particle size, growth, broadening or narrowing of the size distribution. The model is based on the assumption of homogeneous nucleation and transport controlled growth. Experimental results being in concordance with these assumptions can hence clearly be identified, while deviant results allow to draw conclusions about alternative phase separation mechanisms.

The most important factors known to affect particle formation are implemented in **Equation 16, Section 2.3.5**. Most significant among these are the supersaturation S^* as a function of the fenofibrate solubility K_{SP} as well as the interfacial energy γ_{CL} . Under standard conditions (room temperature, no excipients used) the supersaturation can be derived from the measured solubility of fenofibrate in different ethanol water mixtures (**Figure 14**). Variations can be reproduced in the model, indicating an expected rise or fall in particles size when, e.g. the interfacial energy in- or decreases.

Mixing was already shown to gradually decrease particle size under application of higher specific power inputs/flow rates (**Chapter 2**). Despite this observation still no valid conclusion about the underlying phase separation mechanism and the effectiveness of the process could be drawn. As the flow rates applied are not equal for ethanolic and aqueous phase, the organic drug solution might have been pressed to the wall of the container, thereby impairing the mixing efficiency (**Figure 21**). An approach for clarifying the effectiveness of the mixing process in terms of particle size and energy consumption is to gain a broader database. An alternative geometry of the mixing chamber was provided by using a 4-jet impinging jet reactor, which provides a more symmetric flow pattern by introducing the ethanolic drug solution from an additionally added inlet at the top of the mixing chamber.

Also changes in the sizes of the in- and outlets of the mixing chambers used provided additional information on the effectiveness of the mixing process.

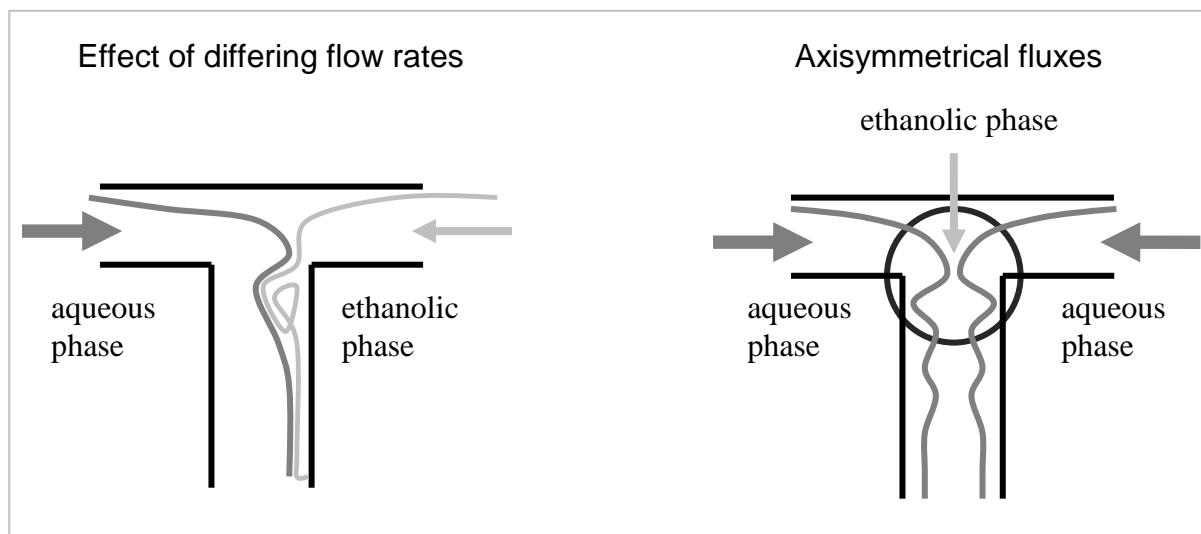


Figure 20: Proposed impact of heterogeneous flow patterns (blue = water, red = ethanolic drug solution)

Mixing effects and changes in the drug concentration can both be directly linked to resulting variations in particle size, as these factors hardly affect other process parameters.

Even more importantly, as these are more difficult accessible by experimental evaluation, the mathematical model also helps to identify in how far interfacial phenomena affect the particle size distribution. Interfacial tension is defined as the work required to increase a surface area divided by that area [91]. Lowering the interfacial tension between two phases means a reduction of the free energy and facilitates the phase separation process as less work has to be employed for creating the new surface.

Within precipitation processes, interfacial phenomena are dynamic processes, as the varying solvent composition continuously changes the interfacial tension between continuous phase and the forming precipitate. This process is best characterized by the surface tension of different ethanol water mixtures (**Figure 21**). The surface tension is the interfacial tension against air and changes upon variations in solvent composition in a comparable manner as the interfacial tension does [92]. With increasing ethanol concentration the surface- and interfacial tensions are lowered.

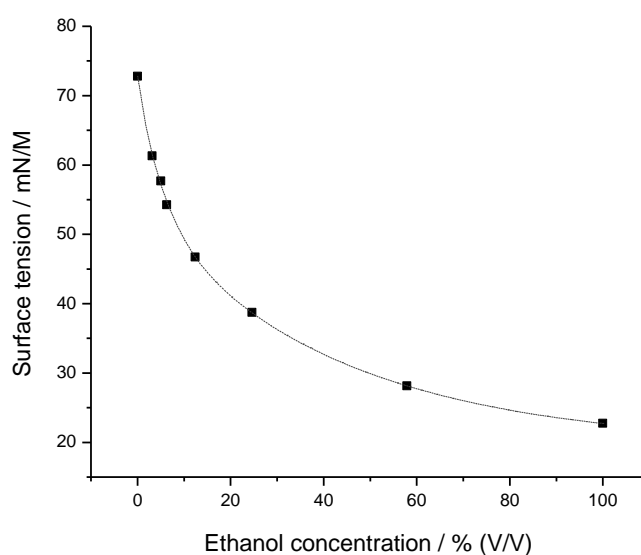


Figure 21: Surface tensions in ethanol water mixtures (modified from [93])

The interfacial tension within the precipitation process can hardly be investigated experimentally, as means varying this factor usually also affect other process parameters, e.g. the drug's solubility. This makes it hard to differentiate between the individual effects. The simulation of the precipitation process is capable to overcome this experimental drawback, as a model based variation of each of the individual parameters can be implemented independently. E.g. a different mixing regime can be superimposed to a given experimental setup with a known solubility profile, to draw verifiable conclusions about whether additional changes in interfacial tension affect the product characteristics.

Another closely related process parameter is the temperature of solvent and antisolvent. Thermoregulation in precipitation processes finds extensive industrial use and is known to have a strong impact on the resulting products [5, 48, 59]. As it significantly influences the solubility of most solutes, it is used to shift the binodal and spinodal curves and to determine the width of the metastable range for precipitation processes [94]. **Figure 22** shows a typical correlation between temperature and the corresponding particle size as it can be observed for the antisolvent precipitation of organic compounds. In the given example, the impact of the antisolvent temperature on the resulting particle size was investigated. As can be seen, particle size increases due to a solubilizing effect at elevated temperatures, which exceeds the impact of simultaneously occurring interfacial phenomena. Although interfacial effects are

known to be temperature dependent [95] the main impact on the particle size distribution is believed to be solubility controlled.

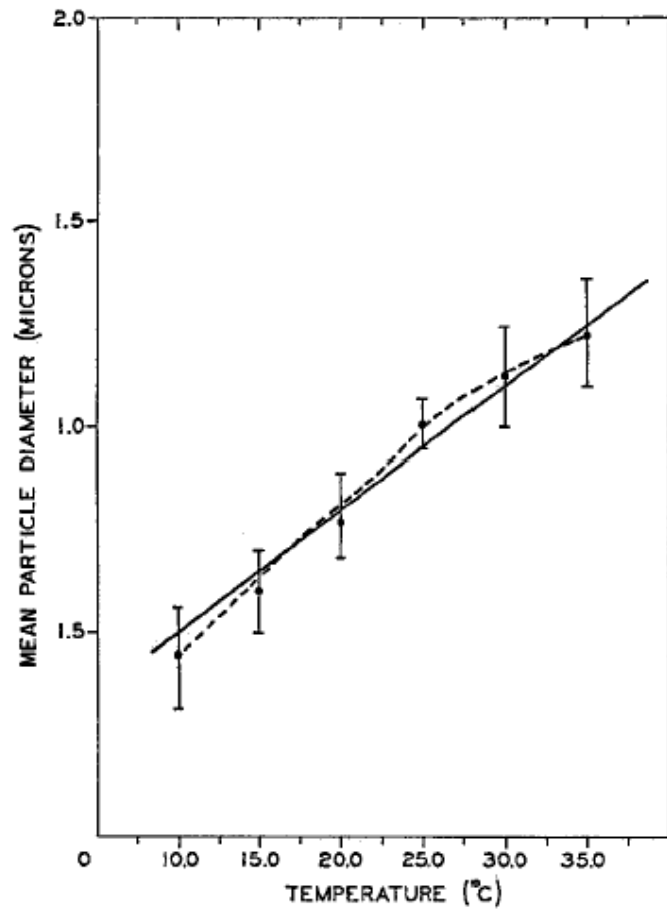


Figure 22: Particle size as a function of temperature [59]

In the following, the impact of size and shape of the mixing chamber, different flow rates as well as a series of experimental parameters affecting the solubility and/or interfacial properties of the fenofibrate dispersions are investigated. All results are critically discussed in awareness of the theoretical predictions. Conclusions are drawn about the underlying phase separation mechanisms.

3.3. MATERIAL AND METHODS

All drug solutions used contained 5% (w/w) of fenofibrate in ethanol absolute undenatured. If not pointed out elsewhere, precipitation experiments were accomplished as described under **Section 2.3.1**. The resulting particle sizes were determined by laser diffraction. For further information also refer to **Chapter 2**.

3.3.1 NON-MIXING RELATED PROCESS VARIATIONS

3.3.1.1. SOLVENT COMPOSITION

The potential influence of the solvent composition on the particle size distributions was addressed by varying the solvent to antisolvent ratio and comparing the obtained particle sizes to the estimations of the mathematical model. Therefore samples were prepared with the pumping setup at a total flow rate of 24 ml/min by using the 0.5 mm i.d. t-piece. For obtaining a specific solvent composition in the final dispersion, the flow rates of ethanol and water were varied according to **Table 1**.

Table 1: Experimental matrix for investigating the impact of solvent composition on particle formation

Ethanol content / % (V/V)	Flow rate / ml/min	
	Ethanolic fenofibrate solution	Water
1	0.25	23.75
5	1.20	22.80
10	2.40	21.60
16	2.00	10.00
25	6.00	18.00
50	12.00	12.00

3.3.1.2. INTERFACIAL TENSION

The interfacial tension between the particle surface and the surrounding liquid is a parameter expected to have a major impact on particle formation. For investigating whether changing it affects particle size to an extend in accordance with the suggestions of the mathematical model, samples were prepared by adding Tween 80 (polyoxyethylen(20)sorbitan monooleate)

to the aqueous phase used for sample preparation. Tween 80 V Pharma was obtained from Uniqema, Middleborough, United Kingdom. It was applied at concentrations ranging from 0.0005% to 5% (w/w) of the aqueous phase. This correlates to concentrations of 4 µg – 4 mg/ml in the final dispersion. With a critical micelle concentration (CMC) for Tween 80 of 14 µg/ml in water [96] and 59.0 µg/ml in a 12.7% (V/V) ethanol water mixture [97], the CMC in a 16.7% (V/V) ethanol water mixture as used for our dispersions was expected to be reached at latest by using the sample containing 0.05% Tween 80 in the aqueous phase, hence 400 µg/ml in the final dispersion. Nanodispersions were prepared at total flow rates of 60 ml/min by using a 0.5 mm i.d. t-piece.

3.3.1.3. TEMPERATURE CONTROLLED EXPERIMENTS

While experiments were generally conducted at room temperature ($23^{\circ}\text{C} \pm 2^{\circ}\text{C}$), additional experiments were accomplished under modification of the educt solutions' temperature. The temperatures of ethanolic and aqueous phase were thereby adjusted with two water baths (UKT 3, Edmund Bühler, Tübingen, Germany and Neslab RTE 111, Neslab Instruments, Inc., Newington, USA). For the aqueous phase temperatures from 1°C to 50°C were used, while the ethanolic drug solution was tempered between 20°C and 50°C . Due to the temperature dependent solubility of fenofibrate the ethanolic solution could not be cooled below 15°C as the solubility product was approached and the drug started to crystallize.

Dispersions were prepared using the 0.5 mm t-piece at a total flow rate of 60 ml/min.

3.3.1.4. DRUG CONCENTRATION

Samples were prepared by varying the drug concentration in the ethanolic phase for explicitly addressing mass density effects on particle formation. For this purpose ethanolic drug solutions were prepared containing 1, 3, 5 and 7% (w/w) of fenofibrate. Additionally a saturated drug solution was prepared by dispersing an excessive amount of drug in ethanol absolute and removing undissolved material by filtration through 0.2 µm Minisart RC 15 syringe filters (Sartorius, Göttingen, Germany). Prior to the filtration the samples had been

incubated over night. Dispersions were prepared using the 0.5 mm t-piece at a total flow rate of 60 ml/min.

3.3.2 THE IMPACT OF MIXING

Different mixing chambers were used for revealing the impact of size and shape of these devices on the particle size distribution. The first experimental set aimed on investigating the impact of the size of equally shaped mixing chambers. Besides the mixing chamber used as standard (i.d. of 0.5 mm, Klaus Ziemer GmbH, Langerwehe, Germany), further t-shaped devices were used with inner diameters of 0.15, 0.25 and 1.0 mm. The 0.15 mm i.d. Upchurch MicroTee Assy and the 1 mm Upchurch Tee Assy were both obtained from Klaus Ziemer GmbH, Langerwehe, Germany. A VICI Tee with a 0.25 mm bore was obtained from Macherey-Nagel GmbH & Co. KG, Düren, Germany. Samples were prepared by coupling the mixing chambers to 2 syringe pumps as described in **Chapter 2, Section 2.3.1**. Total flow rates of 24 and 60 ml/min were applied with a 5+1 ratio of aqueous to ethanolic phase.

As it was open whether the unequal flow rates applied for the solvents result in impaired mixing efficiency, control experiments were accomplished using custom made 4-jet impinging jet reactors prepared by the machine shop of the University of Erlangen-Nuremberg, Chair of Particle Technology. The aqueous phase was directed into these cross shaped mixing chambers from the left and right sides, while the drug solution was introduced from the top inlet as shown in **Figure 23**.

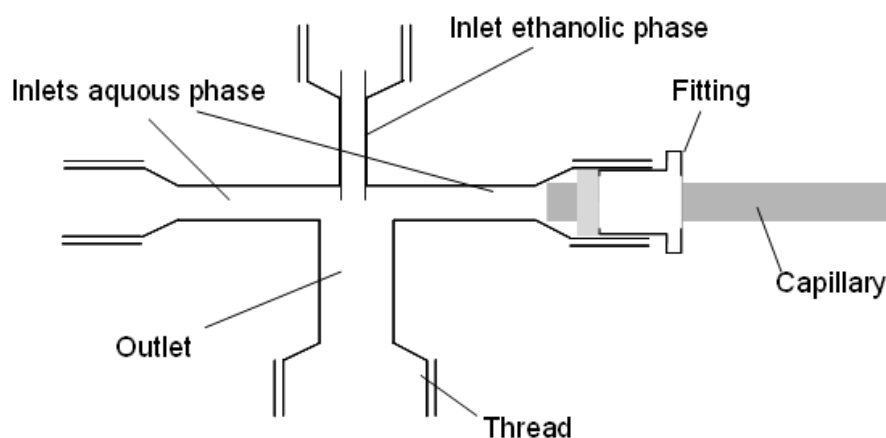


Figure 23: Mechanical drawing of the cross shaped mixing chambers used for nanodispersion preparation

Symmetrical flow conditions were obtained by splitting the flow from the aqueous phase with a PEEK t-piece inserted between the syringe pumps and the mixing chamber (**Figure 24**). A total flow rate including the flows from all three inlets of 60 ml/min was applied for sample preparation.

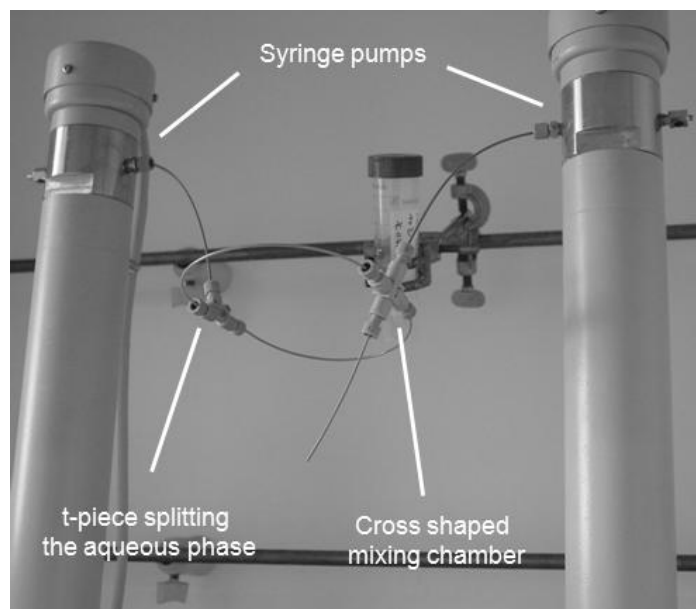


Figure 24: Sample preparation with cross shaped mixing chambers. The aqueous phase is homogeneously split by insertion of a t-piece

No experience existed on the impact of the flow pattern in each of the 3 inlets as well as the outlet of the cross shaped mixing chamber. Therefore mixing chambers with varying sizes of the inlets and outlets were fabricated for covering a wide range of potential mixing properties (**Table 2**). As for the t-pieces, all crosses were prepared from PEEK material.

Table 2: Layout of cross shaped mixing chambers used for nanodispersion preparation

	A	B	C	D
Inlet ethanolic phase / mm	0.2	0.2	0.3	0.4
Inlets aqueous phase / mm	0.5	0.3	0.5	0.5
Outlet / mm	1.0	0.6	1.0	1.0

The mixing efficiency was deduced based on particle size measurements as well as from pressure drop measurements on the differently shaped mixing chambers. Latter were accomplished using the build in pressure sensors of the syringe pumps.

3.4. RESULTS AND DISCUSSION

3.4.1 INFLUENCE OF THE SOLVENT COMPOSITION

When simulating the precipitation process by using increasing amounts of ethanol in the dispersion, the obtained data suggest that the resulting decrease in interfacial tension leads to much higher nucleation rates. In consequence smaller particles are formed. Furthermore, the fenofibrate solubility increases at elevated ethanol concentrations. A lowered supersaturation then leads to a decreased nucleation rate, and hence results in the formation of bigger particles. According to the simulations, these two countervailing processes result in an optimal ethanol concentration, at which a minimum particle size can be obtained. As not only the composition, but also the flow rate ratio between ethanol and water was changed within corresponding experimental evaluation, simulations were accomplished using varying micro-mixing times, reflecting differently intense mixing. As shown in **Figure 25**, the qualitative assumption of an existing optimized ethanol concentration was found to be widely independent from mixing effects. At increasingly fast mixing, the minimum is however shifted towards higher ethanol fractions.

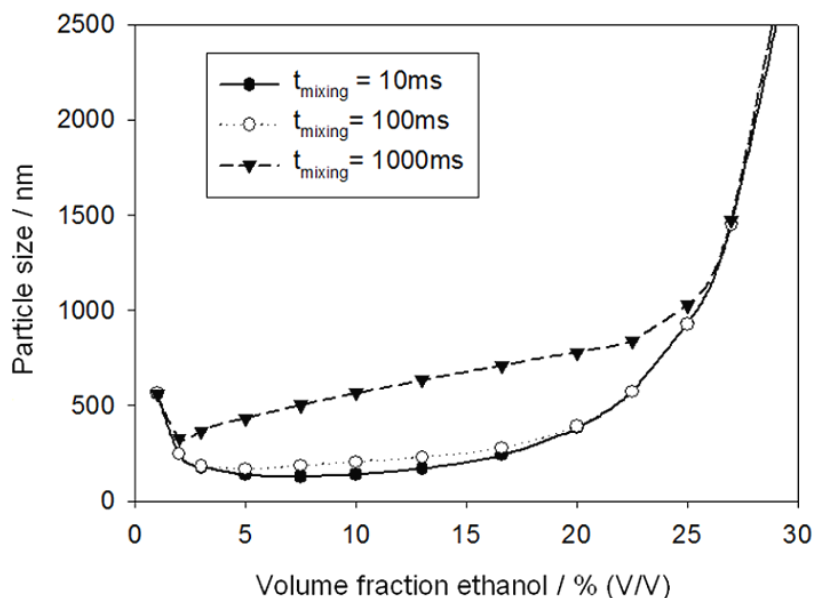


Figure 25: Influence of the solvent composition on the resulting particle size (simulation)

Within the actual preparation of fenofibrate dispersions under varying solvent compositions, the existence of a particle size minimum as suggested by the simulations could not be

confirmed. Indeed, particle size was found to increase continuously with rising ethanol content (**Figure 26**). It was concluded that interfacial events play a subsidiary role compared to the model based expectations, while phase separation mainly depends on the solubility of fenofibrate in the given solvent compositions. In addition, samples became much less stable the more ethanol was contained, immediately crystallizing upon sample preparation. Determination of the size of the primary particles was hindered by the presence of the crystals formed, as is indicated by the wide error bars.

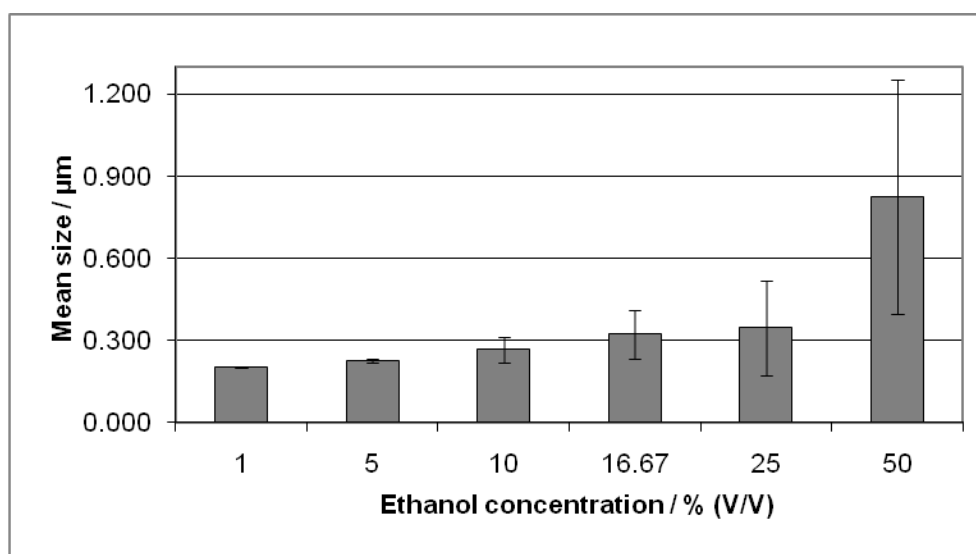


Figure 26: Experimental verification of the impact of the solvent composition on particle size

3.4.2 THE IMPACT OF INTERFACIAL TENSION

While already ethanol alone significantly lowers the interfacial tension between the dispersed and the continuous phase, even stronger effects were anticipated for the additional use of surface active reagents. Tween 80 was shown to decrease the surface tension of ethanol/water mixtures further than ethanol alone. At its critical micelle concentration Kawakami et al. measured a surface tension of ~ 39.4 mN/m, compared to ~ 46.5 mN/m in a corresponding surfactant free ethanolic water mixture (data extrapolated from [93, 97]). The ethanol concentration of $\sim 12.7\%$ (V/V) used by Kawakami is in a comparable range as the one applied in this study (16.7% (V/V)), so that similar effects on surface/interfacial tension can be expected. Due to the ethanol contained in the samples, the reduction in interfacial tension caused by the surfactant is moderate compared to pure water which has a surface tension of 72.8 mN/m [93]. Nevertheless, according to the mathematical model, a decrease in interfacial

energy by just 10% results in a rise of the nucleation rate by up to 5 magnitudes (**Figure 27**). It was expected that especially at low surfactant concentrations interfacial effects dominate the particle formation, while reported solubilization effects of Tween 80 [98] would not be relevant until elevated surfactant levels are applied. Consequently, significantly smaller particles were expected than would form without the surfactant.

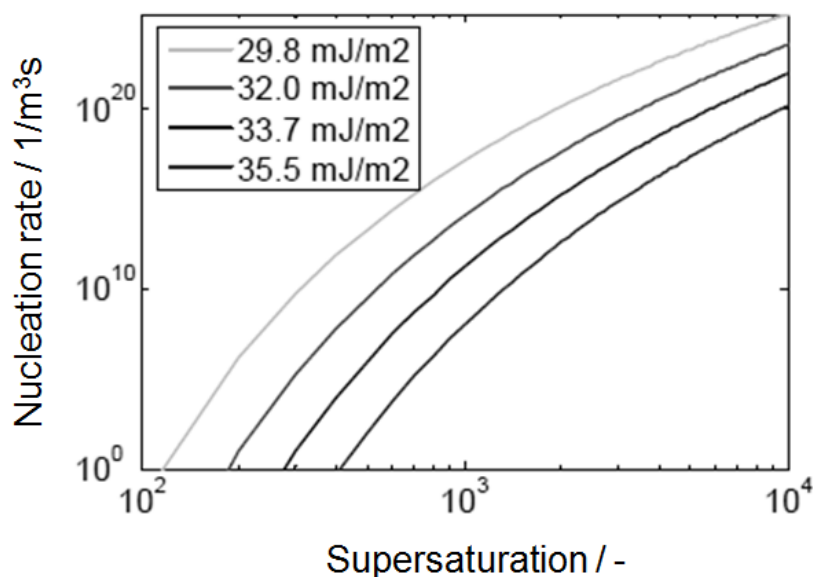


Figure 27: Influence of supersaturation and interfacial energy on the calculated nucleation rate

Compared to the mathematical model, Tween 80 indeed led to a significant particle size reduction (**Figure 28**). Nevertheless, this size reduction lacks behind the immense effects that had been expected from the calculated changes in the nucleation rate.

Experimental data revealed a drop in particle size by ~30% when using Tween 80 at concentrations reaching its expected CMC (**Figure 28**, 0.05% solution). At this Tween 80 concentration the surface of the ethanol water mixture is saturated with surfactant molecules, so that remaining Tween 80 is exclusively available for adsorbing to the emerging precipitate. Particle size reductions at lower Tween 80 concentrations were only moderate, what might be attributed to the interfacial tension lowering effect of ethanol. Only little additional size reduction can be exerted by the surfactant. Also at very high Tween 80 concentrations, only moderate further size reduction was observed. As expected, high Tween concentrations showed distinct solubilizing effects, indicated by an obviously decreasing turbidity of the dispersions prepared from aqueous phases containing 0.5% - 5% of surfactant.

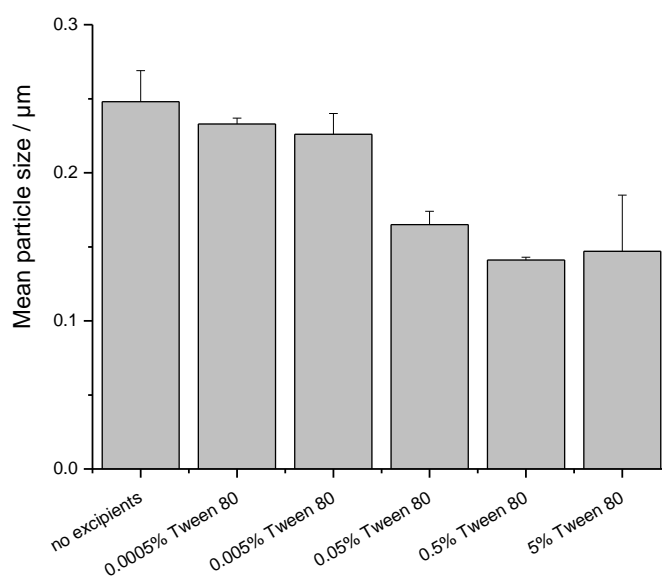


Figure 28: Effect of Tween 80 on fenofibrate particle size

3.4.3 INFLUENCE OF TEMPERATURE

Most substances, like fenofibrate, show an increased solubility at elevated temperatures. In consequence, with increasing temperature the supersaturation in the dispersion is reduced when applying equimolar drug concentrations. According to the mathematical model, lower amounts of larger particles should form due to a decreased nucleation rate.

When performing temperature controlled precipitation experiments, temperature variations only had a limited impact on particle size and size distribution (**Figure 29**). Only under the most extreme conditions applied, when the aqueous phase was cooled to 1°C and the ethanolic phase to 20°C, a slight increase in particle size was observed. At elevated temperatures only insignificant changes in particle size occurred.

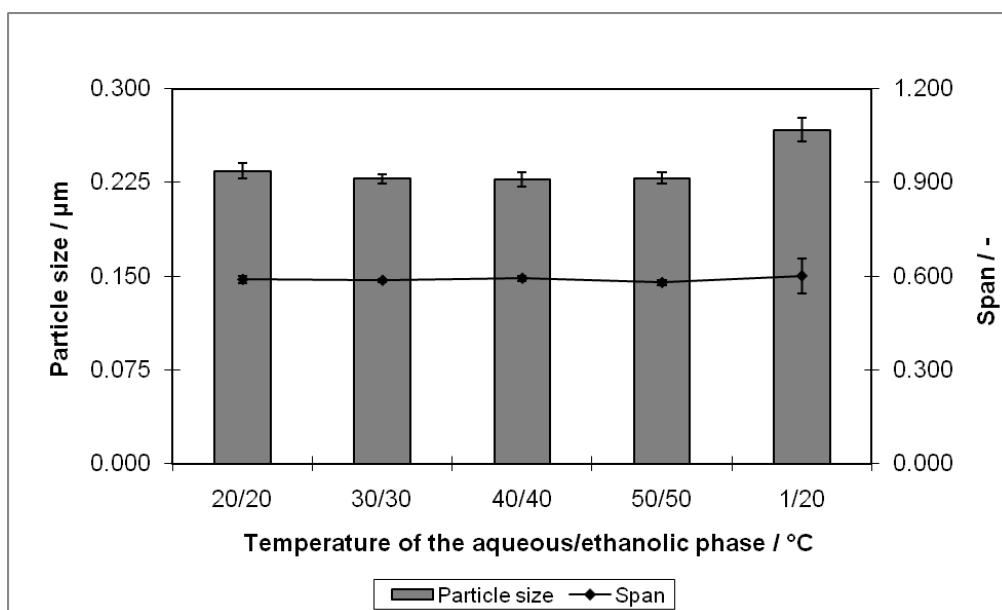


Figure 29: Dependency of particle size and polydispersity (span) on temperature

The fact that almost no changes in particle size can be observed is not only in disagreement with the precipitation model used for accomplishment for the simulations. Also other precipitation models based on heterogeneous nucleation or spinodal decomposition would suggest some change in the particle size distribution. Clearly, other effects exceeding classical phase separation theory must be superimposed to the precipitation process.

3.4.4 INFLUENCE OF DRUG CONCENTRATION

Investigating the impact of varying drug concentrations allows to exclusively monitor supersaturation effects on particle formation, as no other important process parameters are significantly affected. It hence gives the most unambiguous evidence about the underlying phase separation mechanisms. The higher the drug load is, the higher is the resulting supersaturation and the amount of precipitate formed. Simulations of the precipitation process indicate that, due to the higher supersaturation, an increased nucleation rate can be expected. In consequence, a higher amount of smaller particles would form.

For verification of the simulation data, nanodispersions containing different amounts of fenofibrate were prepared with the pumping setup. As for the temperature controlled experiments, experimental data could not confirm the model based expectations. Particle size

was found to increase gradually at elevated drug concentrations (**Figure 30**). Also the polydispersity of the dispersions increased as indicated by the span values.

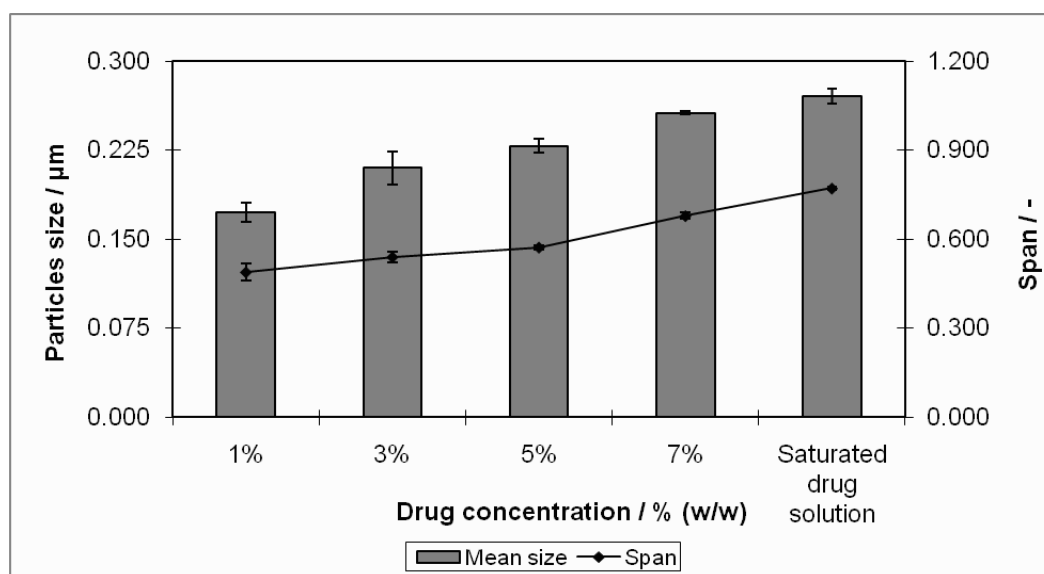


Figure 30: Dependency of particle size and polydispersity (span) on drug concentration

Considering the homogeneous appearance of the precipitate particles and the absence of agglomeration due to the high zeta-potential (**Figure 10**, **Figure 12**), the particle size distribution can be expected to be widely unaffected by ripening effects. It is evident that in the absence of other influencing factors such as interfacial effects or unpredictable changes in drug solubility, homogeneous nucleation and transport controlled growth are not the dominating factors which determine the product characteristics.

3.4.5 IMPACT OF DIFFERENT MIXING DEVICES

Using different t-shaped mixing chambers for the preparation of drug dispersions revealed that the 0.5 mm i.d. device was best suited for the preparation of the dispersions, as it resulted in small particles and narrow size distributions. Mixing chambers having smaller bores were found to be rapidly blocked within sample preparation. The 0.25 mm i.d. t-piece allowed at least for the preparation of sufficient amounts of dispersion for accomplishing particle size measurements, while the 0.15 mm i.d. device immediately showed strong accumulation of

solid drug at the outlet of the mixing chamber. This blockage is surprising, as the diameter of the mixing chamber is at least 600 to 1000 times bigger than the mean particle size.

Comparing the t-shaped mixing devices suitable for sample preparation, particle size became smaller the smaller the mixing chambers were (**Figure 31**). While this effect is insignificant at very high flow rates, the impact of the mixing device was more pronounced at the intermediate flow rate of 24 ml/min. Nevertheless, even when using the smallest possible t-piece at the highest flow rates, the particle size could not be decreased under a minimum value of about 250 nm. This size lacks behind by the order of a magnitude to the particle sizes anticipated under consideration of the energy consumption within the process.

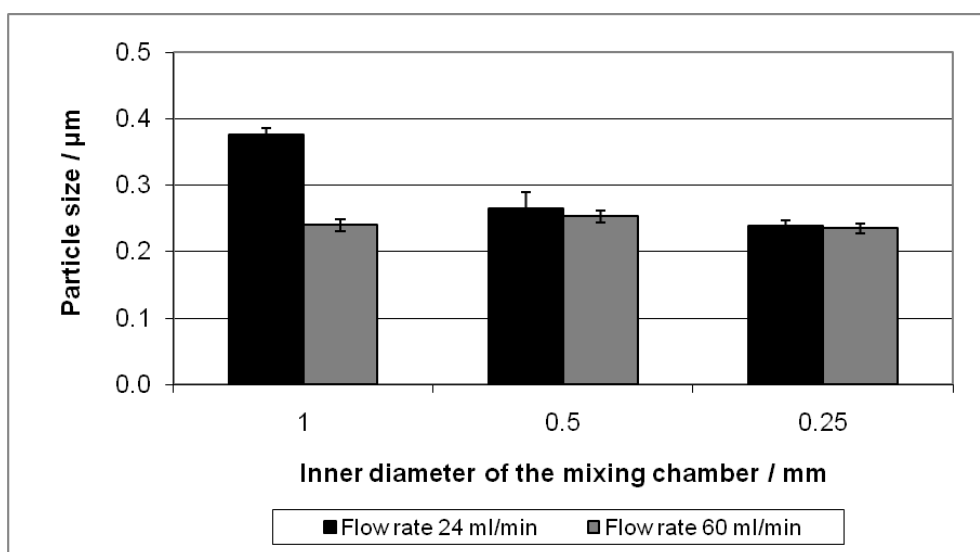
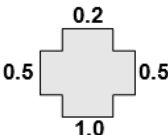
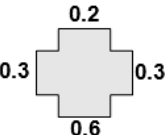
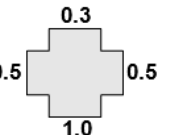
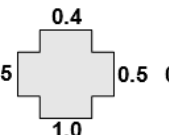


Figure 31: Preparation of fenofibrate nanodispersion with differently sized t-shaped mixing devices

The application of the unequal flow rate ratio of 1+5 for the ethanolic and aqueous phases was thought to be a potential reason for the fraction of µm-sized particles obtained. By splitting the aqueous flow and introducing the ethanolic phase from a third inlet on top of the device, a more effective blending of aqueous and ethanolic phase was expected. However, when preparing drug dispersions using cross-shaped mixing chambers, none of them showed an improvement in terms of further particle size reduction. Those 4-jet reactors having wide inlets for the ethanolic phase even showed particle sizes about 60 nm bigger than the 0.5 mm i.d. t-piece (**Table 3**). Latter effect might be attributed to a more turbulent flow profile in the mixing chamber.

Also energy dissipation was in a comparable range for the crosses and the 0.5 mm i.d. mixing chamber. It was found to be mainly effected by the width of the outlet of the mixing chamber.

Table 3: Comparison of mean particle size and energy dissipation of 4-jet impinging jet reactors and a 0.5 mm i.d. t-piece

Diameter mixing chambers / mm					
Pressure loss upon mixing / bar	1.5	2.0	1.2	1.3	1.4
Average particle size / μm	0.258	0.253	0.315	0.313	0.251
STDEV particle size	0.003	0.003	0.008	0.011	0.007

In conclusion, the flow rate dependency of particle size could be confirmed to be independent of the size and shape of the mixing chamber. Especially the t-shaped mixing devices are very well suited for the highly effective preparation of nanodispersions. Optimal mixing conditions are obtained, resulting in a small sized and homogeneous precipitate. Although neither the size or shape of the mixing chamber, nor the flow rates applied allowed to undercut the experimental particle size limit of ~ 250 nm, phase separation was clearly effected by hydrodynamic effects; particle size and size distribution became smaller upon intensifying mixing.

3.4.6 INTERPRETATION OF THE EXPERIMENTAL DATA

Comparison of the experimental data and the simulations accomplished based on homogeneous nucleation and transport controlled growth showed an overall unsatisfying correlation. Especially an increase in particle size upon application of higher drug loads is in

contradiction to nucleation based particle formation. Using Tween 80 within the precipitation process revealed that phase separation was much less effected by interfacial effects than would have been expected. Furthermore, the fact that in the surfactant free formulations particle size could not be decreased below 250 nm and the existence of endemically contained particles in the low μm -range question the idea of nucleation based phase separation.

Although generally considered unlikely for the phase separation of small molecules, spinodal decomposition represents a plausible explanation for the observed results. Within spinodal decomposition a random precipitate pattern is created, from which subsequently particles are formed by the interplay of thermodynamic, hydrodynamic and friction effects. Assuming spinodal decomposition for the given experimental setup, the spatially varying energy dissipation within the mixing chamber leads to a less effective breakup of the materializing precipitate as soon as the drug concentration is increased. The result is a rise in the average particle size as well as the particle size distribution. In agreement to that, the intensification of the mixing process led to a remarkable particle size reduction. Hydrodynamic effects can reach from macroscopic vortices down to the size of the Kolmogorov eddies, which in the given setup range from approximately 0.9 μm to 6 μm (refer also **Chapter 2**). Further size reduction can only be obtained by friction effects inside the system, which is summarizing referred to as viscous dissipation. Viscous dissipation is the rate at which the kinetic energy in turbulent flows is converted by viscous stress into thermal energy. Upon amplification of the mixing intensity and at elevated flow rates this effect becomes more prevalent [99]. As in a mortar, viscous dissipation is capable to break down the spatially extended precipitate to sizes distinctly smaller than the Kolmogorov scale [75, 100, 101]. A major reason for the obvious accessibility of the precipitates formed by spinodal decomposition is the fact that these primarily do not have a distinguishable interface to the surrounding medium. Such interfaces form within the phase separation process, simultaneously to the hydrodynamical shaping of the precipitate. Until completion of this confinement the precipitate is hence very sensitive to external triggers applied by the mixing process. The interplay of hydrodynamical effects and viscous dissipation define the final particle size distribution.

The particle size reduction observed upon addition of Tween 80 to the aqueous phase is in good agreement with the theory of spinodal decomposition. Upon phase separation, first a spatially poorly defined precipitate is formed, which subsequently assumes a defined shape

by forming distinct interfaces to its environment [102]. Adsorption of surfactant to these interfaces can stabilize them already early within the phase separation process. A decrease in interfacial energy occurs, so that under introduction of the same energy to the system smaller particles with an increased surface area are obtained.

While spinodal decomposition proves to be in good agreement with the experimental results discussed above, this phenomenon alone is not sufficient for explaining the impact of solvent composition and temperature on the precipitate. As observed in the context of concentration dependent changes in particle size (**Section 3.4.4**), a spinodal precipitate is expected to depend on the volume of the precipitate formed. When, due to an increase of temperature or ethanol concentration the solubility of fenofibrate increases, less precipitate forms. Smaller particles would be expected due to a facilitated hydrodynamic and viscous breakdown of the forming precipitate. For temperature controlled experiments, indeed an increase in particle size is observed when decreasing the temperature of ethanolic and aqueous phase below room temperature, so that higher amounts of precipitate form. Why particle size remains constant at elevated temperatures and why it increases at elevated ethanol concentrations (**Section 3.4.1**) cannot be terminally concluded based on the experimental results described here and will be discussed in detail in **Chapter 1**.

3.5. CONCLUSIONS

Comparison between the simulations of the precipitation process and experimental data allowed for identifying spinodal decomposition as the dominating phase separation process. Spinodal phase separation was found to mainly depend on the volume of precipitate formed, as was shown by the fact that particle size increased upon application of elevated drug loads. In addition, the finally obtained particle size distribution is strongly influenced by the transition of the spinodal phase separation product to a particulate precipitate. In the underlying shaping process hydrodynamic and friction effects were found to play a key role, while interfacial effects have a less pronounced impact than would have been expected for homogeneous nucleation as alternative phase separation mechanism. However, also spinodal decomposition as solely phase separation mechanism fails to explain all of the observed phenomena. The missing impact of temperature changes and the increase in particle size when increasing the solvent to antisolvent ratio reveal that phase separation is superimposed by additional mechanisms.

Chapter 4. Structural Characterization of the Precipitate

4.1. ABSTRACT

In **Chapter 2** and **Chapter 3** it was shown how comparison of experimental data and mathematical modeling of the precipitation process allowed to gain a better understanding of the different factors influencing the particle formation process. However, only little information could be gained about the physical properties of the drug particles. Rapid crystallization and light-microscopical observations using cross-polarized filters indicate their non-crystallizing state, but this thermodynamical instability also impaired further detailed analysis. For the experiments described below, sample preparation was optimized in a way allowing particle analysis in an environment as close as possible to that in the original drug dispersions. Scanning electron microscopy showed that particles in the submicrometer range had a homogeneous structure and were most likely amorphous. Sample analysis under varying solvent composition was possible by using wide-field fluorescence microscopy, and allowed detailed insight into dynamic structural variations of the particles. The prevalent opinion that demulsification products obtained from antisolvent precipitation are crystalline or amorphous solids could not be confirmed. In opposite, fenofibrate was found to phase separate as a liquid, gel-like precipitate. Extension of the experiments to atomic force microscopy (AFM), as well as the comparison to further drugs clearly showed that the liquid-liquid phase separation of fenofibrate is not an exception, but can be regularly observed for a wide variety of solutes in antisolvent precipitation. This awareness casts a new light on the investigated phase separation process and facilitates data interpretation for the results obtained concerning the process characterization. After all, the data presented in this chapter allow for a more specific understanding of the impact that certain process parameters have on the precipitates.

4.2. INTRODUCTION

When screening the scientific literature for “antisolvent precipitation”, the vast majority of citations deal with the formation of solid particles. Concerned are not only experimentalists, but to the same extend researchers dealing with the theoretical background and modeling of the corresponding phase separation processes. The precipitation products are found to be either amorphous [56, 103], or consist of varying amounts of crystalline polymorphs [104-107]. Depending on the physical state of the material, the type of salt or the particle size, different dissolution profiles and bioavailabilities can be obtained.

However, considering the thermodynamical background of phase transitions, the formation of a solid precipitate represents only one part of the truth around precipitation processes. Unrecognized by many researchers, besides multiple solid polymorphs, for many substances also a liquid derivate exists. As early as 1897 Wilhelm Ostwald developed his famous rule of stage, describing a systematical order in the occurrence of phase separation products within a precipitation process [108]. Ostwald found, that phase separation preliminarily occurs under the manifestation of the phase with the highest possible Gibbs free energy. For substances following Ostwald’s rule, this phase often is a liquid or oil like precipitate.

The fact that Ostwald’s rule is not universal is nowadays well known. Many substances, especially those with strong intermolecular interactions will bypass the liquid state and directly phase separate as a solid. Reasons therefore are mainly considered kinetical and are extensively discussed in [109]. Whether direct liquid-solid or an intermittent liquid-liquid phase separation occurs is not always obvious, as the liquid state of a precipitate is, due to its thermodynamical instability, often very short lived. In most cases rapid transformation into thermodynamically more stable (solid) forms, e.g. different polymorphs, occurs. However, there are also examples where no crystallization at all is observed and the precipitate remains in its liquid state for weeks or even months [110, 111].

The most realistic impression about the mechanistical background of phase separation processes is probably provided when reviewing the field of crystallization technology. In this sector structural homogeneity of a crystal is often a key factor. Crystallization processes are in consequence carried out slow, aiming on the highest possible product quality and reproducibility. The precipitates are comparably big in size, often in the elevated μm -range, what makes them accessible to direct visual characterization. In combination with a distinct

focus on structural analysis, the likeliness of identifying the occurrence of an intermediate liquid precipitate is higher than for more rapid precipitation processes aiming on amorphous and/or nanoscopic products. Consequently, oiling out, as liquid-liquid phase separation is also called, is considered a regularly observed “problem” in crystallography. It is known to slow down crystallization and impair product homogeneity and reproducibility. Despite this awareness, the pressing interest in gaining a deeper understanding of liquid-liquid phase separation is not even closely reflected by the amount of corresponding research activities [112].

The described mismatch in the knowledge of alternating phase separation processes might at least partly be ascribed to a lack of analytical techniques addressing specimen on the nanoscale. Measurement techniques for bulk materials such as X-ray powder diffraction, Raman spectroscopy or nuclear magnetic resonance are inappropriate for investigating the required nanoscopic structural properties [113]. The target size ranges for some of the most popular particle characterization techniques used in laboratory routine are summarized in **Figure 32**. Although the nanoscale is widely covered by an array of different methods, structural information beyond “just” particle size is hardly accessible. Only AFM, above an already elevated size cut-off also light- and fluorescence microscopy, are indeed capable to distinguish between an amorphous particle or an equivalent droplet. Also electron microscopy is only in rare cases capable to distinguish between solid and liquid samples, as these usually need to be dried or frozen before use. Within the drying process sample solidification can occur. Spectroscopic techniques as dynamic and static light scattering as well as light blockage, the techniques probably most often used in colloidal carrier laboratories, are completely inappropriate with respect to this purpose.

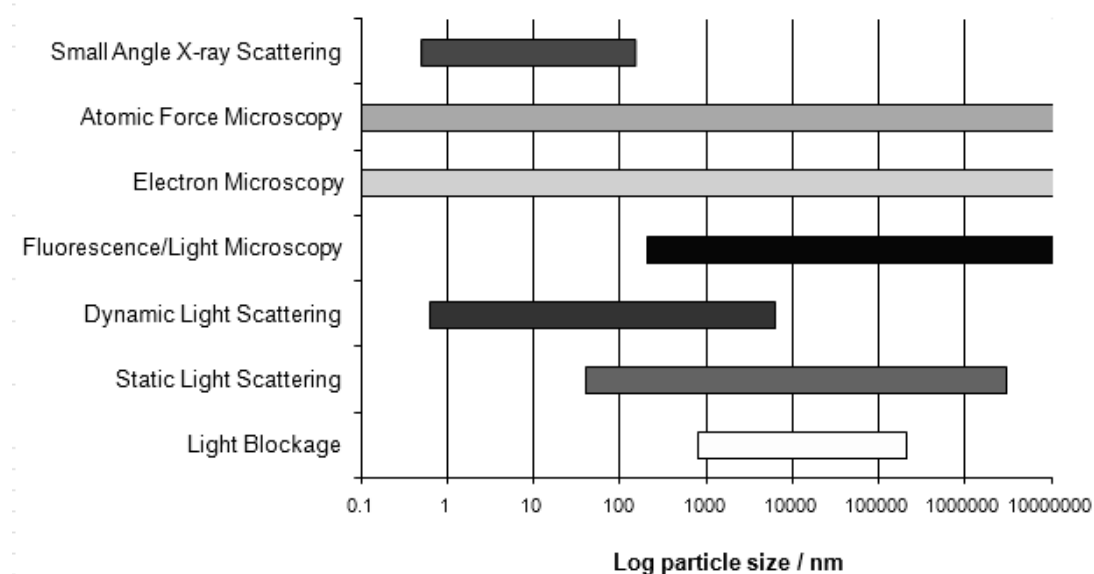


Figure 32: Standard particle characterization techniques

In addition to the analytical challenges, liquid precipitates are not uniform in structure and viscosity. In the literature they are referred to as oil, gel, intractable gum or tar [114]. The border distinguishing between liquid and solid precipitate is fluent. Concerning their mechanical properties, the solute rich phase resembles closest the characteristics of a supercooled liquid [115]. Such precipitates can contain varying amounts and kinds of solvent/antisolvent, which for some systems account for the major part of the constituents. They are known to act as plasticizers in amorphous materials [115] and are capable to distinctly modify their structural characteristics. Often liquid-liquid phase separation is observed in antisolvent processes where semipolar organic solvents as methanol, ethanol, acetone or ethyl acetate are applied [8, 116-121]. For such systems the precipitates typically contain only ~40-70% (w/w) solute. The remaining phase consisted of complexed antisolvent (~7-24% (w/w)) and even more importantly solvent molecules (20-35% (w/w)) [8, 117, 120]. The liquid precipitate is hence connected to its environment via a complex set of intermolecular interactions.

Generally, liquid-liquid and liquid-solid phase separation underlie the same general principles [5, 8, 117]. In both cases demulsification can either occur due to nucleation and growth or due to spinodal decomposition. Interfacial properties and the degree of supersaturation hence determine the outcome of the phase separation process. Nevertheless certain differences exist

between both cases that are fundamental for understanding solubility, stability and downstream processing of dispersions. As will be shown in the following, in the case of fenofibrate observed deviations from the expectations result from the fact that the drug did not phase separate as a solid as had been anticipated, but as a liquid precipitate. In addition to agglomeration, the liquid precipitates are affected by coalescence and mechanical breakup of the particles. In this context also the viscosity of the dispersed phase is a key factor, as it might trigger the potential effects of hydrodynamic and viscous stress on particle breakup [75]. Also solvent complexation plays an important role in liquid-liquid phase separation, and is indeed one of the reasons referred to for explaining its wide prevalence. Often substances with low melting point tend to phase separate as a liquid, as these can frequently underlie critical melting point reduction due to solvent complexation [111].

In this chapter the mechanical properties and the internal structure of the fenofibrate particles are discussed. The impact of the composition of the surrounding continuous phase is evaluated. For comparison, additional experimental data were acquired from the lipophilic drugs lopinavir and loratadine. The obtained data allow for new insights on the phase separation process.

4.3.2 SCANNING ELECTRON MICROSCOPY

Scanning electron microscopy (SEM) was applied for structural analysis of the fenofibrate dispersions. Experiments were accomplished using alternatively a JSM-6500 F (Joel, Ebersberg, Germany) or an ULTRA 55 (Carl Zeiss NTS GmbH, Oberkochen, Germany) field emission scanning electron microscope. The dispersions investigated were prepared as described in **Chapter 2, Section 2.3.1** and **Chapter 3, Section 3.3.1.1**, reflecting the characteristics of samples prepared under defined flow rates and containing defined ethanol to water ratios. Some SEM images were accomplished with the undiluted dispersions as positive control. Most specimens were however diluted about 1:300 to 1:3000 for being capable to investigate individual particles. The dispersions were transferred to SEM carbon pads and dried over night under vacuum in an exsiccator. If available, samples were sputtered with carbon for increasing sample conductivity and reducing the thermal stress applied on the fenofibrate particles.

4.3.3 ATOMIC FORCE MICROSCOPY

Force-distance (f-d) measurements were accomplished from fenofibrate, loratadine and lopinavir dispersions using a Veeco CP-II atomic force microscope (Veeco Instruments, Santa Barbara, USA). For sample preparation about 80 μl of a 5% (w/w) ethanolic drug solution was placed on a freshly cleaved 9.9 mm diameter pelco mica disc (Ted Pella Inc, Redding, USA). The drugs were precipitated by addition of double distilled water. The supernatant was stepwise removed and replaced with additional water until a clear solution was obtained. Measurements using undiluted dispersions were not possible due to light scattering effects of the particles, which strongly attenuated the laser signal intensity. All measurements were accomplished under water using a MicroCell[®] (Veeco Instruments, Santa Barbara, USA) for avoiding drying and crystallization of the samples. Evaporated water was replaced from time to time if necessary. Measurements were accomplished by using Veeco-MLCT silicon nitrile cantilevers with a spring constant of 0.5 N/m. The sample particles were located on the sample holder with the built in optics of the on-axis microscope (5:1 zoom, 10 x objective). The cantilever was placed above the sample particles and aligned between laser and detector (**Figure 34**). Depending on the elasticity of the sample, the bending of the cantilever was recorded and the linear part of the force distant curves was analyzed.

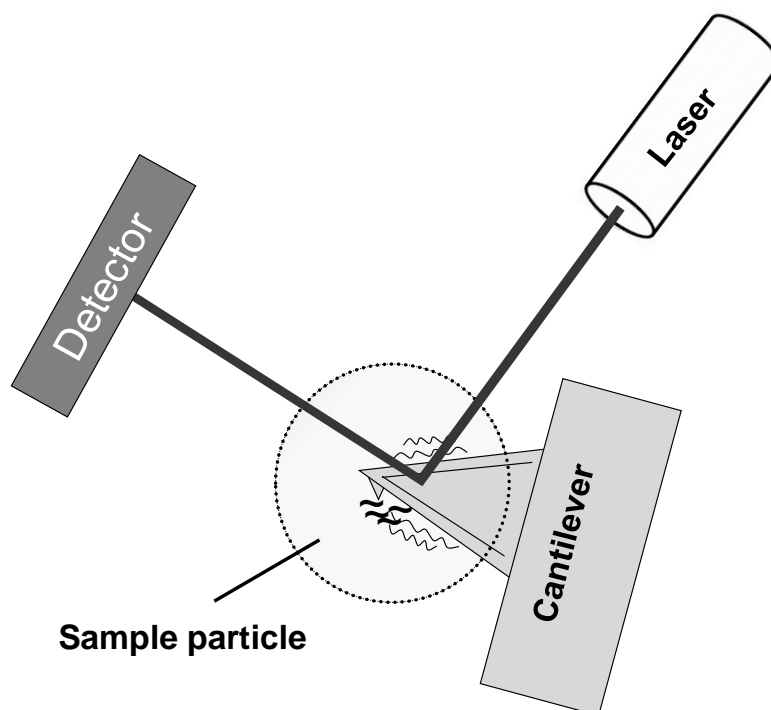


Figure 34: Schematic illustration of AFM force-distance measurements

For calibration, measurements were accomplished on blank mica. The height of the particles was estimated using the position of the cantilever when the first signal was recorded by pressing on a particle, compared to the height of the mica sample holder. AFM measurements were accomplished using freshly prepared dispersion of fenofibrate, lopinavir and loratadine, as well as a crystallized fenofibrate dispersion serving as control for a hard sample. The crystalline fenofibrate sample was prepared by ageing a fenofibrate dispersion over night at room temperature. For each sample about 10 measurements were accomplished with differently sized particles as well as 5 background measurements on the mica surface. Data was analyzed using the linear part of the extension (contact) curve of the cantilever, from which the spring constants of the cantilevers were subtracted. The extension curve represents best the elasticity of the sample. The curves were fitted linearly (loratadine, lopinavir, crystalline fenofibrate) or by an exponential function (fenofibrate). Graphs linearly fitted resembled an elasticity modulus of 1 N/m with standard deviations between 3% and 6%. The exponential fitting for the fenofibrate results had a R^2 value of 0.9320.

4.3.4 WIDE-FIELD FLUORESCENCE MICROSCOPY

Wide-field fluorescence microscopy images of fenofibrate dispersions were recorded with an Eclipse TE200 epifluorescence microscope with a high numerical aperture oil-immersion objective (Nikon Plan Apo 100 x 1.4 N.A. oil, Nikon GmbH, Düsseldorf, Germany). The samples were excited at a wavelength of 633 nm using a He–Ne gas laser with an intensity of 0.25 kWcm^{-2} , or at 532 nm using a diode-pumped solid state laser (DPSS) with an intensity of 0.20 kWcm^{-2} (Cobolt Samba TM Laser, cw, 100 mW LAB, *Cobolt*, Stockholm, Sweden). The fluorescence signal was detected with a back-illuminated electronmultiplying charge-coupled camera in frame transfer mode (Andor iXon DV897, 512x512 pixels, Andor Technology Plc. Berlin-Adlershof, Germany). Incident laser light was blocked by a dichroic mirror (640 nm cutoff) and a bandpass filter (730/140 for the He-Ne gas laser and 675/250 for the DPSS, all AHF Analysentechnik AG, Tübingen, Germany). To record wide-field microscopical movies of the samples, cycle times between 0.0161 and 0.41682 sec per frame were used. A typical movie contained 1000 frames.

The use of the Andor iXon DV897 camera allowed for a temporal resolution of 40 ms, enabling the monitoring of rapid structural changes. The spatial resolution of the images was limited by the pixel-size of 123 nm.

4.3.5 CONFOCAL FLUORESCENCE SPECTROSCOPY

Fluorescence spectra of freshly prepared fenofibrate dispersions as well as the crystalline drug were acquired for investigating whether the fluorescence signals recorded by wide-field fluorescence microscopy were derived from a liquid precipitate, crystalline material or potential impurities. The fluorescence spectra were recorded using a prism-CCD spectrometer (EEV 1300/100-EMB-chip, Princeton Instruments, Trenton, New Jersey, USA) attached to a ZEISS LSM410 confocal laser scanning microscope (Carl Zeiss Imaging Solutions GmbH, Munich, Germany). Light source was a diode pumped cw solid-state laser (DLSOT-50, Soliton Laser und Messtechnik GmbH, Gilching, Germany) with a wavelength of 532 nm. The fluorescence light was collected using a high NA oil-immersion objective (Zeiss Plan Apochromat 63x/1.40 oil) and separated from the excitation light with a combination of a dichroic (HQ 545LP, AHF Analysentechnik, Tübingen, Germany) and a bandpass filter (675/250, Chroma Technology Corp, Bellows Falls, Vermont, USA).

ibidi μ -slides (ibidi GmbH, Martinsried, Germany) were used as sample vessel, in which the dispersions were filled directly after preparation. Details of the setup were described previously [122]. Measurements were accomplished with an undiluted ethanolic solution containing 5% (w/w) of fenofibrate or with dispersions freshly prepared by manually mixing the ethanolic drug solution with highly purified water in a 1+5 ratio. The crystalline fenofibrate sample was prepared by ageing a fenofibrate dispersion over night at room temperature. Spectra of the crystalline drug were accomplished directly on the crystals, which were located on the bottom of the ibidi μ -slides by using the ZEISS LSM410 microscope.

4.3.6 LIGHT MICROSCOPY

For light microscopical observations specimens were prepared under as mild mixing conditions as possible, for not breaking down the precipitate structures below a microscopically observable size range. Therefore ethanolic drug solution and water were blended by slowly pipetting one to the other or by directly mixing them on the microscope slide. Images were recorded directly after sample preparation using a Nikon Labophot light microscope equipped with a JVC digital camera (Model JVC TKC 1380E, Nikon GmbH, Düsseldorf, Germany). Crystallization of the samples was monitored using crossed polarized filters.

4.4. RESULTS AND DISCUSSION

4.4.1 SCANNING ELECTRON MICROSCOPY

Samples prepared by using undiluted fenofibrate dispersions gave a general overview about the dispersions' structure and makeup. **Figure 35** shows a droplet of undiluted suspension prepared by hand-mixing (pipetting) ethanolic and aqueous phase. In the middle potentially amorphous particles are shown, while the dispersion started to crystallize from the rim. Fenofibrate crystals typically had a rhombic shape. When observed in dispersion by light microscopy also cross shaped or five branched structures were observed. On the SEM samples, the presumably amorphous particles were found to be round and embedded in a layer of previously dissolved debris. They consisted of dried precipitate.

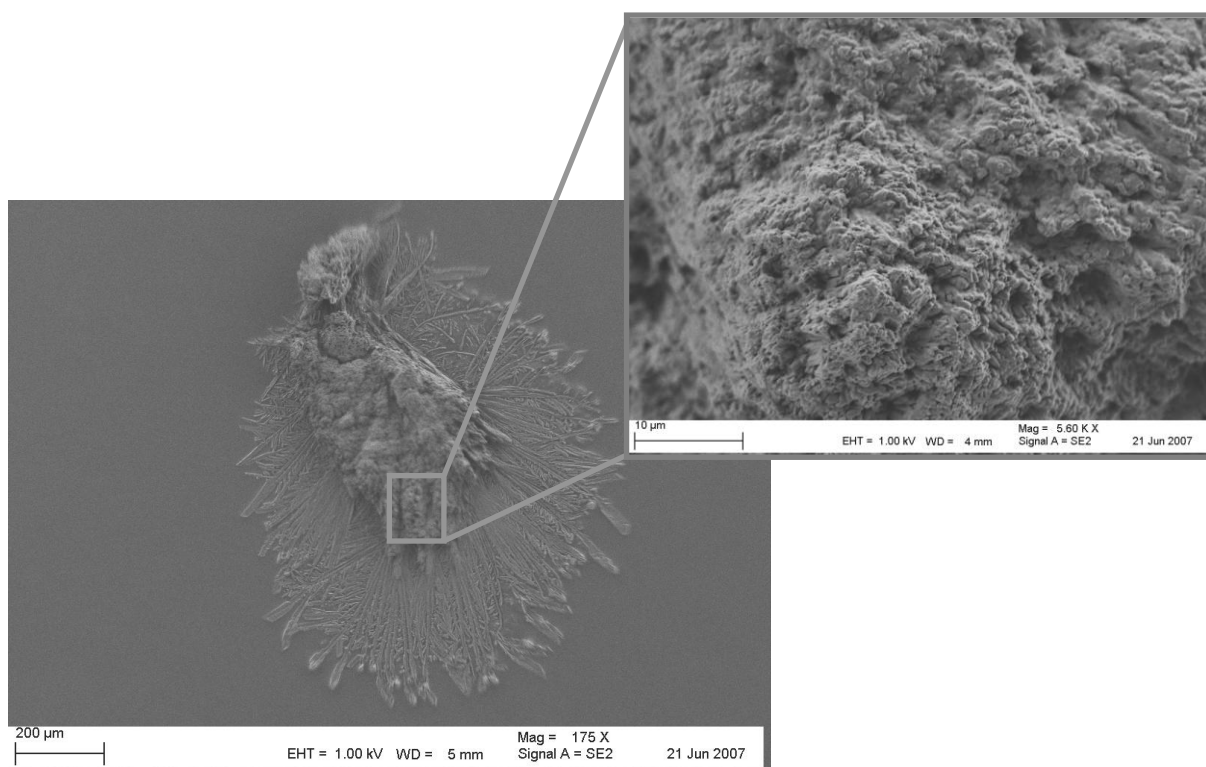


Figure 35: SEM sample prepared from an undiluted fenofibrate dispersion containing 16.7% (V/V) ethanol, mixed by hand, unsputtered sample

In all samples, both crystalline and amorphous material showed a strong tendency to melt once hit by the electron beam of the microscope (**Figure 36**). Potentially amorphous particles darkened starting from the particles' centre. Degradation was so fast, that especially for

unsputtered samples hardly enough time remained for focusing the electron beam on the sample before the particles cleared out. Crystalline material was more resistant, requiring higher working voltages for melting the material. This is a clear indication of the precipitates' thermodynamical instability compared to the crystalline state of the drug. A test measurement performed using transmission electron microscopy for getting a higher resolution and detecting potential nanocrystallites failed, as the particles instantaneously disappeared even at the lowest possible working voltage of 80 kV.

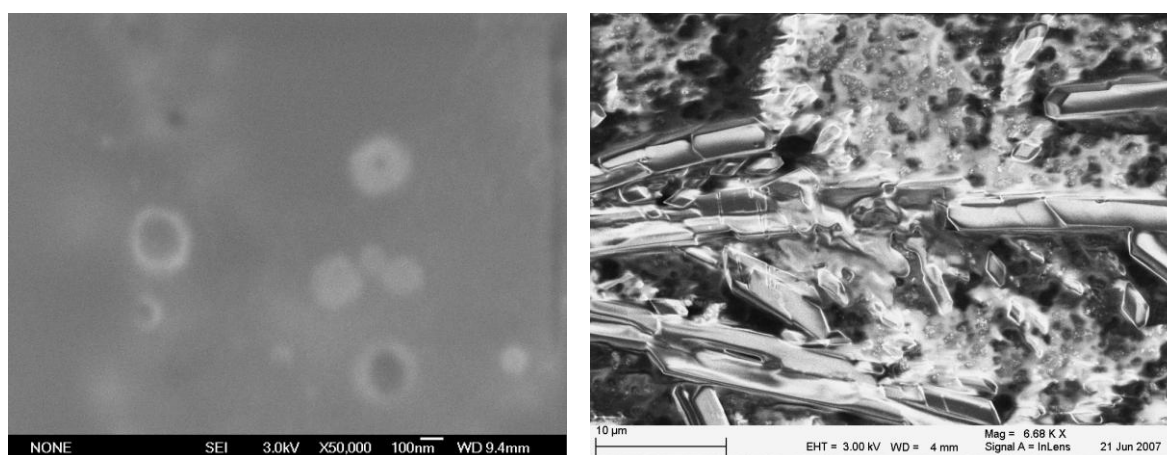


Figure 36: Melting of amorphous (left) and crystalline (right) particles in the electron beam. The samples were prepared with the pumping setup at a total flow rate of 24 ml/min. The ethanol concentrations in the dispersions were 50% (V/V) (left) and 16.7% (V/V) (right)

The investigation of isolated particles was facilitated by sufficiently diluting the dispersions prior to sample preparation. The particles typically had a homogeneous appearance without a distinguishable inner structure or surrounding shell (**Figure 37**). Particles were in the same size range as observed by laser diffraction, with small particle fractions in the low μm -range and down to sizes of about 20 nm. While the particle size distributions were inhomogeneous between different sample spots, the structure of the particles was comparable for all samples, independent from the process conditions applied (e.g. varying ethanol concentrations/flow rates).

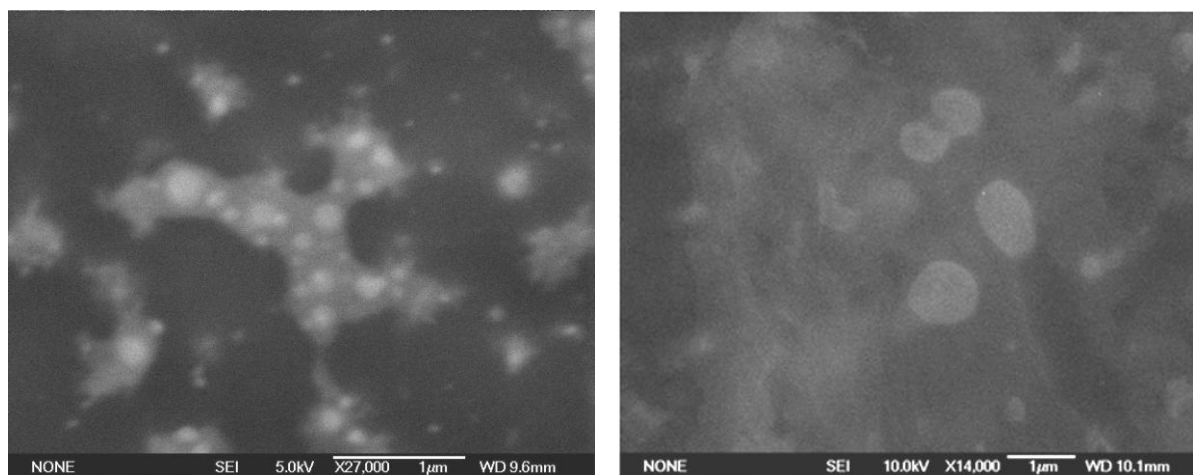


Figure 37: Fenofibrate particles embedded in layers of solvent debris. Particles appear homogeneous without an internal structure. The samples were prepared at total flow rates of 12 ml/min (left) and 24 ml/min (right). The ethanol concentrations in the dispersion were 16.7% and 50% (V/V)

4.4.2 ATOMIC FORCE MICROSCOPY

Force-distance measurements were accomplished for investigating the mechanical properties of the fenofibrate precipitates. For comparison, measurements were extended to the poorly soluble compounds loratadine and lopinavir.

Figure 38 shows the correlation between particle size and the corresponding elasticity moduli derived from f-d measurements. Crystalline fenofibrate, loratadine and lopinavir showed elasticity moduli around 1 Nm^{-1} with a slight tendency towards lower elasticity moduli at increasing particle size. This means that these samples had an elasticity in the same range or even below that of the cantilever used. As the cantilever deformed stronger than the sample did, no further mechanical differentiation between the samples was possible.

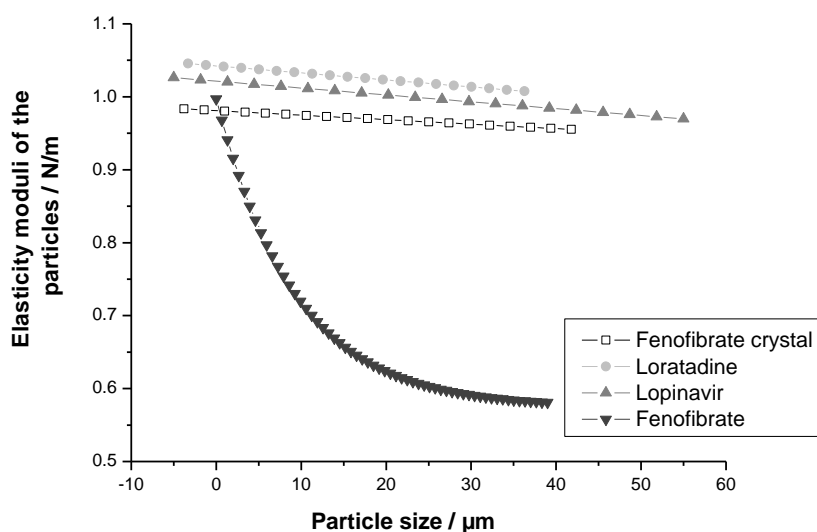


Figure 38: Elasticity of the precipitate vs. particle size. Smaller fenofibrate particles were found to have higher spring constants, meaning they appear to be harder to their environment than bigger particles

In contrast, the fenofibrate precipitate was found to be much easier deformable, and showed a strong dependency of its elasticity moduli on particle size. In fact, the particles' elasticity increased exponentially corresponding to the reciprocal particle radius, thereby satisfying the La Place equation (**Equation 21**, [123]). The equation states that at constant surface tension, the elasticity of a specimen decreases at smaller particle sizes. Smaller samples appear to be harder. Originally developed for describing the pressure differences across curved gas-liquid interfaces, the La Place equation was found to also apply to liquid-liquid systems [124].

Undetectable by laser diffraction, PCS or SEM, the AFM measurements proved that fenofibrate particles were liquid rather than consisting of solid amorphous material as might have been anticipated. As described by the La Place equation, only when reaching sufficiently small particles sizes, the precipitate particles approach the mechanical properties of a solid. Nevertheless, the composition of the precipitate was expected to be comparable for all particle sizes.

$$\Delta P = P_d - P_a = \frac{2\gamma}{r}$$

Equation 21

Loratadine and lopinavir samples were found to be much harder compared to the fenofibrate precipitate. Nevertheless, also these particles had a round shape, lopinavir even formed stream like structures on the sample holder (**Figure 39**). It was concluded that the precipitates of all three drugs phase separate by passing a transient liquid state and subsequently harden when being exposed to the aqueous environment in which the AFM measurements were accomplished.



Figure 39: Lopinavir particles exhibiting mechanically robust, solidified structures, indicating a transient liquid state of the precipitate during phase separation

While the AFM cantilevers are constructed to predefinedly deform when exposed to vertical pressure, their stronger resistance to horizontally applied force was used for gaining a deeper understanding of the mechanical properties of the precipitates. As a needle, the cantilevers were used to horizontally pierce the particles. While loratadine and lopinavir had shown comparable f-d patterns within regular AFM measurements, significant differences were observed when exposing them to stronger mechanical stress. The mechanical behavior of loratadine was clearly dominated by viscoelastic deformation, resulting in particles having an almost putty like mechanical behavior (**Figure 40**). In addition, the loratadine precipitate showed an extreme stickiness, so that after contact with the cantilever, filaments stretching over multiple times the length of the original particles could be drawn. The particles obviously consisted of a homogeneous matrix without any observable inhomogeneities.

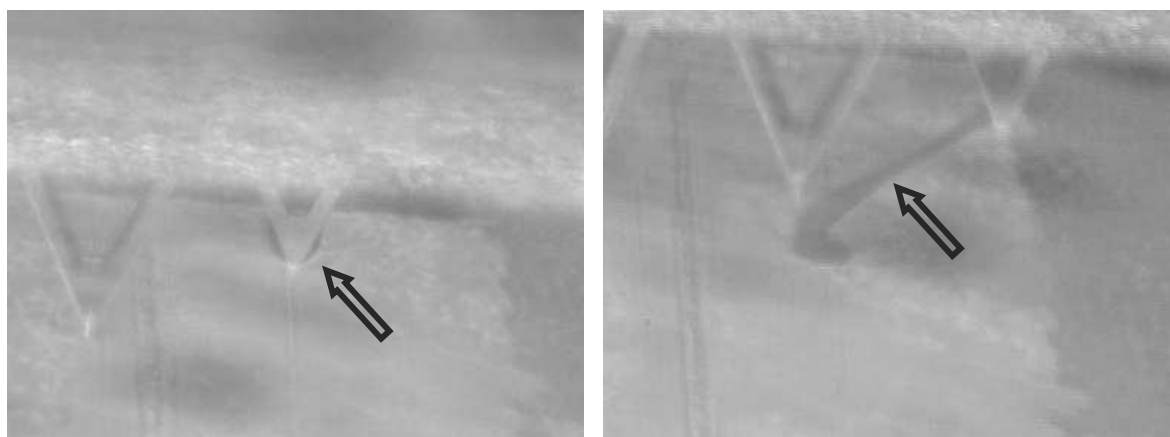


Figure 40: Video snapshots of the mechanical straining of a loratadine particle. Center left: loratadine particle attached to the cantilever. Right: long, viscoelastically deforming filaments can be pulled out of the particle

The lopinavir precipitates represent a further step towards complete solidification of the precipitate. Being the most lipophilic of the drugs investigated, lopinavir no longer showed deformability, even under application of significant mechanical stress. The particles were less sticky than loratadine and withstood the force applied by the cantilever (**Figure 41**). The cantilever deformed when pressed on the particle, while the particle itself appeared structurally unchanged. Whether the manifestation of the lopinavir particles can be considered a glass transition, with corresponding viscosities of the precipitates being larger than 10^{12} Pa s [91] cannot be appraised based on the above shown data, and might strongly depend on the environmental conditions of the measurements.

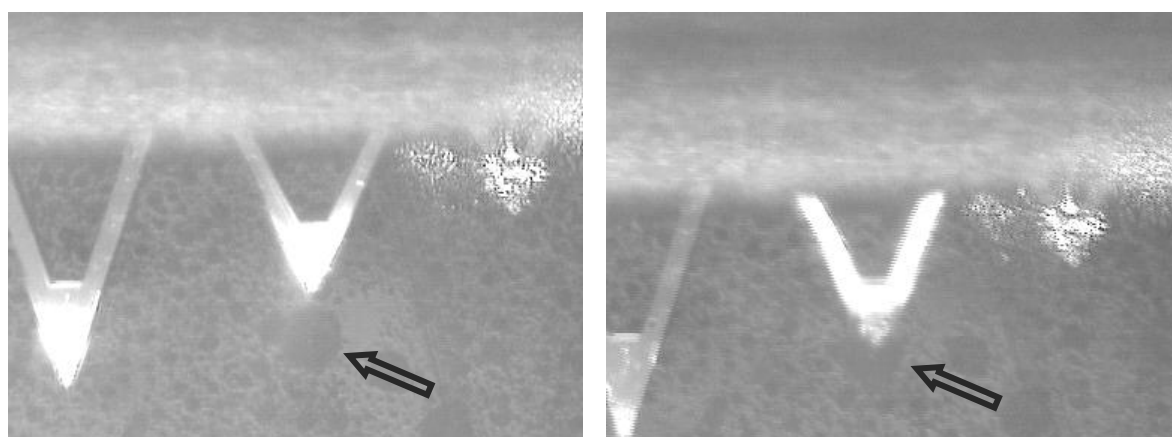


Figure 41: Lopinavir particle under application of mechanical stress from the cantilever. The particles remain stiff and undeformable, while the cantilever (middle of the right image) bends tremendously

For comparison, **Figure 42** resembles the liquid state of the fenofibrate particles previously described by f-d measurements. Their viscosity is tremendously lower than that of the other samples, actually resembling a true liquid. The particles did not burst or change in size when being penetrated by the cantilever, and immediately resumed their round shape after its removal. The cantilever easily penetrated almost the whole depth of the particles and was even capable to divide them into smaller subparticles.

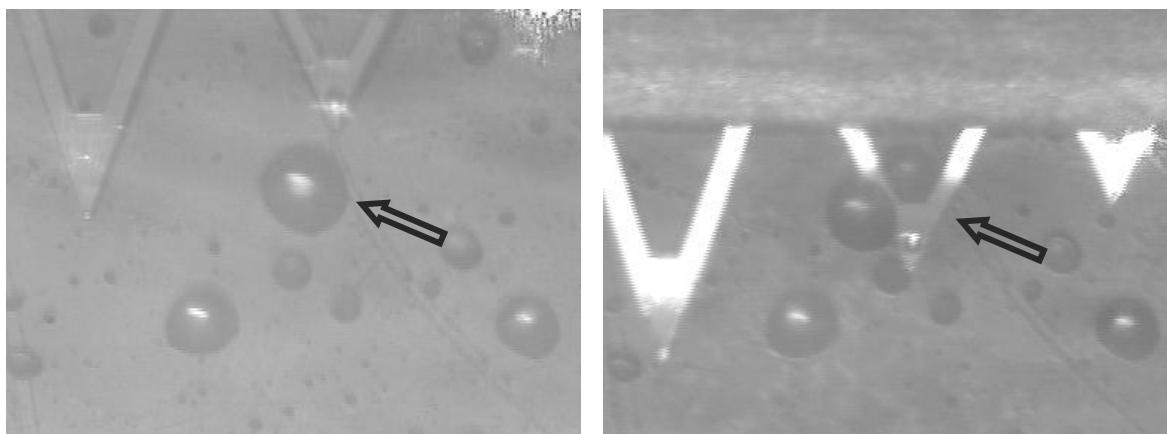


Figure 42: Fenofibrate particle pierced with a cantilever. The precipitates behave as a liquid with relatively low viscosity

It is self-evident that in liquid-liquid phase separation the physical state and viscosity of the precipitate depend on the interaction potential between the drug molecules and the solvent. The more solvent is complexed and the weaker the short range interaction potential (e.g. hydrogen bonds, ionic interactions) between the drug molecules is, the lower will be the viscosity of the liquid precipitate. Considering the lipophilicity of the compounds used for the AFM measurements, it should be pointed out that loratadine and lopinavir, with logP values of 5.9 and 6.3, form much harder precipitates than the more hydrophilic fenofibrate with a logP value of 4.8. It is hence assumed that the solidification of the precipitate is related to the capability to continuously complex solvent molecules within the framework of long-range interactions between the drug molecules. The aqueous environment of the experiments abets this process, leading to a stronger desolvation of the more lipophilic compounds.

Comparing the above described observations to the results obtained for fenofibrate dispersions prepared with the pumping setup, it can be anticipated, that especially in the early stage of the precipitation process, when an equilibrium between the precipitate and the

continuous phase has not yet leveled off, the ethanol rich precipitate is easily accessible to hydrodynamical and viscous stress. Within the phase separation process, ethanol will leak out of the drug rich dispersed phase, leading to an increased viscosity and surface integrity towards the predominantly aqueous continuous phase. In good agreement, post-preparational morphological changes were found to occur almost exclusively due to Ostwald ripening and crystallization, rather than coalescence or rupture of the particles.

4.4.3 WIDE-FIELD FLUORESCENCE MICROSCOPY

For gaining additional information about the inner assembly of the particles, wide-field fluorescence microscopy images were accomplished from fenofibrate dispersions prepared without the additional use of excipients. Fenofibrate intrinsically shows intense fluorescence signals, so that the observations could be performed without the need of using fluorescent dyes, which might have altered the precipitates' structure.

Figure 43 shows a light-microscopical image of a diluted fenofibrate dispersion accomplished with the wide-field fluorescence microscope. The sample was prepared under the same conditions as were applied for the sample preparation within the AFM measurements. Correspondingly, the particles have a comparably big size and apparently homogeneous constitution. However, when observing the fluorescence signal of the same sample spot by wide-field microscopy fluorescence microscopy, the presence of a fluorescent particulate species inside the mother particles was revealed (**Figure 44**). This fluorescent species (subsequently called subparticles) moved rapidly inside an obviously liquid environment enclosed by the mother particle. The smallest subparticle size differentiable from the background fluorescence signal consisted of complexes of 2 to 3 pixels, corresponding to a side length of ~240-400 nm. The presence of the subparticles could hence be confirmed for mother particles with diameters > 1 μm . Whether such substructures were also present in mother particles in the nm-range could not be verified.

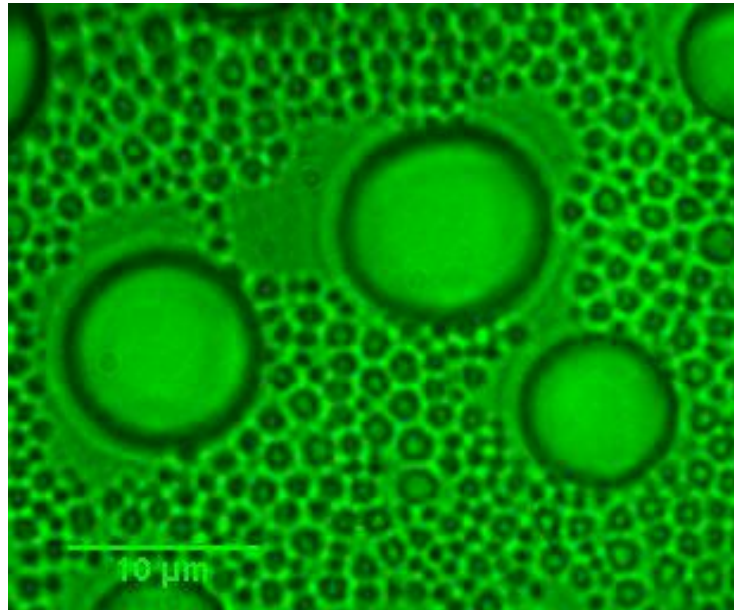


Figure 43: Light microscopical image of a fenofibrate dispersion. The particles have a homogeneous appearance

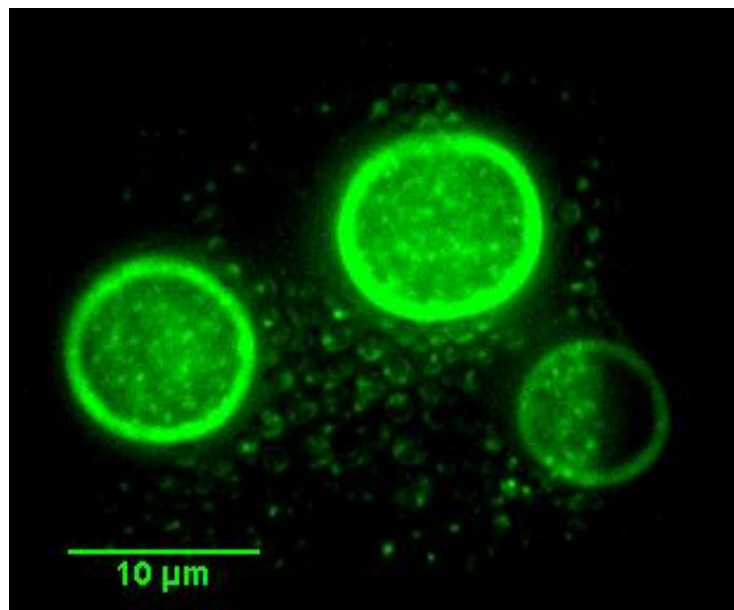


Figure 44: Snapshot of the wide-field fluorescence microscopy movie shown in Figure 43. Subparticles are rapidly moving inside bigger precipitate particles

Especially for very big mother particles a fluorescent outer layer with a thickness up to 5 μm was observed (**Figure 44**), which surrounded the inner dispersion. The precipitate did hence not consist of a pure liquid or a structurally homogenous phase as was anticipated based on

AFM measurements, but of a core shell structure with a solute rich outer layer. Also SEM imaging (**Section 4.4.1**) was incapable of resolving this structural feature, as the particles solidified upon drying, falsely suggesting an apparently homogeneously structure. Only upon exposing the particles to the electron beam, melting was found to occur starting from the inside of the precipitate, potentially indicating a denser outer layer (**Figure 36**). Such core shell structures have also been described in the literature [125], however, only under crystallization of the outer shell. Considering the flexibility and robustness of the fenofibrate precipitate upon application of mechanical stress, the surface layer of the mother particles must have a certain flowability and elasticity, preventing leakage of the contained dispersed phase. Presumably it is the bad wettability of the hydrophobic drug molecules that leads to rapid contraction and sealing of the particle surface one lacerated by the AFM tip.

The formation of a mechanically stable outer layer of the fenofibrate precipitate is attributed to solvent depletion from the precipitate surface. As observed for loratadine and lopinavir, this depletion leads to an increase in sample viscosity. The fact that the outer layer of the particles only spans nanometers to micrometers in thickness, as well as the observation of rapid solidification of the lopinavir precipitate (**Figure 39**), suggests, that the surface equilibration with the continuous phase completes within seconds or even milliseconds. Neither within the AFM measurements, nor within wide-field fluorescence microscopy, structural changes were observed within the measurement time (up to 1 hour for wide-field fluorescence microscopy, up to 4 hours for AFM measurements), indicating the complete formation of a surface layer prior to the start of the measurements.

The dependency of the particle surface properties on the composition of the continuous phase was also shown by accomplishing additional wide-field microscopy measurements using undiluted fenofibrate dispersions, hence containing ~16.7% (V/V) ethanol. In opposite to the samples observed in an exclusively aqueous environment, the particles had a hardly distinguishable outer shell with a thickness of less than 2 pixels \approx 246 nm, indicating a lower degree of solvent depletion compared to an exclusively aqueous environment. In one case even the bursting of a particle and spilling of the contained dispersion was observed (**Figure 45**).

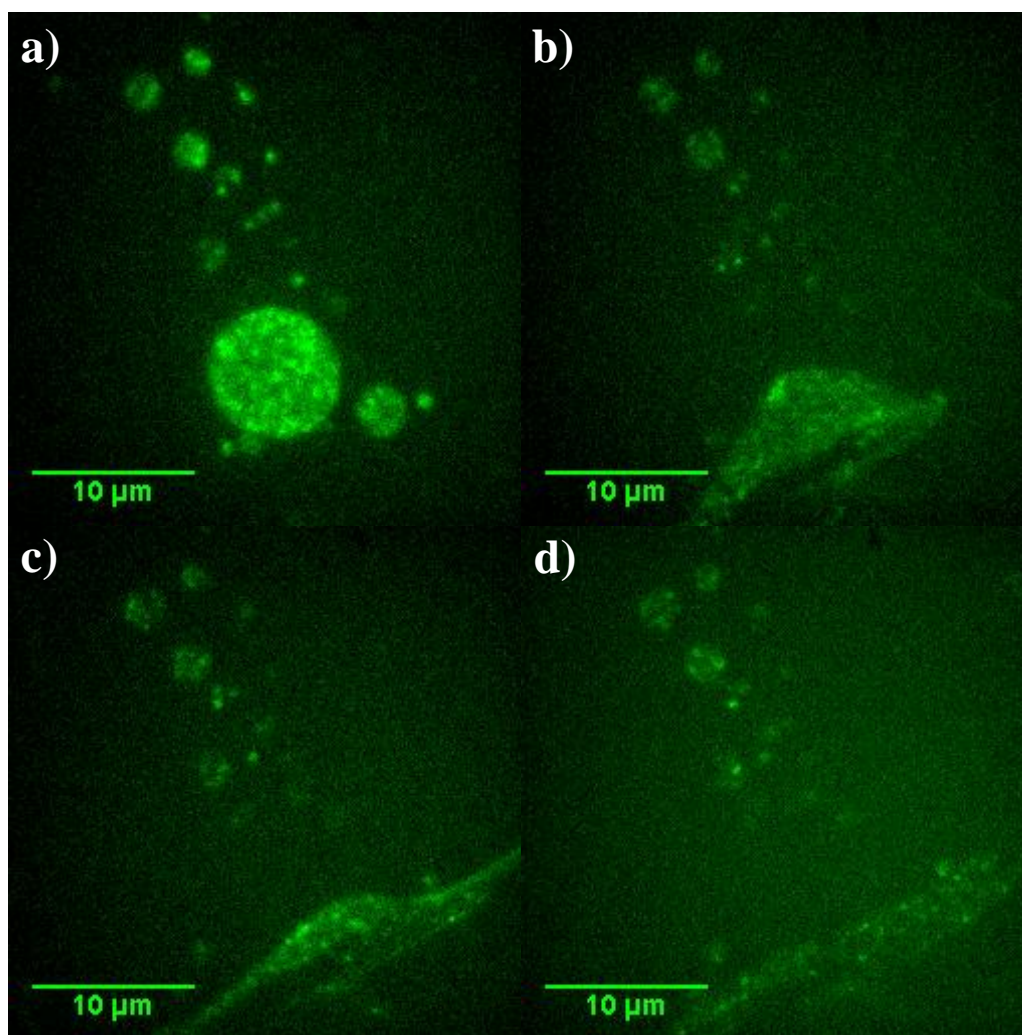


Figure 45: Video snapshot of an undiluted fenofibrate dispersion. The interior of the particles remains rather liquid; particles are prone to Ostwald ripening and coalescence. The particle in the middle (image a) bursts, its content pours out

4.4.4 CONFOCAL FLUORESCENCE SPECTROSCOPY

Spectra were accomplished by confocal fluorescence spectroscopy for investigating whether the subparticles were crystalline or rather having the same liquid-amorphous state as the mother particles. Surprisingly no shift between the spectra of dissolved drug, crystallized fenofibrate or the liquid precipitate were observed, so that it was not possible to spectrometrically differentiate between the samples (**Figure 46 - Figure 48**). Neither water nor the ethanol used for preparation of the dispersions showed a fluorescence signal, so that the fluorescence observed was caused by fenofibrate alone, and not by potentially contained

impurities. Intensity variations of the signals were observed due to fluctuations in the local particle concentration.

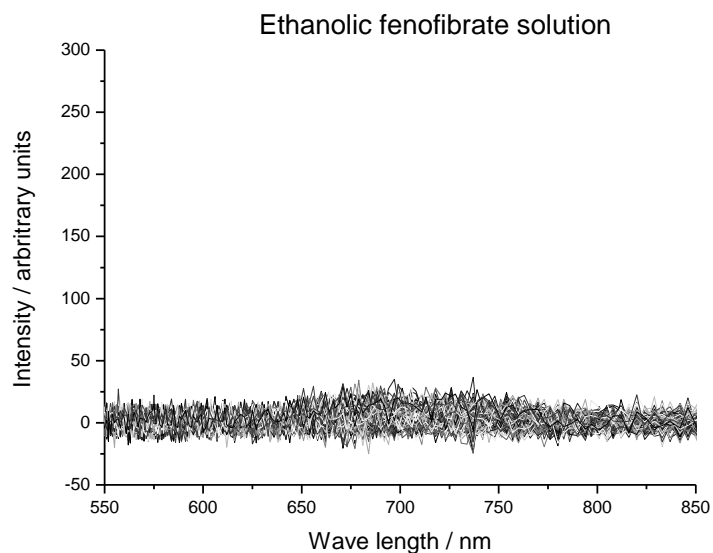


Figure 46: Fluorescence spectra of a 5% (w/w) ethanolic fenofibrate solution. Only weak signals are obtained for the dissolved drug

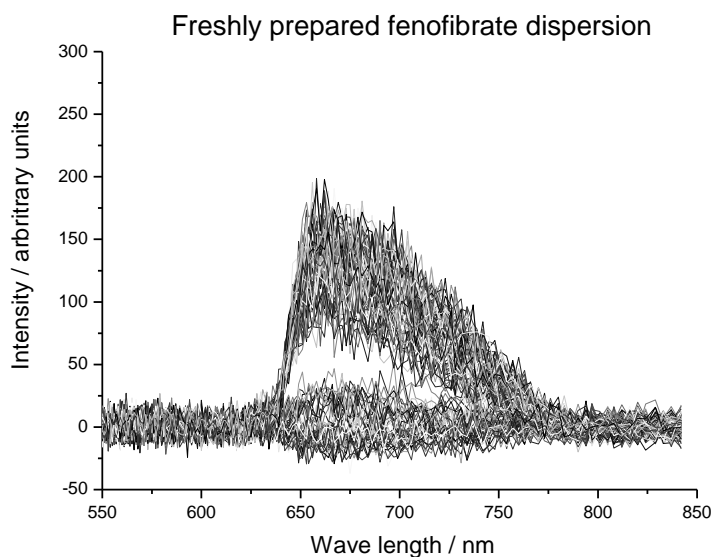


Figure 47: Fluorescence spectra of a freshly prepared dispersion containing 7 mg fenofibrate/g dispersion. Depending on local concentration fluctuations, differently strong signals for the dispersed phase as well as dissolved drug were observed

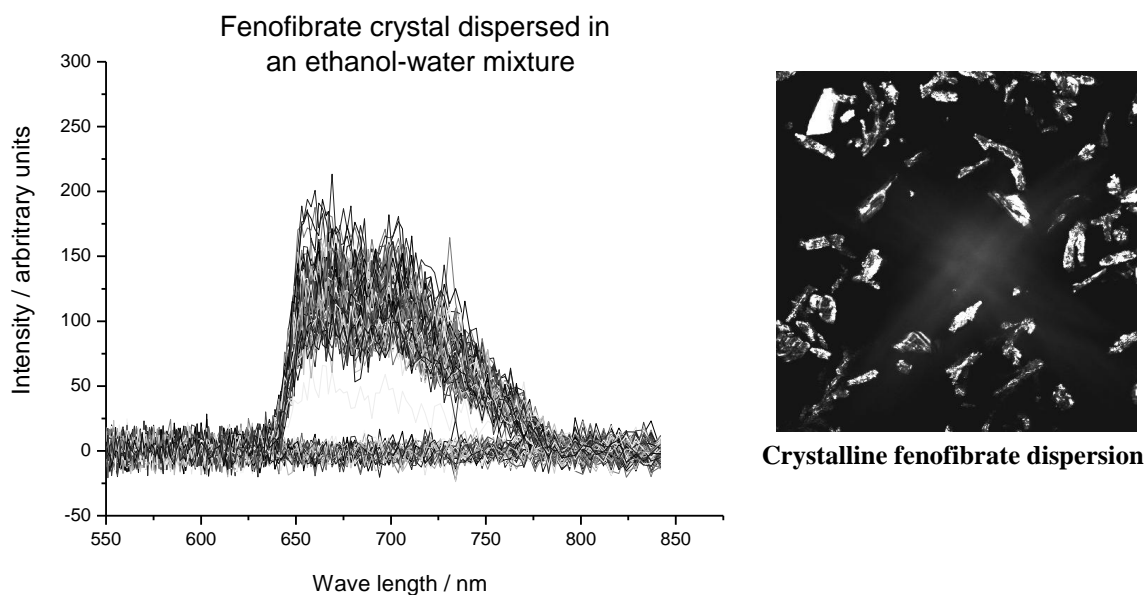


Figure 48: Fluorescence spectra acquired from a crystallized fenofibrate dispersion. Signals are comparable to those of the liquid precipitate were obtained

The fluorescence signals of the liquid precipitates were much stronger than for the dissolved drug and very comparable to those obtained from the crystalline drug. This similarity indicates a comparable interaction pattern of the fenofibrate molecules in the crystals and those in the freshly prepared precipitates. This is surprising, considering the much higher molecular mobility in the liquid precipitate. How many of the drug molecules contribute to the fluorophor of the drug has not been reported in literature, making further evaluation of the interaction pattern difficult.

4.4.5 LIGHT MICROSCOPY

Light microscopy was intended to complete the dataset for being able to fully retrace the underlying mechanisms of the particle formation process. Adopting the very gentle sample preparation conditions from AFM measurements and wide-field fluorescence microscopy, precipitates in the elevated μm -range could be generated (**Figure 49, right**). Still rarely observed, the thereby obtained macroscopic particles helped to confute the impression of homogeneity gained when investigating the samples prepared under more rigid mixing

regimen (**Figure 49, left**). It could be confirmed that the result of the precipitation process is a complex multiple emulsion system, with substructures forming inside the mother particles. The continuous phase of the subparticle-dispersion comprised inside bigger particles apparently had a comparable viscosity/composition as the continuous phase surrounding the mother particles.

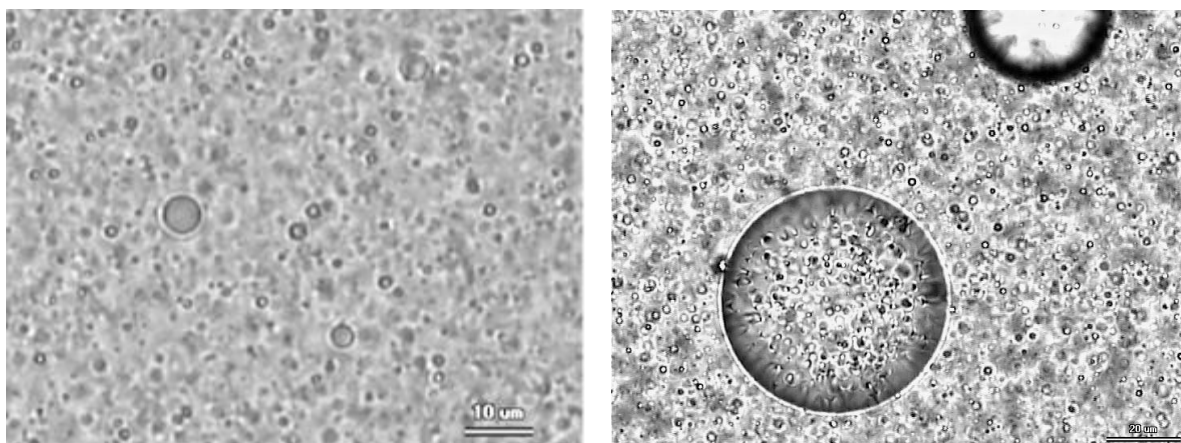


Figure 49: Fenofibrate dispersions prepared under normal (left) and very gentle (right) mixing conditions. Even particles up to 10 µm have an optically homogeneous appearance

Fenofibrate particles did, in opposite to the crystalline drug, not give any signal when being observed by using cross polarized filters. These optical properties in combination with the above described melting pattern within the SEM imaging provide strong evidence for the non-crystallinity of the fenofibrate precipitate. Further evidence for the absence of crystalline material in the precipitate is provided by thermodynamical reasons. The chemical potential of the drug inside the precipitate as well as in the drug depleted continuous phase is the same [120], so that the formation of the thermodynamically favorable crystalline state can occur in either of the phases, depending on kinetic factors. Crystallization was however found to exclusively occur outside the particles. The presence of hardly detectable nanocrystallites would have contradicted the free formation of crystals in solution, as they would have served as seeds, promoting crystallization in their direct environment, meaning inside or at the surface of the precipitate particles. Facing the non-crystallinity of the subparticles, and considering the comparable optical properties of the subparticles and the surrounding outer layer, it can be anticipated that both, the subparticles and the shell are composed of the same material.

A more detailed observation of the particle formation process could be accomplished regarding the viscous precipitates of lopinavir and loratadine. Better than for fenofibrate, the viscosity of the precipitates of these two drugs was high enough to withstand the hydrodynamic effects present within the mixing process. It can be nicely seen that the phase separation of loratadine and lopinavir underlies typical spinodal patterns as they are known e.g. for polymeric systems [91].

In a first step, the concentration density fluctuations arising from blending the ethanolic drug solution and water lead to the actual event of phase separation. A poorly defined precipitate is formed. Subsequently, the newly formed phase gains shape by forming a well-defined interface. The third step resembles the shape transformation of the interface. An interconnected structure of precipitate is formed from which substructures constrict, forming individual particles. Also the formation a multiple emulsion system as it was shown to exist for fenofibrate could be tracked as well for loratadine and lopinavir (**Figure 50 - Figure 52**). It can nicely be seen how the subparticles constrict from the same solute rich matrix that later forms the shell of the mother particles.

The observed spinodal decomposition is presumably conveyed by noninstantaneous mixing of ethanol and water, as it is known to occur due to interfacial effects [89]. An indication therefore is the observation of entrapped droplets of organic solvent inside the precipitate particles (**Figure 52**). These ethanol droplets, infrequently observed within precipitation experiments of all three drugs, were distinguishable from the liquid precipitate due to their color and a strong tendency to coalescence.

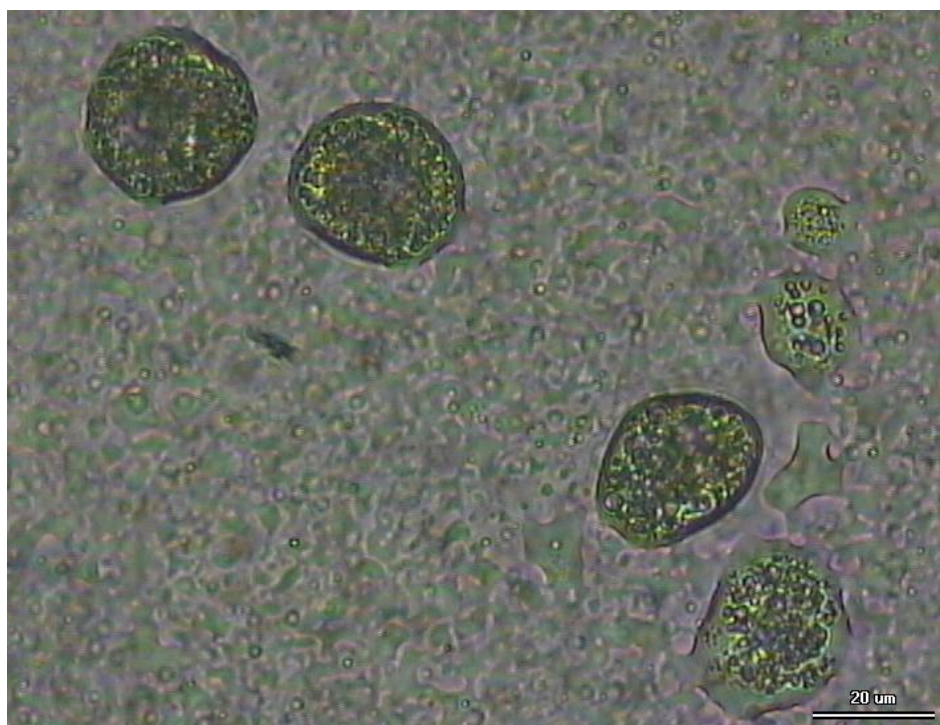


Figure 50: Lopinavir dispersion prepared under weak mixing conditions. The process of decomposition and shaping of individual sample particles can be observed

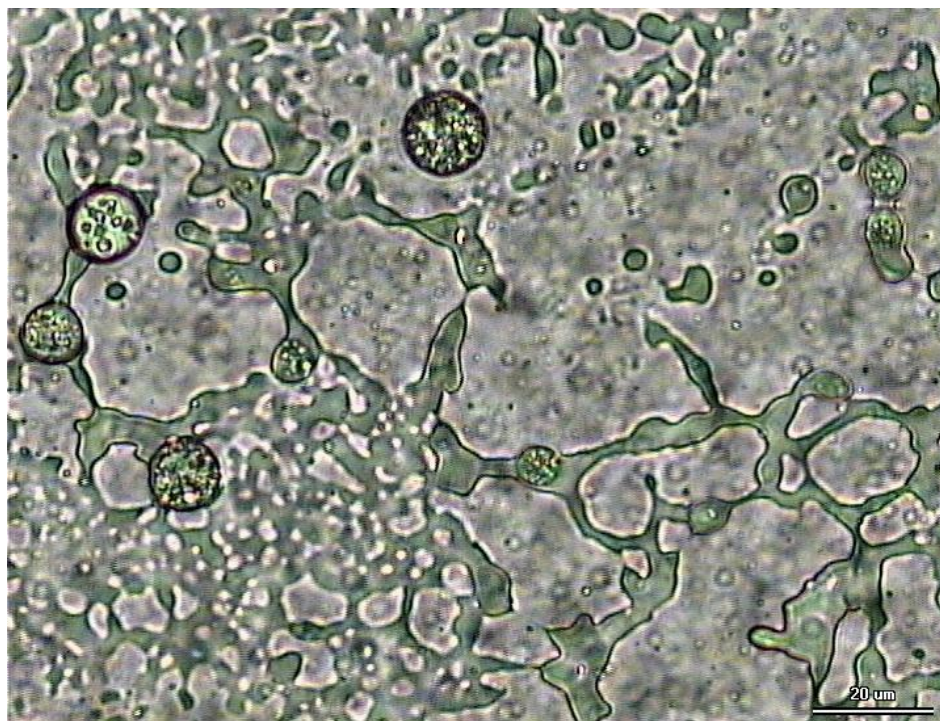


Figure 51: Dispersion of lopinavir prepared under weak mixing conditions. Formation of an interconnected gel like network of which subparticles constrict



Figure 52: Dispersion of loratadine prepared under weak mixing conditions. As for the other drugs, droplets of organic solvent entrapped in the precipitate (centre) could be observed

Although the intermediate interconnectivity found for the lipophilic compounds lopinavir and loratadine (e.g. **Figure 51**) could not directly be confirmed for fenofibrate, it is very likely that all three drugs phase separate according to the same mechanisms. The reason for the rare manifestation of spatially extended fenofibrate structures might be the low viscosity of its precipitate, as it was revealed by AFM measurements (**Figure 38**). This makes the precipitate too fragile to withstand the hydrodynamic and surface energy dependent rapid decay post sample preparation. Another explanation is, that the formation of individual fenofibrate particles might occur at an early state of the of the spinodal decomposition, prior to the manifestation of interconnected structures (see also [126]).

4.4.6 NEW INSIGHTS ON THE IMPACT OF THE PROCESS CONDITIONS ON PARTICLE FORMATION

The fact that not a solid, but a liquid precipitate is formed, shifts the interest from supersaturation defined effects on the particle size distributions to the impact of friction and

hydrodynamic processes going on during phase separation. The liquid state of the precipitate provides a wide accessibility to particle breakup, depending on the mixing intensities applied. Under weak mixing conditions, e.g. hand-mixing of ethanolic and aqueous phase, core shell structures were formed, upon whose rupture the contained particles were found to be released into the continuous phase (**Figure 45**). Also, at low flow rates of 12 - 24 ml/min a binodal particle size distribution could be observed (**Figure 9, Chapter 2**), potentially reflecting the release of nanoparticles from destroyed bigger structures. At higher flow rates, this bimodality gets lost, as the size reduction of bigger structures reaches a limit. It can be expected that spatially extended precipitate structures do no longer persist, but are directly destroyed by the intense mixing forces applied at elevated flow rates. The energy required for breaking up the precipitate structures in the mixing setup is reflected by the high energy dissipation and the linear shape of the pressure drop obtained within antisolvent precipitation (**Figure 17**). At intermediate mixing intensities an increasing amount of energy is consumed for breaking up primarily formed structures into smaller subparticles, thereby exceeding the specific power input needed for mixing just ethanol and water (blank). When the particle size is reduced to a minimum under very intense mixing conditions, no additional energy is consumed for further size reduction. Energy dissipation lags behind the blank values and remains on a comparably low level. Presumably interfacial effects beyond the stabilization of the oily phase take place, facilitating the flow through the mixer. The coalescence of particles, which one could anticipate to occur in the mixing setup, most likely only has an insignificant impact on the final product properties, as the resulting coalescent underlies the same hydrodynamic effects as the primarily formed particles. Typically, an equilibrium levels off between particle breakup and recombination.

Solvent complexation was found to play a determining role concerning the mechanical properties of the precipitate. For fenofibrate the viscosity respectively the thickness of a solvent depleted outer shell of the particles was found to increase with decreasing ethanol concentration in the continuous phase of the dispersions (**Section 4.4.3**). Also for loratadine and lopinavir strong indications for a solidification of the precipitate post operation were observed within the AFM measurements. It is evident, that besides the elasticity of a sample also its volume is affected by the observed solvent complexation. In comparable antisolvent precipitation experiments, the organic solvent was found to contribute ~30-60% of the total mass of the precipitate [8, 117, 120]. Lafferrère et al. [117] found a correlation between temperature and precipitate composition in antisolvent precipitation. In their study they

showed, that the fraction of the contained drug decreased by 25% in favor to complexed solvent/antisolvent when the temperature was increased from 10°C to 50°C. Considering the unchanged particle size obtained when varying the process temperatures in our setup (**Chapter 3**), the interaction between drug and solvent provides the most reliable explanation. The increasing solubility of fenofibrate at elevated temperatures is countervailed by the complexation of solvent, keeping the total volume of precipitate constant. Only by decreasing the temperature of the aqueous phase tremendously, a higher volume of precipitate, and hence bigger particles are formed.

In the same context, the dependency of particle size on solvent composition has to be seen. Particle size increased continuously as the ethanol content in the dispersions was increased (**Figure 26**). Neither interfacial nor solubility related effects alone can explain this increase. In fact, the reason therefore presumably was an increasing amount of solvent, especially ethanol, complexed in the framework of intermolecular interactions of the precipitate.

4.5. CONCLUSIONS

The above described observations give a good impression about the compositional and structural makeup of the precipitated drugs. Beyond the structural analysis of the precipitates, the results allow to clarify many questions raised by the observation of differences between the simulations accomplished and the experimental results (refer also to **Chapter 2** and **Chapter 3**).

Already at very low supersaturations (hand mixing) spinodal decomposition was observed for loratadine and lopinavir, as indicated by the spatially extended and gradually shaped precipitate. Comparable product characteristics suggest the same phase separation mechanism for fenofibrate. The precipitates examined within our experiments were no transient solvent particles as suggested by other authors [55], but the liquid precipitate was stable until crystallization of the drug. AFM as well as wide-field fluorescence measurements indicate that the elasticity of the particles primarily depends on the lipophilicity of the drugs as well as on the interaction potential with the solvent. The varying complexation of solvent/antisolvent molecules at different temperatures and solvent/antisolvent ratios represent a conclusive explanation of the previously described particle size dependencies. In conclusion, the particle formation process was governed by three major processes:

- a) Spinodal decomposition
- b) Complexation of solvent and antisolvent in the framework of drug molecules, which determine the volume and mechanical properties of the precipitate
- c) Shaping of the resulting precipitate by hydrodynamic and interfacial effects

A liquid precipitate shell at the particle surface and the existence of incorporated nanoparticles was observed by light- and wide-field fluorescence microscopy. While for lopinavir and loratadine clear evidence was found, indicating that besides the main precipitate also such secondary particles are formed within the spinodal decomposition process, nucleation based phase separation of the subparticles cannot be excluded for fenofibrate, as the intermediate state of the demulsification process could not be monitored. The absence of

crystalline material after sample preparation as well as the comparable optical properties of the shell and the contained particles (light- and wide field fluorescence microscopy) indicates that the dispersed particles most likely have a comparable composition as the surrounding shell. Evidence was provided supporting the idea that the mother particles as well as the subparticles do not contain crystalline drug, which might have formed by nucleation or subsequent to the phase separation process. Nevertheless, a distinct interaction potential exists between the fenofibrate molecules in the liquid dispersions, resulting in fluorescence spectra comparable to that of the crystalline drug.

If and to what extent amorphous or liquid nanoparticles below the resolution of the wide-field fluorescent microscope ($\sim 1 \mu\text{m}$) exist could not be determined. The required drying of the specimens and their observed thermal instability within electron microscopy measurements prohibited further investigations with sufficient spatial resolution. For loratadine and lopinavir solvent complexation was found to be temporarily short lived, leading to particles with an homogeneous inner structure and the loss of a potentially existing inner dispersed phase as was observed for fenofibrate.

Chapter 5. Stabilization of the Dispersions

5.1. ABSTRACT

The physical stability of a formulation is essential for assuring a sufficiently long shelf life as well as for providing the experimental freedom required for downstream processing during manufacturing. This is especially the case for substances as fenofibrate, whose bioavailability can suffer significantly following phase transformations, namely crystallization [127]. Fenofibrate represents a worst case substance concerning phase transition stability. Different approaches were accomplished to inhibit the drugs crystallization, coalescence of the amorphous drug particles as well as to slow down Ostwald ripening. Most successful of these was the coprecipitation with a second liquid-liquid phase separating substance in combination with surfactants. Crystallization could thereby be delayed from 1 min to 1 hour. Wide-field fluorescence microscopy, AFM measurement and also the structural analysis of lyophilizates of the drug dispersions allowed to gain further insights in the structural habits of the precipitates. It was concluded, that the presence of butylated hydroxytoluene (BHT), which was used as model-coprecipitant and stabilizing agent, decreases the likelihood of nucleation due to its structural affinity to fenofibrate and the resulting constraint of the homologous interaction between fenofibrate molecules. Side effect of the weakened fenofibrate-fenofibrate interaction pattern was a liquefaction of the coprecipitate particles, which was, besides fenofibrate, also observed for the poorly soluble drugs lopinavir and loratadine. It indicates the potential for a wide applicability of this stabilizing approach. To the knowledge of the author, such analysis of the structural properties of liquid-liquid phase separating substances has so far not been accomplished, and the proposed approach to inhibit crystallization is new in the field of pharmaceutical sciences.

5.2. INTRODUCTION

The stability of drug dispersions can be affected by a multitude of potential destabilizing mechanisms. Although most publications dealing with the preparation of such dispersions claim to produce “stable” formulations, this term is not always properly defined. It can refer to the stability of a certain physical state of the primary product, e.g. a certain polymorph, to a given size distribution, or to both.

The means applied for assuring dispersion stability are mostly derived from classical emulsion or crystallization technology, e.g. the use of certain excipients, dilution with a non-solvent or the removal of solubilizing compounds. However, why a certain stabilization measure applies to one formulation but not to another is poorly understood [128], especially concerning the amount and kind of excipients to use. The absence of a commonly accepted formulation guideline must at least in part be addressed to an incomplete understanding of the morphology of the dispersions and the interaction mechanisms between the excipients and the main compounds.

Within the scope of this work the stability of fenofibrate formulations is primarily defined as the absence of crystallization. Secondly, the mean particle size was thought to remain in a range allowing for parenteral application of the drug dispersions, preferentially below 1 μm .

Considering the tremendous instability of amorphous fenofibrate dispersions against crystallization, the development of a marketable formulation was not a target. Rather, knowing that often liquid-liquid phase separating substances exhibit an extraordinary intrinsic stability against crystallization [110, 111], a subsequent transfer of the developed formulation approaches to compounds with a higher thermodynamical stability was aspired. For such substances a significantly extended and commercially attractive shelf-life seems attainable even without the application of classical long term stabilization techniques, such as freeze- or spray drying of the formulations.

For fenofibrate a 30 min target time was established, in which crystallization and considerable particle growth should be avoided. Thinking beyond early formulation studies, 30 min were thought to guarantee enough experimental freedom for implementing additional stabilizing means to allow for further downstream processing. Therefore the work was based on using dispersions in their unchanged post preparational state, without the application of solubility diminishing means as solvent removal or dilution. The applied stabilization

techniques aimed on a reduction of particle agglomeration as well as coalescence by fusion of the liquid dispersed phase. Most important was however to inhibit interparticulate mass transfer in terms of crystallization and Ostwald ripening.

In the following, the destabilization mechanisms found to be relevant within this work are briefly outlined in the context of potential counteracting measures. In the **Results and Discussion** part (**Section 5.4**), their applicability to fenofibrate dispersions is experimentally investigated. In addition, a completely new approach for inhibiting the crystallization of liquid drug dispersions is presented: the modification of the molecular interaction profile inside the precipitate particles by coprecipitation with a second substance showing liquid-liquid phase separation. Lyophilization as downstreaming operation for the conservation of the dispersions and adjusting the postoperational excipient content is discussed. Results from lyophilization studies as well as wide-field fluorescence microscopy and AFM measurements gave further insight into the structural properties of the fenofibrate precipitates.

5.2.1 CRYSTALLIZATION

Crystallization generally occurs due to thermodynamical reasons, as the highly ordered state of crystals is energetically favorable compared to the amorphous (or liquid) state of a substance. Fenofibrate is a particularly good example for a substance being sensitive to crystallization. In dispersions prepared by antisolvent precipitation, the first crystals can be observed directly after preparation of the dispersions, independently from the mixing conditions applied. The driving force for crystallization increases with increasing supersaturation of the solute, growth kinetics accelerate at elevated solubilities in the continuous phase (**Figure 53**). The higher the solubility is, the higher is the diffusion rate of molecules from an energetically less favorable particle towards a more stable polymorph [129]. Developing a formulation with the aim of increasing drug solubility, hence unavoidably threatens the dispersions' physical stability. In antisolvent precipitation crystallization depends on the amount of solvent, temperature, the size and physical nature of the precipitate as well as the presence of excipients.

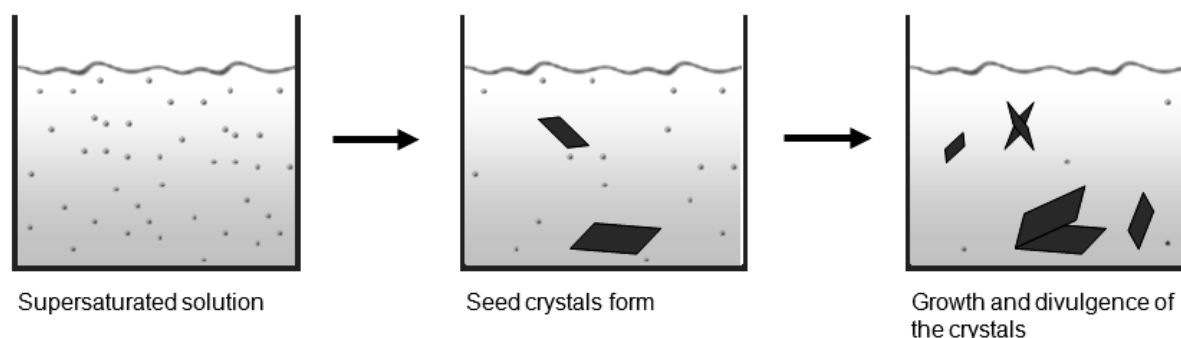


Figure 53: Crystallization in a supersaturated solution

The bulk phase of liquid precipitation products can be interpreted as a supercooled liquid with an exceptionally strong interaction potential with the available solvent (and antisolvent). Upon liquid-liquid phase separation, the solvent thereby acts as plasticizer, which lowers the viscosity of the sample. In consequence, the samples' glass transition, and also its crystallization behavior, can be influenced by any parameter affecting the interaction between solute and solvent.

For substances showing liquid-liquid phase separation, crystallization can occur either in the continuous phase, in the solute rich dispersed phase or at the interphase between both. Generally, crystallization inside or at the surface of the dispersed phase is favored within a range of optimal molecular mobility, as was described for other amorphous systems [130]. In the case of homogeneous nucleation, it hence depends on the intensity and duration of the homogeneous molecular interaction between the solute molecules. In the case of heterogeneous nucleation, crystallization additionally depends on the interaction pattern with foreign nucleation sites, e.g. impurities. In both cases the molecular mobility needs to be high enough to allow for an oriented arrangement of the molecules. In the case of homogeneous nucleation, the duration of the interaction needs to be long enough to assure an interaction pattern sustainable enough to allow for the condensation of an amount of molecules exceeding the critical nucleus size (refer also to **Section 2.3.5**). It was shown in **Chapter 1** that the viscosity and hence the molecular mobility of precipitates obtained by liquid-liquid phase separation can vary strongly. It depends on the solvation of the solute inside the precipitate, which can lower the homogeneous interaction between the solute molecules. The glass transition of the precipitate is reached when the interaction between the solute molecules becomes strong enough to increase the precipitates' overall viscosity to

$\geq 10^{12}$ Pas, accompanied by a corresponding reduction in molecular mobility. For temperature controlled systems, this state is characterized by the glass transition temperature T_g (**Figure 54**) [91]. The Kauzmann temperature T_K marks the condition at which the entropy of the supercooled system reaches that of the corresponding crystal and the configurational entropy of the system becomes zero.

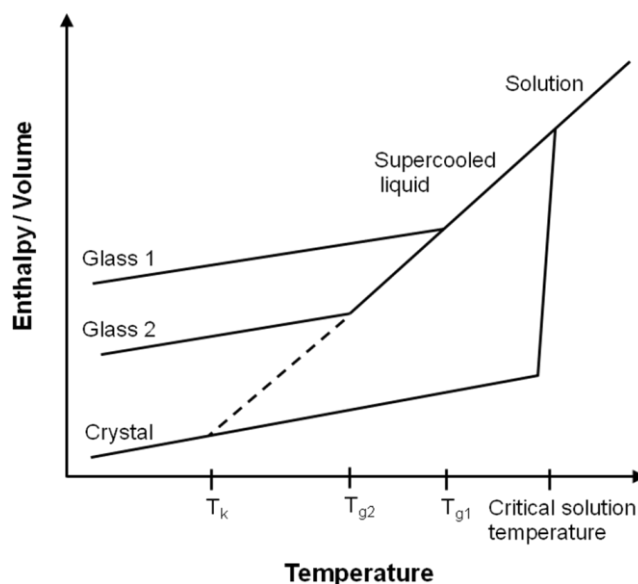


Figure 54: Schematic description of the enthalpy variation with temperature (adopted from [131])

Crystallization is only possible, as long as a sufficiently high mobility is assured, and hence usually occurs at temperatures between T_g and the critical solution temperature (**Figure 55**). The exact position of the nucleation optimum for the amorphous phase depends on the interaction pattern between solute and solvent and is hence poorly predictable. For substances forming solvates, a strong interaction with the solvent can facilitate crystallization, as the solvent can conciliate a certain periodicity between the solute molecules. Other substances were found to be impossible to crystallize from a liquid precipitate, as their high molecular mobility prevented sufficiently strong molecular interaction [132]. Only solvent removal by lyophilization and careful rehydration allowed for the agglomeration of sufficient amounts of material to reach the critical nucleus size. For certain systems crystallization is favored at the interface between the dispersed and the continuous phase, again underlining the impact of the interaction between solute and solvent/antisolvent [106, 125, 133-135]. For fenofibrate, whose structure lacks the presence of hydrogen donors and which is not known for forming solvates [136], crystallization would be expected to increase at lower molecular mobility, as

this would allow for a closer approximation and more permanent interaction of the drug molecules.

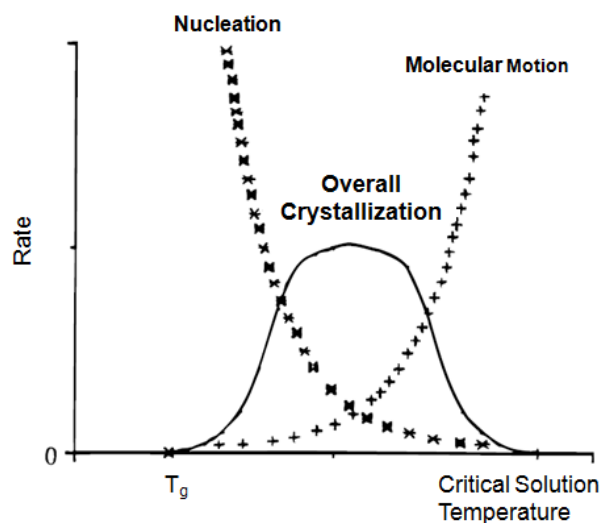


Figure 55: Schematic illustration of the parameters controlling crystallization from the amorphous state (adopted from [115])

For liquid-liquid phase separating substances, crystallization not only occurs inside or at the surface of the solute rich precipitate, but can also take place in the solute depleted continuous phase, which is in the presence of amorphous material supersaturated compared to crystalline polymorphs. The correlation between the different crystallization patterns is nicely shown when referring to the example of temperature controlled systems. As observed by Lafferrère et al. [117] and conceivable for other systems, the composition of the precipitates tends to increasingly comprise solvent at elevated temperatures. Neglecting gelation effects, the solvent complexation causes an increase in molar mobility inside the precipitate until the solubility limit is reached, and the precipitate dissolves. For most substances also the solubility in the continuous phase increases, which is directly associated with the crystal nucleation and growth rate. A temperature shift hence not only affects the crystallization behavior inside the dispersed phase, but simultaneously alters crystallization in the continuous phase. Primarily kinetical factors finally determine whether crystallization will preferentially occur in the continuous, or the solute rich dispersed phase.

To inhibit crystallization is difficult. Crystal nuclei form on a molecular level by agglomeration of a certain amount of solute molecules. Crystallization inhibitors in the classical sense prevent nuclei formation on a sub-critical size, so that molecular agglomerates

redissolve before forming a thermodynamically stable solid [137]. However, due to the experimentally difficult identification of nanoscopic nuclei, it can be expected that the stabilizing effects described in literature can in many cases also be attributed to shielding effects of adsorbing excipients on the crystals surface, so that already existing crystallites do not grow to an observable size.

Crystallization inhibitors are substances with a high interaction potential with the solute. For inhibitors additionally binding to the crystal surface, the inhibitor-crystal interaction needs to be comparably unspecific, as the multiple faces of a crystal have different structural surface habits. To prevent crystal growth, an inhibitor needs to bind to all of such surfaces simultaneously. Mainly polymers such as polyvinylpyrrolidone (PVP), cellulose derivatives or poloxamers were used as crystallization inhibitors [138-140]. Their positive effects on dispersion stability were attributed to an increase of the viscosity of the continuous phase, the formation of a steric barrier for solute adsorption on existing crystals and/or specific interaction between the drug and the stabilizer, e.g. by hydrogen bonding. Hydroxypropylmethylcellulose (HPMC) and PVP are known to be generally capable to inhibit precipitation from a solution, indeed indicating interaction with the solute on a molecular level [138, 139].

Almost no research has been accomplished on the stabilization of small molecules showing liquid-liquid phase separation. In 1910 Flaschner and Rankin [141] developed an approach to influence the morphological properties of precipitation products. Intending to experimentally determine the critical solution temperature of different small organic molecules, they succeed to artificially induce liquid-liquid phase separation by the addition of a second poorly soluble compound and to avoid, resp. postpone, crystallization. The excipients used typically had a lower solubility than the solute of interest and a higher interaction potential between both solutes than between the solutes and the continuous phase. Galkin et al. [142] used a comparable technique when studying crystallization phenomena in lysozyme formulations, using salt, glycerol or nonadsorbing polymers to cause liquid-liquid phase separation and to direct the phase separation mechanism. Post precipitational stabilization of liquid precipitates is widely neglected in research, as liquid-liquid phase separation in the context of crystallization technology is widely considered undesirable and scientific focus it put on its avoidance.

Within this work, in a preliminary trial a series of excipients previously used for the stabilization of fenofibrate and other drug formulations were studied for their stabilizing functionality in the current sample system. These classical formulation approaches were subsequently further developed by an innovative formulation approach, the coprecipitation of the API with an additional liquid-liquid phase separating compound. It takes on the idea of influencing the morphological properties of the precipitates used by Flaschner and Rankin [143]. Fenofibrate was combined with a second poorly soluble compound, the antioxidant 2,6-di-tert-butyl-4-methylphenol (butylated hydroxytoluene, BHT). Not mentioned in the literature in the context of having effects on the physical stability of dispersions, the antioxidant was selected based on its low toxicity [144-146] as well as structural properties indicating a strong interaction potential with fenofibrate. With a logP value of 5.3 BHT is even more lipophilic than fenofibrate, and with its aromatic structure not only accessible to lipophilic, but also to (induced) dipole-dipole interaction, as is fenofibrate. Experimental investigations were accomplished for controlling the physical state of the coprecipitates. BHT's potential to increase dispersion stability was refined by combination with classical formulation strategies, namely the addition of surface active and polymeric excipients.

5.2.2 OSTWALD RIPENING

Ostwald ripening was, besides crystallization, found to be the main cause for structural modifications in fenofibrate dispersions. As already discussed under **Section 1.4**, Ostwald ripening describes the growth of bigger particles at the expense of smaller ones [147] (**Figure 56**). The driving force for the mass transfer is the higher surface energy of smaller particles, which have a detrimental surface to volume ratio compared to bigger particles. Overall, Ostwald ripening leads to a reduction in the total surface area of the dispersed phase.

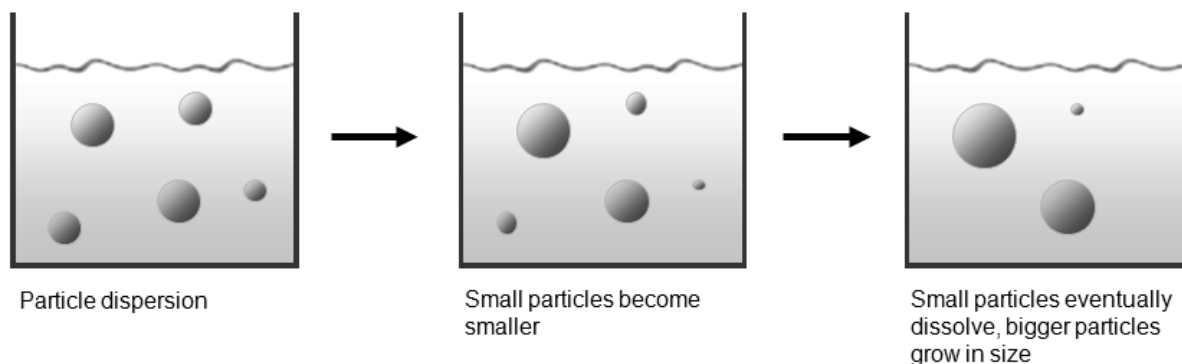


Figure 56: Ostwald ripening

As shown above for crystallization phenomena, also Ostwald ripening increases at high concentrations of solute in the continuous phase. It applies to crystalline, amorphous as well as liquid particles, will however in most cases be fastest with liquid and amorphous materials, as these show a higher solubility and facilitated surface integration of the adsorbing solute molecules. As Ostwald ripening depends on the mass transfer between individual particles; systems containing a wide particle size distribution are most prone to Ostwald ripening. The preparation of dispersions with a homogeneous size distribution is hence an effective strategy for increasing their stability. In addition, Ostwald ripening might be decreased in the presence of adsorbing polymers as PVP as well as surface active additives. They lead to a reduced diffusion coefficient between the particles by shielding the particle surface [140].

A further technique for the reduction of Ostwald ripening is the addition of a second, poorly soluble compound, such as medium chain triglycerides, to the dispersed phase [148-151]. Diffusion controlled mass transfer of both compounds leads to varying concentrations inside the differently sized particles and, in consequence, to an equilibration of their chemical potentials. The mass transfer between the particles is reduced, and the stability of the dispersion can be maintained. The same mechanism was postulated to also apply to amorphous nanoparticles [34, 152]. BHT, primarily intended to be used as crystallization inhibitor, at least theoretically also has the potential to be used as Ostwald ripening inhibitor for fenofibrate. Prerequisite for a successful application is however the complete miscibility of both compounds.

5.2.3 OSTWALD RIPENING IN SAMPLES CONTAINING DIFFERENT POLYMORPHS

In cases where crystalline as well as amorphous/liquid material is present in solution, crystallization and Ostwald ripening compete with each other. Mass transfer depends on the solubility pressure of the individual particles and the energetical advantage realized by the transition process (

Figure 57). Generally, material is transferred following an energy cascade from energetically less favorable small particles to bigger ones and towards a thermodynamically more stable polymorph.

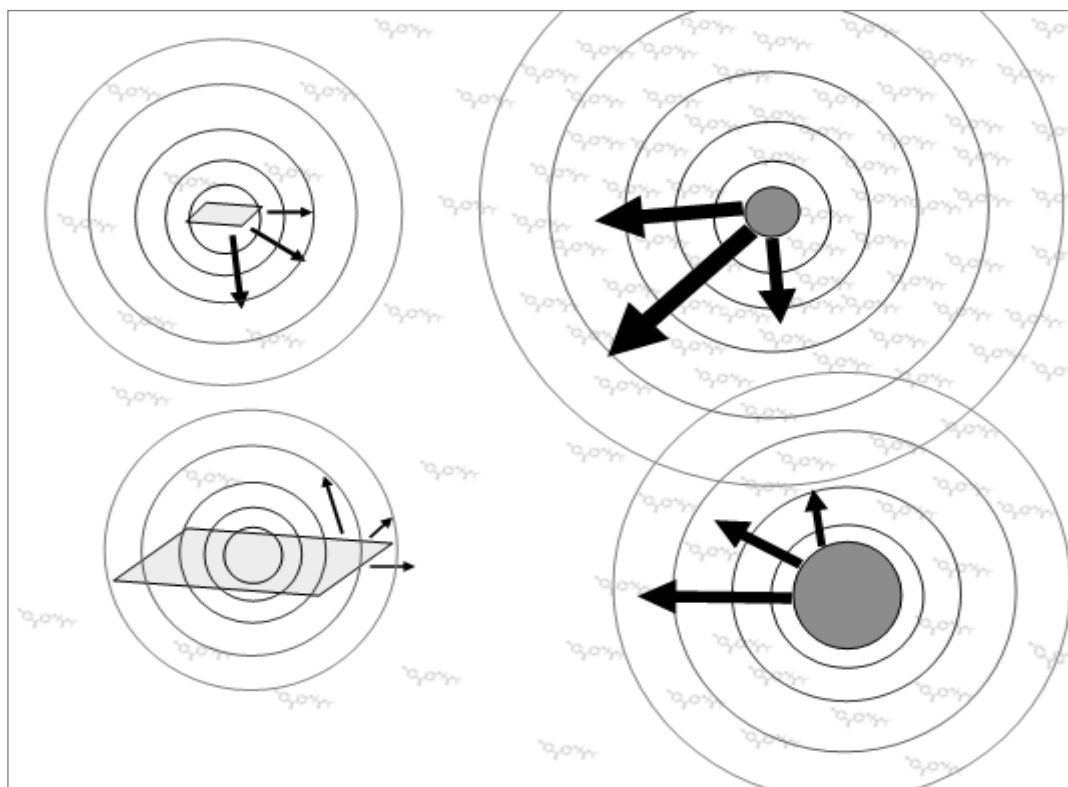


Figure 57: Solubility pressure and mass transfer of different particles in dispersion. Mass transfer takes place from small particles to bigger ones and from liquid/amorphous material to crystals

Whether Ostwald ripening or crystallization dominates the ripening process also depends on the surface integration of solute molecules into the target structure. Surface integration into amorphous or liquid surfaces such as the fenofibrate precipitate is considered less critical than in the highly ordered molecular lattice of the crystalline drug. Crystal growth requires an oriented approach of solute molecules to fit into the surface lattice structure. Also the use of

excipients can modify the surface integration. Despite being thermodynamically disadvantaged, Ostwald ripening can dominate the ripening process in the case that kinetical reasons slow down crystallization. In most cases, Ostwald ripening and crystallization occur simultaneously with different growth rates for each polymorph (**Figure 58**).

Analytical differentiation between Ostwald ripening and crystallization dominated processes is best possible using optical methods, as e.g. PCS or static light scattering are hardly capable to differentiate between amorphous and crystalline particles.

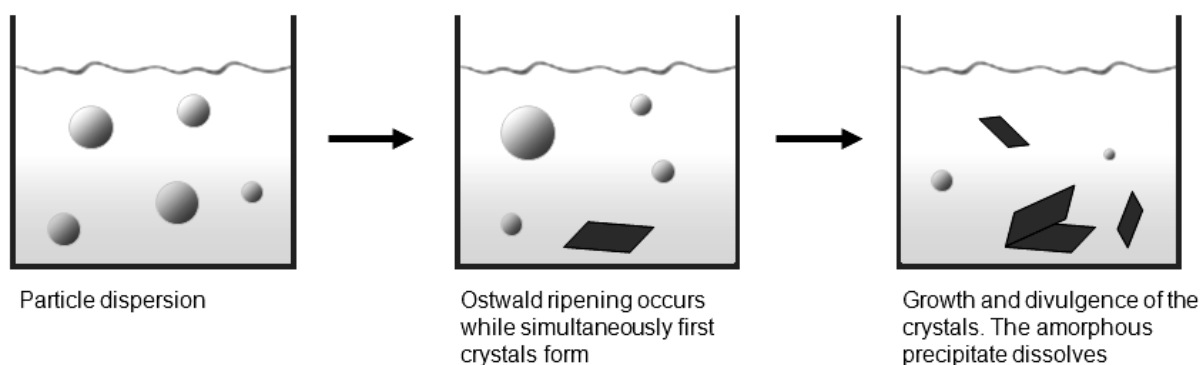


Figure 58: Ageing of a dispersed phase by Ostwald ripening and crystallization

5.2.4 AGGLOMERATION, COALESCENCE AND MECHANICAL PARTICLE

DISRUPTION

Besides the described solubility related phenomena, the homogeneity of dispersions can also be affected by agglomeration and coalescence of the contained particles. Agglomeration (**Figure 59**) especially occurs for samples containing species with opposed or very weak surface charges. High contents of salts can shield the surface charge, thereby destabilizing a formulation. In opposite, adsorption of peptizing agents with excessive positively or negatively charged functional groups can prevent agglomeration by electrostatic repulsion. Certain polymers can stabilize the dispersion upon adsorption to the particle surface by forming sterically repulsive layers on the particle surface.

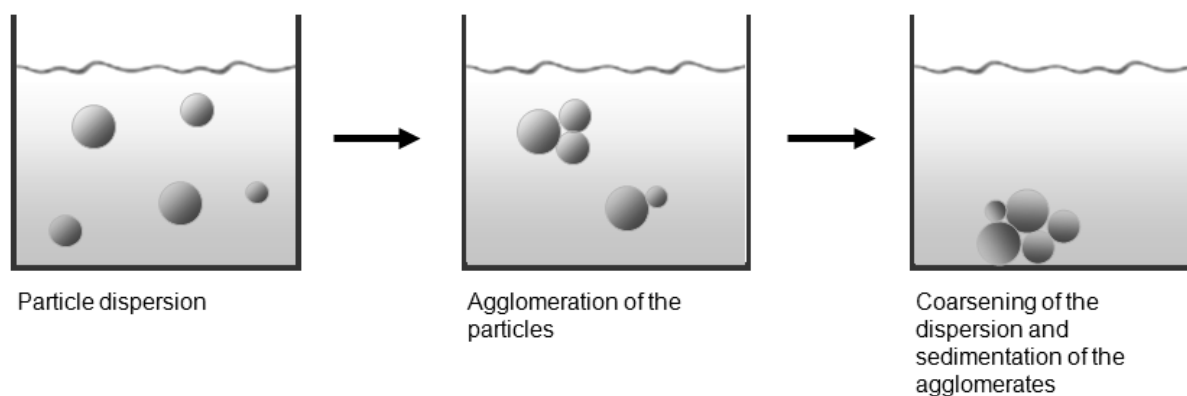


Figure 59: Agglomeration and sedimentation

Agglomeration can be tremendously affected by mechanical stress as is often applied during sample processing, leading to an increased collision rate and intensity. In the case of liquid dispersed phases, the amplified collisions can also boost coalescence, the fusion of particles (**Figure 60**).

The extent to which particle fusion occurs depends on the constitution of the interfacial layer separating dispersed and continuous phase. Important factors are e.g. the packaging, the electrical charge, the intermolecular interaction and the dimensions of the molecules forming the interfacial layer [148]. Especially liquid particles without the protective shield of a surface tension lowering surfactant are sensitive to coalescence. Raising the dispersions' viscosity can be used as additional stabilizing mean. At elevated viscosity the kinetical energy of the particles and the probability of collisions can be reduced [153]. As discussed in **Chapter 2** and **Chapter 3** neither agglomeration nor coalescence of the particles was observed post preparation in the excipient free fenofibrate formulations. Nevertheless, the hydrodynamic pressure imposed on the samples during preparations with the pumping setup suggests, that such phenomena can occur within the mixing process, but are negated by the simultaneously occurring breakdown of the precipitate (refer also to **Section 4.4.6**).

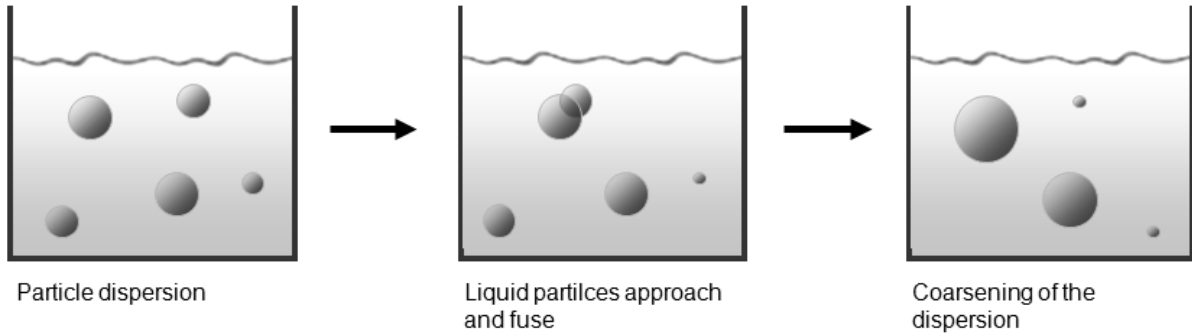


Figure 60: Coalescence of a liquid dispersed phase

Simultaneously to particle fusion, mechanical stress yields in a breakup of existing structures and the fragmentation of the particles (**Figure 61**). The deformation of a particle is proportional to its viscosity, so that the likeliness for particle breakup decreases at higher viscosities of the dispersed phase [148]. However, for breaking up a liquid particle in a mixing process, the disruptive forces applied must exceed the interfacial forces which hold the particle together. In core-shell particles with weak cohesive forces, these superficial forces might contribute the major part to samples' stability.

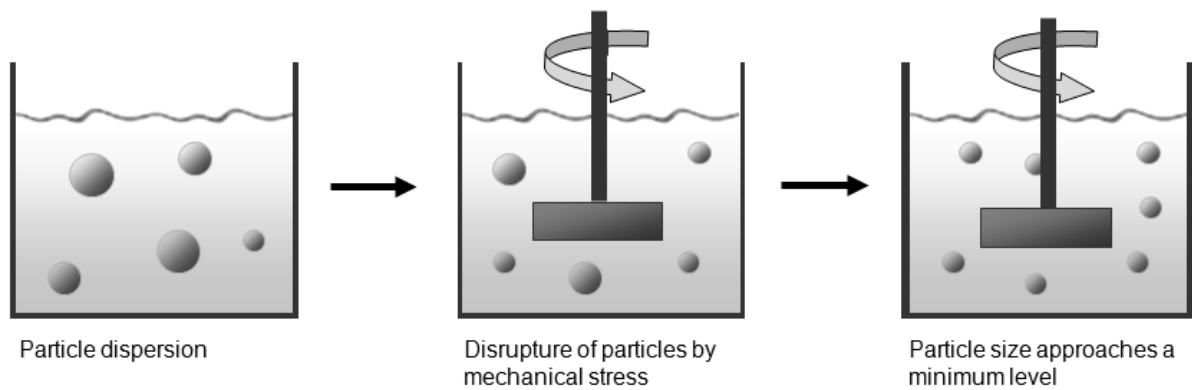


Figure 61: Particle size reduction within mixing processes

5.2.5 SEDIMENTATION AND FLOCCULATION

Sedimentation and flocculation describe a density dependent separation of the dispersed phase. Both mechanisms depend on the density ratio between continuous and dispersed phase, as well as the particle size. According to the Stokes-Einstein equation (**Equation 19, Chapter 2**) [29], both mechanisms apply stronger to bigger particles and agglomerates, while

the movement of small particles (up to 5 μm) is dominated by their Brownian motion [154]. Best measures for preventing sedimentation and flocculation are hence the prevention of agglomeration (**Section 5.2.4**), the preparation of small scaled precipitates as well as an alignment of the densities of dispersed and continuous phase. Both, sedimentation and floatation of the dispersed phase will not be discussed in detail within the scope of this work, as they have been found to be irrelevant for the formulations under investigation.

5.2.6 DOWNSTREAM PROCESSING

It is self-evident that substances that show liquid-liquid phase separation are not necessarily inert, but can exhibit a certain array of side effects. Also BHT, well known as antioxidative reagent for years [144-146], has not been applied at elevated concentrations for improving the physical stability of a drug delivery systems. The intention to use such substances as stabilizing agents hence inevitably brings with it the need to apply them at concentrations in a pharmaceutically applicable range. Therefore processing techniques not only allowing for long term stabilization of the formulations, but also to optimize the excipients concentration in the final product are considered highly beneficial in terms of downstream processing. The functional use of, in this case BHT, can thereby be extended beyond the use as liquid-liquid phase separation mediator and crystallization inhibitor to serve as antioxidant at concentrations suitable and commonly accepted for this purpose.

Lyophilization is well known for its ability to remove not only solvents from pharmaceutical and food products [155], but also to reduce the concentration of other volatile compounds [156, 157]. The sensitivity of the compounds to sublimation within the lyophilization process correlates to their vapor pressure [158]. BHT, with a vapor pressure of 0.8 Pa (25 °C) can be expected to significantly lack behind the sublimation rates of water and most organic solvents used in freeze drying [71, 155], making it an ambitious task to evaluate the extent to which the BHT levels in the samples can be purposefully adopted. Some examples for the vapor pressures of solvents used in lyophilization are given in **Table 4** [71]. For comparison, also the vapor pressure of fenofibrate is shown.

Table 4: Vapor pressures of different solvents used for lyophilization as well as fenofibrate and citric acid and BHT

Solvent / solid compound	Vapor pressure / Pa (25°C), [71]
Acetic acid	1853
Acetone	46396
Acetonitrile	22798
Ethanol	11039
Isopropanol	10839
Methanol	35330
n-Propanol	3506
tert-Butanol	6133
Water	3266
BHT	0.8
Fenofibrate	0.000007

In a series of experiments, the impact of the lyophilization process on the content of BHT in the freeze dried product was evaluated. Thereby different excipients previously used for the stabilization of the dispersions were investigated for their impact on the sublimation behavior of BHT. In addition also trehalose, a cryoprotectant widely used in freeze drying [159], was used for evaluating the applicability of BHT in commonly applied freeze drying processes. Trehalose preferentially forms amorphous lyophilization cakes with a fine filamentous structure when being rapidly cooled [160] as was done within the experiments described here. Without providing heterogeneous nucleation sides, trehalose was expected to scarcely affect the physical nature of the other compounds, namely fenofibrate and BHT. Beyond the impact of lyophilization on the composition of the dispersions, structural variations of the fenofibrate particles caused by the freeze drying process were investigated.

5.3. MATERIAL AND METHODS

5.3.1 EXCIPIENT SCREENING

5.3.1.1. LITERATURE BASED STABILIZATION APPROACHES

Based on bibliographic references about fenofibrate and comparable drugs, a variety of polymeric and surface active reagents were investigated for their stabilizing effects. Only excipients applicable for parenteral administration were used. If necessary, substances with distinct parenteral toxicity were replaced by less toxic alternatives with corresponding functionality. The kind and amount of excipients was adjusted according to **Table 5**. The employed concentrations were selected based on literature data or citations referring to related excipients. The excipients were either dissolved in a 5% (w/w) ethanolic fenofibrate solution, or in the aqueous phase which was used for preparation or subsequent dilution of the dispersions. For increasing the experimental throughput, the dispersions were prepared by hand-mixing (pipetting) of ethanolic and aqueous phase.

D- α -tocopherol-polyethylene-glycol-1000-succinate and gelatin type A were obtained from Sigma-Aldrich, Steinheim, Germany; Tween 80 was purchased from Uniqema, Middleborough, United Kingdom. Phospholipon 100H was a kind gift from Phospholipids GmbH, Köln, Germany. Medium chain triglycerides were a gift from Nordmann, Rassmann GmbH, Hamburg, Germany. Mannitol was purchased from Riedel-de Haen, Seelze, Germany.

Table 5: Literature based formulation screening for fenofibrate dispersions

No.	Excipient content in the ethanolic fenofibrate solution / % (w/w)	Excipient content in the aqueous phase / % (w/w)	Dilution medium	Literature source
1.	1% Phospholipon 100H	0.2% Tween 80 5.5% mannitol	-	[161]
2.	Phospholipon 100H (varying conc.)	Tween 80 (varying conc.)	-	[161]
3.	1% Phospholipon 100H, 1.25% medium chain triglycerides	0.2% Tween 80 5.5% mannitol	-	[34, 161, 162]
4.	-	-	1:1 dilution with an aqueous 0.25% D- α -tocopherol-polyethylenglycol-1000-succinat solution	[163]
5.	0.34% D- α -tocopherol-polyethylenglycol-1000-succinat + 0.66% Phospholipon 100H	-	-	[161, 163]
6.	-	-	16.5% gelatin type A and 1% ascorbyl palmitate	[61]

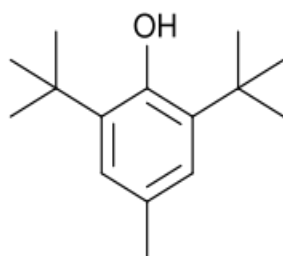
Further screening experiments were accomplished based on a standardized dispersion, to which aqueous excipient solutions were added. These dispersions were prepared using a 5% (w/w) ethanolic fenofibrate solution and water as antisolvent. Preparations were accomplished using the pumping setup comprising a mixing chamber of 0.5 mm i.d. Flow rates of 5 ml/min from the aqueous phase and 1 ml/min from ethanolic phase were applied. Post preparation the dispersions were combined with the aqueous stabilizer solutions in a 1:1 ratio according to **Table 6**. The dispersions were optically and microscopically monitored for signs of agglomeration and crystallization. In case phase separation or unwanted morphological changes (agglomeration, crystallization) occurred, the experiments were aborted. An excipient free fenofibrate dispersion served as positive control.

Table 6: Empirical investigation of stabilizing reagents

No.	Excipient	Excipient content in the stabilizer solution / % (w/w)	Literature source	Substance supplier
1.	Positive control (just fenofibrate)	-	-	Abbott GmbH & Co. KG
2.	Hydroxyethyl starch (Mw 200 kDa)	0.5% 2.5%	[164]	Fresenius Kabi AG, Bad Homburg von der Höhe., Germany
3.	Poloxamer 188 (Lutrol F 68, block copolymers based on ethylene oxide and propylene oxide)	0.5% 2.5%	[9]	BASF Aktiengesellschaft, Ludwigshafen, Germany
4.	Polyethylene glycol 660 12-hydroxystearate) (Solutol HS 15)	0.5%	[91]	BASF Aktiengesellschaft, Ludwigshafen, Germany
5.	Polyvinylpyrrolidone (Kollidon 12 PF)	0.5%	[59, 165-167]	BASF Aktiengesellschaft Ludwigshafen, Germany
6.	(Polyoxyethylen(20) sorbitan monooleate) Tween 80 V Pharma	0.5%	[161, 168]	Uniqema, Middleborough, United Kingdom
7.	PEG-35 castor oil (Cremophor EL, Cremophor ELP)	0.5%	[169]	BASF Aktiengesellschaft Ludwigshafen, Germany
8.	Gelatin (type A)	0.5% 1.0%	[61, 170]	Sigma-Aldrich, Steinheim, Germany
9.	D- α -tocopherol-PEG-1000-succinat	0.25%	[171]	Sigma-Aldrich, Steinheim, Germany

5.3.1.2. BHT AS CRYSTALLIZATION INHIBITOR

In addition to the literature based excipient screening BHT was investigated as potential crystallization inhibitor. Its chemical structure is shown in **Figure 62**.

**Figure 62: Butylated hydroxytoluene**

Coprecipitates with fenofibrate were prepared by adding appropriate amounts of BHT to a 5% (w/w) ethanolic fenofibrate solution, which was subsequently precipitated by addition of the aqueous phase. Further excipients, such as different surfactants and citric acid were added to either the aqueous or the ethanolic phase for further improving the dispersion stability and investigating the impact of varying ionic strength. As for the screening of classical excipients, dispersions were first prepared by hand mixing. The most promising formulations were subsequently transferred to the pumping setup, for optimization of the final composition.

The hydrophilic compounds citric acid and Tween 80 were dissolved in the aqueous phase used as antisolvent, while the lipophilic surfactants dipalmitoyl phosphatidyl choline (DPPC), dipalmitoyl phosphatidyl glycerol (DPPG) and Phospholipon 100H were dissolved in the ethanolic phase. In a series of experiments the impact of BHT on dispersion stability was investigated under varying BHT to fenofibrate ratios according to **Table 7**. In addition, the concentrations of the surfactants were varied extensively for finding an optimal concentration range.

Table 7: Weight ratios of fenofibrate and BHT applied for investigating dispersion stability

BHT / % (w/w)	Fenofibrate / % (w/w)
10	5
5	5
4	5
3	5
2	5
1	5
0.5	5
0.2	5
0.1	5
0.05	5
0.01	5
5	0

For further characterization of the coprecipitates of BHT and fenofibrate, one of the samples was centrifuged using a Sigma 4k15 laboratory centrifuge (DJB Labcare Ltd., Newport Pagnell, England). The obtained residue was colored with methylene blue and sudan red (both Merck Darmstadt, Darmstadt, Germany) for evaluating the precipitates' lipophilicity.

Following the first screening experiments, sample preparation was shifted from manual mixing to the more reproducible preparations using the pumping setup. Latter comprised a 0.25 mm t-piece and PEEK tubing with the same i.d. for the in- and outlets of the mixing chamber. Total flow rates of 60 ml/min were applied for preparation of the dispersions, from which 10 ml/min were derived from the ethanolic phase, 50 ml/min from the aqueous phase. After discarding the forerun, each time about 5 ml of suspension were prepared. Post preparation, the suspensions were stored in 15 ml falcon tubes without dilution or other treatment (besides slight shaking for avoiding decomposition of the dispersions). All experiments were conducted at room temperature. The concentrations of the surface active compounds were adjusted for obtaining the best stabilizing effects in the dispersions, which typically had a much smaller particle size distribution than the hand-mixed samples. Citric acid was not used for dispersions prepared with the pumping setup, as it did not provide additional stabilization compared to an appropriate use of surfactants.

In addition to the excipients used within the screening experiments, brief test runs were accomplished using triacetine, PVP as well as the pegylated phospholipid MPEG-2000-DSPE (1,2-Distearoyl-phosphatidylethanolamine-methyl-polyethyleneglycol conjugate-2000) as stabilizing agents.

For the experiments using triacetine, a saturated triacetine solution was prepared by adding 8.5 g of triacetine to 100 g of highly purified water. After equilibration the supernatant was used as antisolvent for the preparation of the dispersions.

PVP was applied in combination with DPPC and DPPG as well as BHT as stabilizing agents. Besides PVP, which was added to the aqueous phase, all compounds were dissolved in the ethanolic fenofibrate solution. The concentrations applied were 4.2 mg of PVP/g dispersion, 6.7 mg/g dispersion of fenofibrate, 4.1 mg/g dispersion of BHT, 0.1 mg of DPPC and 0.02 mg/g dispersion of DPPG.

MPEG-2000-DSPE was added to the ethanolic phase at 1% and 10% (w/w) of the total amount of phospholipids used. Corresponding to the weight of MPEG-2000-DSPE, the amount of DPPC in the formulations was reduced.

Citric acid monohydrate and triacetine were obtained from Carl Roth GmbH & Co., Karlsruhe, Germany. BHT and triacetine were purchased from Fluka Chemie GmbH, Buchs, Switzerland. PVP (Povidone K-12) was a gift from BASF, Ludwigshafen, Germany. DPPC and DPPG were purchased from Lipoid GmbH, Ludwigshafen, Germany. MPEG-2000-DSPE was a kind gift of the same company.

5.3.1.3. SAMPLE ANALYSIS

Within the excipient screening, sample stability was mainly investigated by taking samples at regular time points and performing light-microscopy, as well as by monitoring the presence of crystalline material using cross polarized filters. The light microscope used was a Nikon Labophot equipped with a JVC digital camera Model JVC TKC 1380E (Nikon GmbH, Düsseldorf, Germany). Also macroscopical observations were found to be an important indicator for dispersion stability, as crystals often adsorbed to the wall of the sample container, withdrawing them from microscopical observation.

For selected formulations, the impact of BHT on dispersion morphology was investigated by wide-field fluorescence microscopy as well as AFM measurements. AFM measurements allowed to gain a deeper insight in the mechanical properties of the precipitates. Force-distance measurements were used for the analysis of coprecipitates containing a 3:5 ratio (w/w) of BHT and fenofibrate as well as of the precipitation products of the individual compounds. For comparison the measurements were extended to coprecipitates of BHT with loratadine and lopinavir. As for fenofibrate, these samples were prepared from 3:5 mixtures of BHT with the drugs. Double distilled water was used as antisolvent. The precipitates containing just BHT or fenofibrate were prepared from a 5% (w/w) ethanol solution. Force distance curves obtained by AFM measurements were fitted exponentially. The resulting R2 values are summarized in **Table 8**.

Table 8: R² values for the exponential fit from the elasticity data obtained from force-distance measurements

BHT to drug ratio	R²
BHT	0.8680
BHT:Fenofibrate 3:5	0.9928
BHT:Lopinavir 3:5	0.9441
BHT:Loratadine 3:5	0.9973

Instrumentation, sample preparation, measurement conditions and data analysis for the accomplishment of the AFM and wide-field fluorescence microscopy measurements were equivalent as described in **Chapter 1, Sections 4.3.3 and 4.3.4**.

For those dispersions prepared using the pumping setup, as well as redispersed samples from lyophilization experiments (see also **Sections 5.3.2 and 5.4.2.2**), samples were additionally monitored by static light scattering using a Horiba LA-950 (Retsch Technology, Haan, Germany). The mean particles size was investigated after sufficient dilution of the samples. The particle size distribution in the dispersions was analyzed using the Span values. Span values < 1 were considered to represent a homogeneous particle size distribution. Measurement conditions for the laser diffraction measurements were the same as applied in **Chapter 2, Section 2.3.1**. Some of the lyophilization products were additionally exposed to the field of an ultrasonic bath (Bandelin Sonorex super RK 510 H; Bandelin electronic GmbH & Co. KG; Berlin; Germany) for breaking down contained agglomerate structures.

5.3.2 LYOPHILIZATION

5.3.2.1. SAMPLE PREPARATION

Lyophilization was used for downstream processing of the fenofibrate dispersions in terms of solvent removal and optimizing of the BHT content. Two test runs were accomplished using differently concentrated dispersions composed of an ethanolic fenofibrate solution and water, hence containing the drug as sole solute. In addition, the impact of different excipients on the freeze drying process was evaluated according to the experimental matrix shown in **Table 9**. Thereby different amounts of BHT, the surfactants Tween 80 and Phospholipon 100H, trisodium citrate as well as the cryoprotectant trehalose were investigated.

Table 9: Differently composed fenofibrate dispersions used for lyophilization (values represent the composition in the final dispersions prior to the lyophilization process)

No.	Compound	Concentration / g/g dispersion
Dispersion 1	Fenofibrate	0.009
	BHT	0
	Phospholipon 100H	0
	Tween 80	0
	Trisodium citrate	0
Dispersion 2	Fenofibrate	0.007
	BHT	0
	Phospholipon 100H	0
	Tween 80	0
	Trisodium citrate	0
Dispersion 3	Fenofibrate	0.007
	BHT	0.007
	Phospholipon 100H	5.4E-05
	Tween 80	3.4E-07
	Trisodium citrate	0.006
Dispersion 4	Fenofibrate	0.007
	BHT	0.0003
	Phospholipon 100H	5.4E-05
	Tween 80	3.4E-07
	Trisodium citrate	0.006
Dispersion 5	Fenofibrate	0.007
	BHT	0.007
	Phospholipon 100H	5.4E-05
	Tween 80	3.4E-07
	Trisodium citrate	0
Dispersion 6	Fenofibrate	0.007
	BHT	0
	Phospholipon 100H	5.4E-05
	Tween 80	3.4E-07
	Trisodium citrate	0.006
Dispersion 7	Fenofibrate	0.007
	BHT	0.007
	Phospholipon 100H	0
	Tween 80	0
	Trisodium citrate	0

No.	Compound	Concentration / g/g dispersion
Dispersion 8	Fenofibrate	0.007
	BHT	0.007
	Phospholipon	2.6E-05
	Tween 80	8.4E-07
	Trisodium citrate	0.006
	D (+) Trehalose	0.01
Dispersion 9	Fenofibrate	0.006
	BHT	0.006
	Phospholipon	2.4E-05
	Tween 80	7.0E-07
	Trisodium citrate	0.048
	D (+) Trehalose	0.04
Dispersion 10	Fenofibrate	0.006
	BHT	0.006
	Phospholipon	2.4E-05
	Tween 80	6.6E-07
	Trisodium citrate	0.045
	D (+) Trehalose	0.07

All samples were flash-frozen by directly injecting the freshly prepared dispersions into a Dewar containing liquid nitrogen (**Figure 63**). The flow rate of the dispersion was adjusted the way that clearly distinguishable frozen droplets sized about 0.8 mm in diameter were obtained. The suspensions were prepared with the pumping setup at a total flow rate of 36 ml/min (30 ml/min for the aqueous phase, 6 ml/min for the ethanolic phase). If possible, the dispersions were prepared using a 0.25 mm i.d. t-piece as mixing chamber. Dispersions no. 1, 2, 4 and 6 shown in **Table 9**, had to be prepared using a 0.5 mm mixing chamber, as the 0.25 mm mixing chamber partly blocked due to adsorbing solute within the preparation of the dispersions.

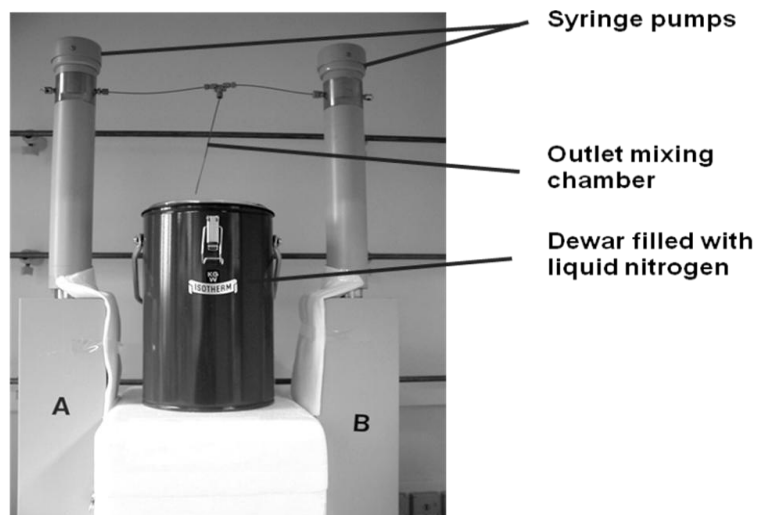


Figure 63: Setup for flash freezing the fenofibrate dispersions

The lyophilization of dispersion 1 was accomplished using an Epsilon 2-12 D, dispersions 2 to 10 were lyophilized using of an Epsilon 2-6D freeze dryer (both Martin Christ Gefriertrocknungsanlagen GmbH, Osterode am Harz, Germany). The shock frozen dispersions were placed on lyophilization plates and cooled with liquid nitrogen until the onset of the vacuum of the freeze dryer. The freeze dryer was started in advance for cooling the plates down to -45 to -50°C and warming up the vacuum pump to assure a continuous freeze chain and avoid thawing of the samples. The freeze drying protocols were varied within the individual experimental sets, for optimizing the method and evaluating the robustness of the process. The protocol applied for dispersion 1 is shown in **Table 10**, the one for dispersion 2 in **Table 11**, the protocol applied for dispersions 3-7 is shown in **Table 12** and the one for dispersions 8-10 in **Table 13**.

Table 10: Freeze drying protocol applied for the lyophilization of fenofibrate dispersion 1

No.	Process phase	Time / hh:mm	Temperature /°C	Vacuum / mbar
1	Sample loading	00:00	-50	---
2	Main drying	00:01	-50	0.045
3	Main drying	00:05	-50	0.045
4	Main drying	10:00	-16	0.045
5	Main drying	50:00	-16	0.045
6	Main drying	00:01	-16	0.007
7	Secondary Drying	05:00	5	0.007
8	Secondary Drying	15:00	10	0.007

Table 11: Freeze drying protocol applied for the lyophilization of fenofibrate dispersions 2

No.	Process phase	Time / hh:mm	Temperature /°C	Vacuum / mbar
1	Sample loading	00:00	20	---
2	Freezing	01:30	-45	---
3	Freezing	02:00	-45	---
4	Freezing	00:30	-20	---
5	Main drying	00:10	-10	0.25
6	Main drying	47:59	-10	0.25
7	Main drying	06:30	0	0.25
8	Secondary Drying	00:01	10	0.001
9	Secondary Drying	02:01	20	0.001
10	Secondary Drying	11:59	20	0.001

Table 12: Freeze drying protocol applied for the lyophilization of fenofibrate dispersions 3-7

No.	Process phase	Time / hh:mm	Temperature /°C	Vacuum / mbar
1	Sample loading	00:00	-50	---
2	Main drying	00:40	-30	0.1
3	Main drying	05:00	-30	0.1
4	Main drying	00:40	-10	0.1
5	Secondary Drying	00:01	-10	0.009
6	Secondary Drying	01:00	20	0.009
7	Secondary Drying	99:00	20	0.009

Table 13: Freeze drying protocol applied for the lyophilization of fenofibrate dispersions 8-10

No.	Process phase	Time / hh:mm	Temperature /°C	Vacuum / mbar
1	Sample loading	00:00	-50	---
2	Main drying	00:40	-30	0.05
3	Main drying	05:00	-30	0.05
4	Main drying	65:00	-30	0.05
5	Secondary Drying	00:01	-10	0.009
6	Secondary Drying	01:00	20	0.009
7	Secondary Drying	99:00	20	0.009

5.3.2.2. HPLC ANALYSIS

The concentration of fenofibrate and BHT in the lyophilizates was determined by HPLC using a Dionex unit (Dionex Corporation GmbH, Germering, Germany) equipped with a P680 HPLC pump, an ASI-100 automated sample injector, a STH 585 column oven and an UVD 170U diode-array detector. The HPLC column used was a Lichrospher 100 RP-18 endcapped (5 μm) equipped with a Lichrocart 4-4 Lichrospher 100 RP-18 precolumn (both Merck KgaA, Darmstadt, Germany). A detection wavelength of 278 nm was used for both, BHT as well as fenofibrate. The oven temperature was set to 35°C, the flow rate was 1.2 ml/min and the temperature of the HPLC vial rack was set to 25°C. 195 μl of the samples were transferred to the HPLC vials containing volume reducing glass inserts. Data analysis was performed using the Chromeleon version 6.60 SP3 Build 1485 software.

5.3.2.3. SCANNING ELECTRON MICROSCOPY

Scanning electron microscopy images were accomplished using a JSM-6500 F field emission scanning electron microscope (Joel, Ebersberg, Germany). Samples were directly spread on carbon pads placed on a copper sample holder. Before the measurements they were sputtered with carbon.

5.3.2.4. RESIDUAL ETHANOL CONTENT

The ethanol content in the lyophilizates was determined using static headspace gas chromatography. Samples were analyzed using a DANI 6000 equipped with a HS 850

automated headspace sampler and a flame ionization-detector (Dani, Monza, Italy). A DB-WAX capillary column 60 m x 0.32 mm i.d. and 0.5 μm film thickness was used (Agilent Technologies Sales & Services GmbH & Co.KG, Waldbronn, Germany). Helium was used as the carrier gas at a flow rate of 5 ml/min. Injections were carried out in split mode, with a total split of 1 ml/min (1:1). The injector temperature was 160°C and the detector temperature was set to 240°C. The oven temperature remained constantly at 60°C. Samples were provided in 20 ml headspace vials conditioned in the headspace oven at 80°C under continuous gentle shaking for 2 h. The loop temperature was set to 110°C with a transfer line temperature of 120°C. Pressurization time for the vial, loop equilibrium and the injection time were adjusted to 0.16 min. Methanol was used as internal standard (Hydranal[®]-Methanol dry, Riedel-de Haën, Sigma-Aldrich GmbH, Seelze, Germany).

5.3.2.5. RESIDUAL WATER CONTENT

The moisture in the lyophilizates was determined by coulometric Karl-Fischer titration using a 737 KF Coulometer equipped with a 703 ti Stand sampling unit (both Deutsche Metrohm GmbH & Co, Filderstadt, Germany). For analysis ~180 mg of each sample were dissolved in methanol (Hydranal[®]-Methanol dry, Riedel-de Haën, Sigma-Aldrich GmbH, Seelze, Germany). The exact mass of methanol was determined gravimetrically. Samples were prepared in a glove box purged with dry nitrogen for avoiding sample hydration by the surrounding atmosphere. Aliquots were withdrawn with a syringe and transferred to the measurement cell with the titration solution (Hydranal[®]-Coulomat AG, Riedel-de Haën, Sigma-Aldrich GmbH, Seelze, Germany).

5.3.2.6. X-RAY POWDER DIFFRACTION

Wide angle X-ray powder diffraction (XRD) was used to study the physical state of the fenofibrate bulk substance as well as the lyophilized dispersions 1 and 2. Samples were placed on a quartz sample holder and analyzed using a XRD 3000 TT diffractometer equipped with a copper anode (40 kV, 30 mA, wavelength 0.154178 nm), (Richard Seifert & Co, Ahrensburg, Germany). Analysis was accomplished in an angular range from 5-40° (2 theta), with steps of 0.05° at a duration of 2 s per step.

5.3.2.7. DIFFERENTIAL SCANNING CALORIMETRY

40 µl crimped aluminum pans (ME-26763, Mettler Toledo GmbH, Gießen, Germany) were filled with ~8 mg of sample and closed with aluminum caps. Measurements were accomplished using a DSC 821e differential scanning calorimeter equipped with a TS0801RO Sample Robot (both Mettler Toledo GmbH, Gießen, Germany) and a vacuum oven type VO 200 (Memmert GmbH & CoKG, Schwabach, Germany). Samples of the fenofibrate bulk substance as well as the lyophilized dispersions 1 and 2 were used. They were cooled from 20°C to -50°C and reheated to 100°C with a scanning-rate of 2°C/min. Data analysis was performed with the STARe Software Version 9.01 (Mettler Toledo GmbH, Gießen, Germany).

5.4. RESULTS AND DISCUSSION

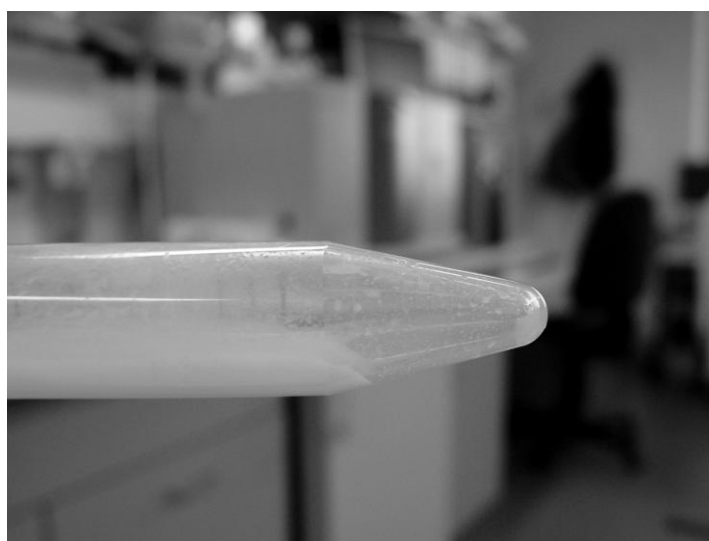
5.4.1 EXCIPIENT SCREENING

5.4.1.1. CLASSICAL STABILIZATION APPROACHES

Lagging behind the expectations [34, 161-163], the literature based formulation approaches only allowed for a moderate stabilization of the fenofibrate dispersions. Significant crystallization occurred in all cases latest 20 min after preparation of the dispersions. Also the application of medium chain triglycerides as Ostwald ripening inhibitor did not fulfill its purpose to a comparable extend as was described in literature [34]. Latter might be attributed to the exchange of the parenterally unacceptable sodium dodecyl sulfate mentioned in the reference [34], by the less toxic surfactants Tween 80 and Phospholipon 100H. An overview of the results is presented in **Table 14**, with the individual formulations being rated in comparison to the stability of an excipient free drug formulation. Experimental data could only be qualitatively evaluated, as adhesion of crystals to the sample container (**Figure 64**) and the formation of air bubbles for dispersions prepared with the pumping setup prohibited proper size determination and quantification of the experimental data.

Table 14: Literature based excipient screening for fenofibrate dispersions. (+) improved stability compared to the excipient free drug formulation; (\pm) equivalent stability, (-) destabilizing effect

No.	Excipients used	Stability relative to excipient free fenofibrate formulation
1.	Phospholipon 100H Tween 80 Mannitol	\pm
2.	Phospholipon 100H Tween 80 (varying concentrations)	-- to ++ (depending on the concentrations applied)
3.	Phospholipon 100H Tween 80 Mannitol Medium chain triglycerides	+
4.	1:1 dilution of the dispersion with an aqueous 0.25% D- α -tocopherol-polyethylenglycol-1000-succinat solution	+
5.	D- α -tocopherol-polyethylenglycol-1000-succinat Phospholipon 100H	+
6.	Gelatin Ascorbyl palmitate	-

**Figure 64: White junks of agglomerated fenofibrate crystals partly adhere to the sample container upon crystallization of the dispersions**

Also the screening for the stabilizing effects of the hydrophilic excipients introduced via an aqueous stabilizing solution post preparation of the dispersions led to unsatisfying results. For most substances, crystallization, as the main destabilizing factor, was significantly increased

compared to the excipient free formulations (**Table 15**). The observed stabilizing effect of gelatin was predominantly attributed to an unspecific increase in sample viscosity.

Table 15: Investigation of the stabilizing effects of individual excipients. (+) Improved stability compared to the excipient free drug formulation; (±) equivalent stability, (-) destabilizing effect

No.	Excipients used	Stability relative to excipient free fenofibrate formulation
1.	Positive control (just fenofibrate)	±
2.	Hydroxyethyl starch	---
3.	Poloxamer 188	---
4.	Polyethylene glycol 660 12-hydroxystearate	-
5.	Polyvinylpyrrolidone	-
6.	Tween 80	-
7.	Cremophor EL & ELP	-
8.	Gelatin	+
9.	D- α -tocopherol-PEG-1000-succinat	-

In summary, the combination of different surfactants exhibited the best stabilizing effects on the fenofibrate dispersions (see **Table 14** and **Table 15**). This could be best observed in the case of Phospholipon 100H, which was, at low concentrations and in combination with Tween 80, capable to decrease crystallization by the formation of a protective surfactant layer on the particle surface. However, the effective concentration range for the surfactants was found to be extremely narrow. Phospholipon 100H dispersions being originally homogeneous after preparation showed distinct agglomeration upon ageing of the dispersions (**Figure 65**). Already the decrease in total surface area due to Ostwald ripening of the dispersed phase was sufficient to provoke additional destabilization once a surfactant concentration required for surface coverage of the particles was exceeded. Also, some of the lipophilic surfactant enclosed inside of the precipitate particles by the precipitation process might diffuse to the particles' surface, additionally increasing the local surfactant concentration and boosting aggregation. The formulations were also sensitive to changes in the concentrations of the other surfactants applied. While the described agglomeration behavior was found to be typical for Phospholipon 100H, crystallization became distinctly more pronounced for all surfactants when applied at inappropriately high concentrations. The reason therefore was attributed to a solubilization of fenofibrate in the continuous phase, going along with an

increased diffusion rate and mass transfer. Indeed, this high sensitivity of fenofibrate to the narrow effective concentration range of excipients applied might in part be responsible for the failure of some of the excipients, and outlines the need for an ongoing optimization process within formulation development.

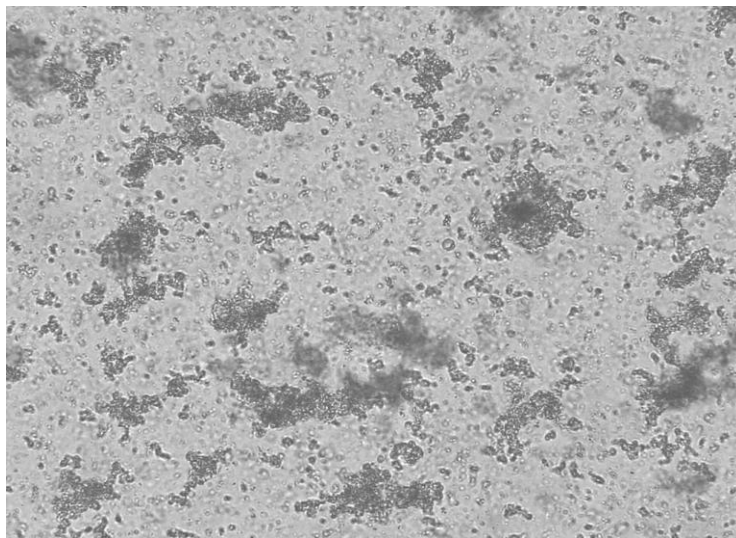


Figure 65: Agglomeration of a dispersion containing excessive amounts of Phospholipon 100H

Knowing that the fenofibrate formulations consist of a liquid dispersed phase, the mechanisms proving to be most effective in stabilizing the dispersions were found to be equivalent to those being generally applied for emulsions. These are namely an increase in the viscosity of the continuous phase (gelatin), and the adsorption of a protective layer of surface active reagents. The functionality of the surfactants is not necessarily based on a reduction of the particles' surface tension, but rather represents a mechanical barrier for mass transfer from and to the drug particles, thereby minimizing Ostwald ripening and crystallization. In contrast, at the concentrations applied, most polymeric excipients failed to improve dispersion stability, as they partly led to agglomeration of the particles, and more importantly increased the crystallization rate. For some of these macromolecular excipients, it can be anticipated that they impaired the surface integrity of the precipitate particles.

5.4.1.2. INFLUENCE OF BHT ON DISPERSION MORPHOLOGY AND STABILITY

Dispersions prepared from ethanolic BHT solutions without fenofibrate were found to contain a thermodynamically metastable liquid precipitate, comparable to the dispersed phase observed for the drug (**Figure 66**). Crystallization set on at the surface of the dispersions or at the container walls, which served as nucleation sides. Once Crystallization started, the whole amount of BHT crystallized within about 10 min.

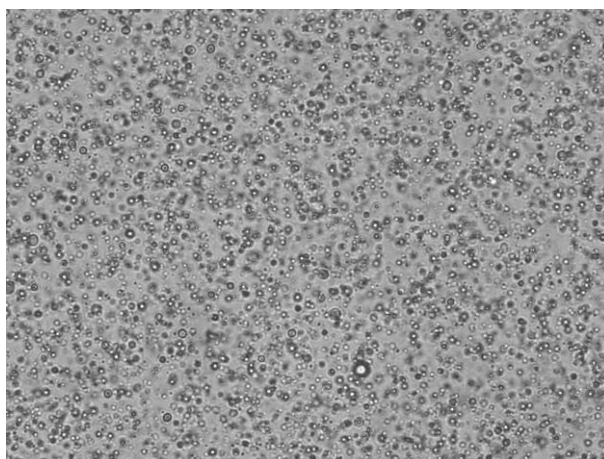


Figure 66: Dispersion obtained from an ethanolic BHT solution upon addition of water

In combination with fenofibrate, BHT formed apparently homogeneous, lipophilic coprecipitates. Upon centrifugation of the samples containing a 5:5 mixture of BHT and fenofibrate, strong coalescence of the particles was observed (**Figure 67**), with the dispersed phase being highly viscous and ductile, drawing filaments when being mechanically disrupted.

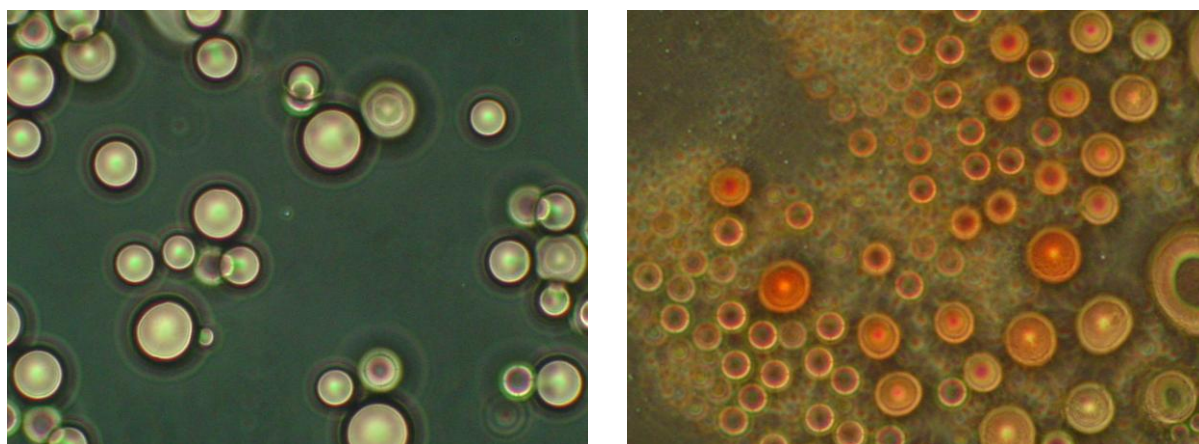


Figure 67: Coprecipitates of BHT and fenofibrate in a 5:5 ratio (w/w) coloured with methylene blue (left) and sudan red (right)

For dispersions containing fenofibrate and BHT which were prepared with the pumping setup, the obtained particle size distributions became broader at increasing BHT concentrations. This effect was attributed to the elevated volume of the precipitate. It was accompanied by a tremendous reduction in mixing chamber and capillary blocking (see also **Section 5.4.2**) due to a liquefaction of the particles which facilitated the passage through the mixing chamber. Particles were thought to have a higher deformability compared to the BHT free fenofibrate formulations when being exposed to hydrodynamical and viscous stress. Indeed, when investigating a 3:5 mixture of BHT and fenofibrate by atomic force microscopy, the precipitate was found to have elasticity moduli distinctly lower than those obtained for fenofibrate or BHT alone (**Figure 68**). Extending the experiments to the drugs lopinavir and loratadine, it was found that this liquefaction did not occur due to a specific interaction between fenofibrate and BHT, but is a general phenomenon also applying to other lipophilic substances. The coprecipitates of lopinavir and loratadine with BHT showed explicitly reduced elasticity moduli compared to the individual compounds. All particles prepared from the same educts had a comparable appearance and mechanical properties, proving the homogeneity of the precipitation process without separation of the two solutes.

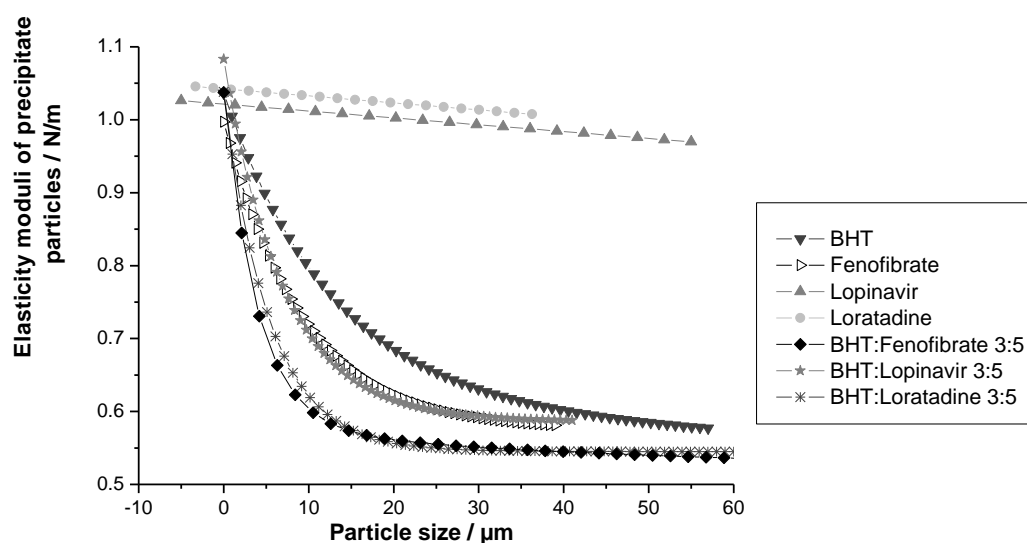


Figure 68: Elasticity of the coprecipitates of 3:5 mixtures of BHT with fenofibrate, lopinavir and loratadine. For comparison, also the force-distance curves for precipitates of the individual substances are shown

The coprecipitates had a gel to rubber like appearance and were easily mechanically penetrable, e.g. by piercing them with an AFM tip (**Figure 69, left**). While the coprecipitate particles prepared from loratadine and fenofibrate rapidly resumed their original round shape after removal of the mechanical stress, lopinavir, the most lipophilic of the compounds, was found to form viscoelastic and extremely ductile coprecipitates that only partly reconstructed (**Figure 69, right**). None of the particles burst or showed leakage of the inner phase when being penetrated with the cantilever, indicating a highly flexible and cohesive surface structure. The exclusively aqueous environment of the continuous phase provided within the AFM measurements thereby seemed to promote surface integrity due to strong repulsive effects on the lipophilic precipitates.

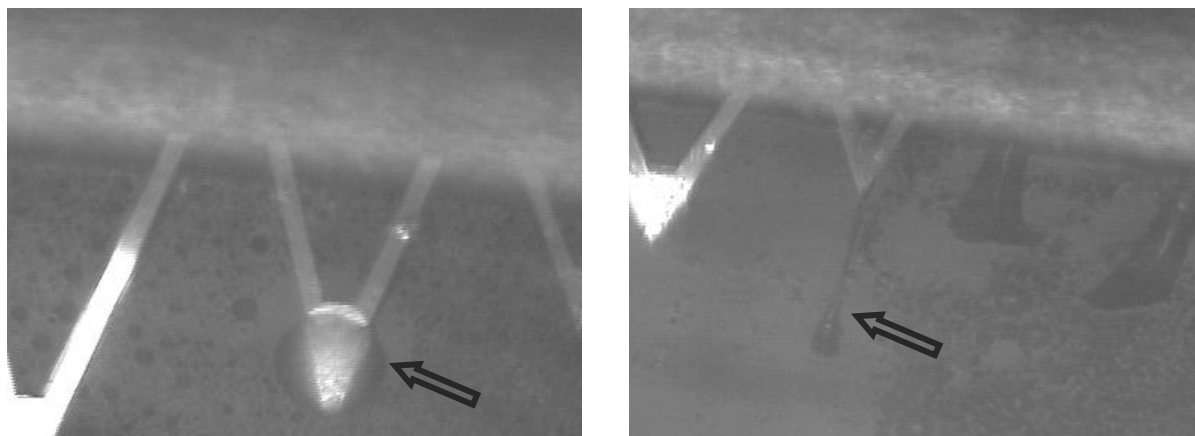


Figure 69: Mechanical stress applied on the coprecipitates of BHT with loratadine (left) and lopinavir (right). Viscoelastic, chewing gum like filaments form from the lopinavir coprecipitates, while the BHT:loratadine particles showed predominantly elastic behavior

Interestingly, when further investigating the fenofibrate dispersions by light microscopical observation, it was found that the addition of BHT not only affected the structural characteristics of the precipitate, but also led to a distinctly reduced crystallization rate, indicated by a decelerated and quantitatively reduced observation of crystalline material. Both effects were found to be concentration dependent, as an increase in the ratio of BHT to fenofibrate improved the dispersions' stability against crystallization and decreased the dispersed phases' viscosity. Most pronounced were these effects at weight ratios of BHT to fenofibrate of 1:5 to 5:5 (corresponding to mole fractions of BHT of 0.2 to 0.6). A saturation of the stabilizing properties of the excipient was even at BHT concentrations exceeding that of the drug not observed. This indicates, that a tight and hence saturable drug-excipient interaction, e.g. due to complexation of fenofibrate, did not occur. In addition, a long lasting molecular interaction would have abolished the liquid state of the precipitate in favor to a solid amorphous or crystalline phase. The liquefaction caused by the addition of BHT hence shows nicely, that the molecular interaction with the drug is only temporary. Other than classical crystallization inhibitors, BHT did not bind tightly to the target molecules, but statistically reduced the likelihood of homogeneous drug-drug interactions by the formation of transient drug-BHT interactions.

Summarizing, the addition of BHT had the following effects on the fenofibrate dispersions:

- **On a molecular level:** Transient molecular interaction between fenofibrate and BHT
- **On a macroscopical level:** Modification of the drug particles' mechanical properties (liquefaction)
- **Thermodynamically:** Concentration dependent stabilization of the liquid dispersed phase and reduction of the crystallization rate

The above mentioned effects of BHT on crystallization as well as the mechanical properties of the precipitate were more pronounced when the nucleation kinetics were shifted from the continuous phase towards the dispersed phase, e.g. by addition of further excipients such as citric acid (for background information on the varying crystallization sides refer also to **Section 5.2.1**). As with BHT, also citric acid was found to affect the structural integrity of the precipitate, providing further insights into the mechanisms defining dispersion stability. Originally intended to be used as peptizing agent for minimizing particle agglomeration within the precipitation process, citric acid was found to distinctly increase the particles' viscosity, especially in dispersions containing no or low amounts of BHT. In addition, the particles' structural integrity was tremendously impaired, leading to coalescence and particle rupture, upon which the coalescent particles often remained frozen in a viscous, irregular shaped state. Wide-field fluorescence microscopy measurements showed nicely, that the interaction potential of the subparticles remained weak and occurring subparticle clusters did not span space to form a coherent system inside the particles (**Figure 70**). The increased viscosity of the particles was hence not caused by a gelling effect, as was regularly reported for colloidal systems [172-174].

It was concluded, that, as for BHT, the impact of citric acid on the particle structure was based on interactions on a molecular level. Obviously, salting out effects caused by the acid led to an intensified interaction of the lipophilic fenofibrate molecules. The resulting reduced molecular mobility caused a viscosity increase in the interstitial space between the subparticles and an incapability to countervail structural inhomogeneities in the particles'

interfacial layer to the continuous phase, making the particles more sensitive to coalescence. The effects of citric acid were found to be independent from the dispersions' pH.

Summarizing, the addition of citric acid had the following effects on the fenofibrate dispersions:

- **On a molecular level:** Salting out effect on fenofibrate, leading to an impaired molecular mobility and an impaired surface integrity (resistance to fusion or bursting) of the particles
- **On a macroscopical level:** Coalescence and rupture of the particles; concentration dependent shift of the crystallization kinetics from the continuous phase towards the dispersed phase
- **Thermodynamically:** Crystal nucleation inside or at the surface of the precipitate particles; reduced crystallization rate in the continuous phase

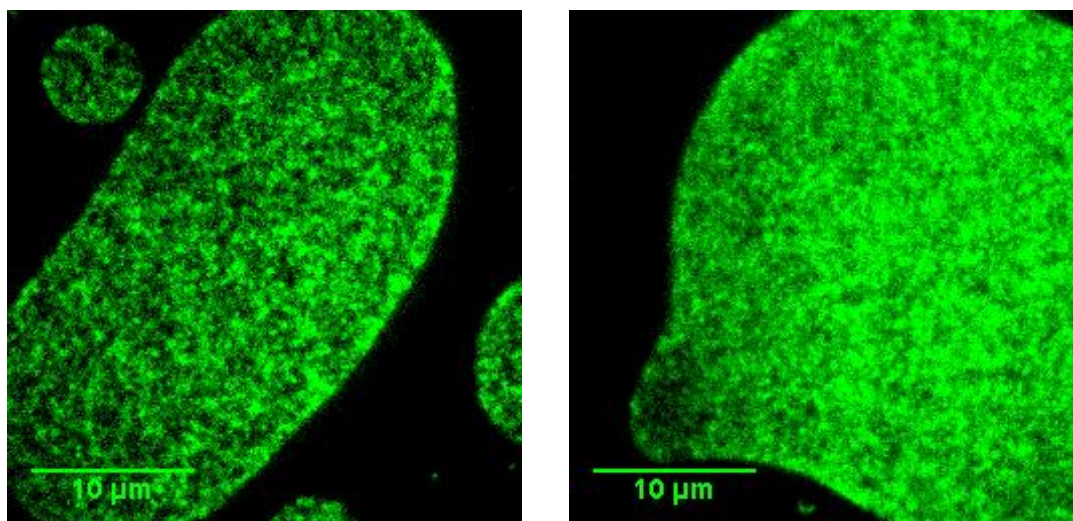


Figure 70: Coalescence of highly viscous precipitate particles as a result of the presence of citric acid in the continuous phase (sample composition: BHT:fenofibrate ratio 0.05:5, Phospholipon 100H, and Tween 80, citric acid)

When using BHT as coprecipitant in the presence of citric acid, already BHT to fenofibrate ratios as low as 0.01:5 further amplified particle coalescence. At higher BHT concentrations

also the particles' viscosity decreased, while the obviously occurring interaction between fenofibrate and BHT remained too weak to allow for the formation of a sustainable interfacial layer at the particle surface. The additional use of surfactants in combination with BHT was found to overcome this drawback. It allowed to increase the colloidal stability, as well as to reduce diffusion controlled interparticulate mass transfer. By the use of e.g. combinations of Tween 80 and Phospholipon 100H, coalescence of the particles and Ostwald ripening could be slowed down remarkably, while at the same time the crystallization inhibiting effect of BHT could be maintained. At optimized surfactant concentrations, stabilization of the dispersions against crystallization became so effective that the additional use of citric acid was no longer necessary for adjusting the crystallization kinetics between the continuous and the dispersed phase. The application of citric acid and other ionic compounds can be considered a backup option in the formulation of fenofibrate dispersions. Most importantly, its use provides an effective mean for understanding the underlying mechanisms which define the physical state of the precipitates.

Summarizing, the concerted combination of citric acid, surfactants and BHT had the following effects on the fenofibrate dispersions:

- **On a molecular level:** Counteracting effects of BHT (increased molecular mobility) and citric acid (salting out, intensified molecular interaction); concentration dependent dominance of either effect
- **On a macroscopical level:** Stable particles due to internal stabilization by BHT and particle surface stabilization by the surfactants
- **Thermodynamically:** Crystallization is shifted from the continuous towards the dispersed phase, and simultaneously suppressed by the addition of BHT; overall reduced crystallization rate in the continuous as well as in the dispersed phase

Despite the given interaction potential of fenofibrate and BHT, the miscibility of the compounds was not necessarily complete on a molecular level, as full inhibition of Ostwald

ripening, which might have been expected to occur in the case of complete miscibility, could not be obtained. Also, above BHT to fenofibrate ratios higher than 3:5, sufficient compositional stability of the particles could no longer be assured. Even in the presence of surfactants, Ostwald ripening led to the formation of liquid, BHT rich particles, identifiable by their elevated size and their adhesiveness to the sample container and drug crystals. In consequence, the 3:5 ratio was found to be the optimal concentration in terms of crystallization inhibition and colloidal stability of the dispersions. Also the effectiveness of the surfactants was found to be very sensitive to variations in the concentrations applied. Exceeding the concentrations required for stabilization of the dispersions, surfactants induced crystallization in the continuous phase by increasing fenofibrate's solubility and hence interparticulate mass transport.

The above described results hence clearly demonstrate the available pathways for influencing the fenofibrate dispersions' structure and stability, the necessity of a combination of different kinds of surfactants however also highlights the distinct need for a fine tuning of the dispersions composition. As especially the concentration of the surfactants applied depends on the accessible particle surface and hence the amount and particles size distribution' of the precipitate. The particles' morphology mandatorily needs to be considered during formulation development.

5.4.1.3. APPLICATION OF THE STABILIZING MEASURES TO THE PREPARATION OF DISPERSIONS WITH THE PUMPING SETUP

The insights gained on the stabilizing effects of certain excipients were transferred from screening experiments to nanoparticle preparations using the pumping setup. Purpose of the transfer was to prepare dispersions with a reproducible particle size distribution and hence a narrow, measurable crystallization pattern. Sample preparation concentrated mainly on using surface active reagents as well as BHT. The use of citric acid was only accomplished to a moderate extend, as no additional stabilizing effect compared to the sole use of surfactants was expected.

As anticipated, excipient free formulations were extremely prone to crystallization, which set in immediately after sample preparation (**Figure 71**). The elevated Span values as well as the

width of the error bars indicate the presence of significant amounts of crystals. Due to the increased solubility pressure of the small particles, the instability of the dispersions was more distinct than was observed for the dispersions prepared under weak mixing conditions, which contained bigger particles directly after preparation.

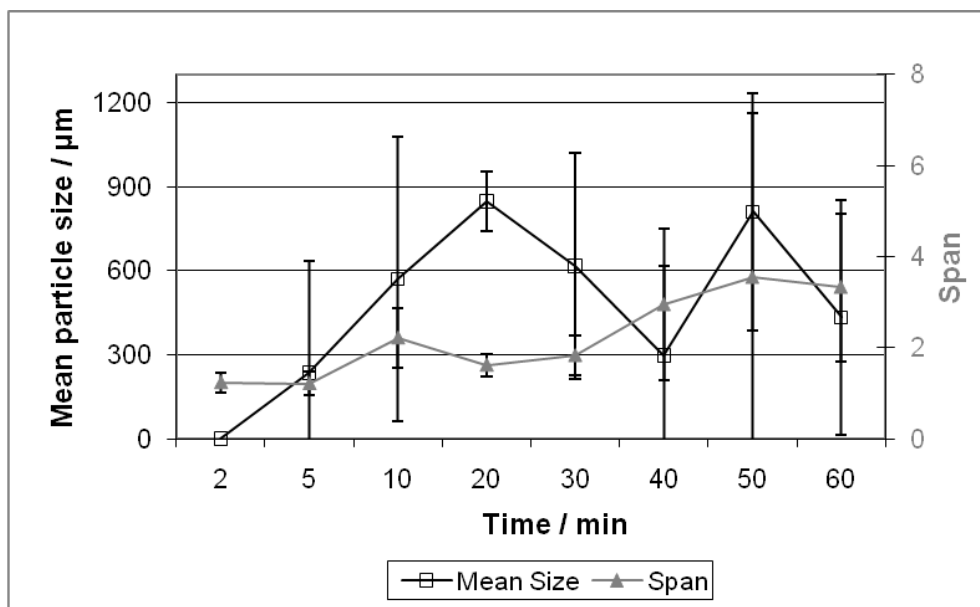


Figure 71: Fenofibrate dispersion prepared without the use of any additional excipients. Crystallization started directly after sample preparation and rapidly comprised the whole dispersed phase

As for the preliminary experiments, the stability of the dispersions against crystallization and Ostwald ripening could be improved by the addition of combinations of surfactants. The concentration and weight ratio of the surfactants used had to be adjusted depending on the composition of the formulation and the process conditions applied. First positive results were obtained by using Tween 80 (conc. 0.002 mg/g dispersion) in combination with Phospholipon 100H (conc. 0.02 mg/g dispersion) and BHT (conc. 7 mg/g dispersion) for stabilization of a 7 mg/g fenofibrate dispersion. An apparently linear particle growth was obtained, accompanied by a slowed down crystallization (**Figure 72**). Nevertheless, Ostwald ripening and the formation of BHT rich particles impaired the dispersions' stability. A sudden drop in Span values already 5 min after sample preparation indicates a turning point, where ripening of the dispersion switched from an Ostwald ripening controlled pattern, to dominating crystallization. A certain amount of crystals adhered to the container wall and were subsequently no longer analytically detectable. Microscopical observation revealed an onset

of particle agglomeration by the end of the experiment due to the local enrichment of Phospholipon 100H.

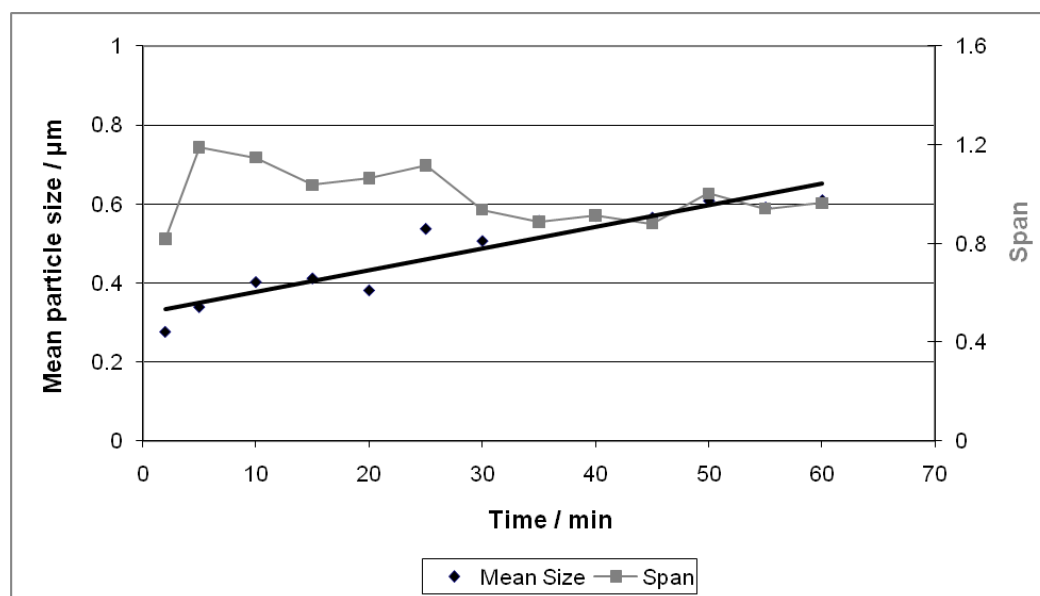


Figure 72: Stabilization of a dispersion containing BHT and fenofibrate in a 3:5 ratio, stabilized with Phospholipon 100H and Tween 80

The formulation could be further optimized by replacing the previously used surfactant combination with DPPC and DPPG. These phospholipids were found to be best applicable in a ratio of 80% (w/w) DPPC and 20% DPPG. Dispersions thus prepared were less sensitive to particle agglomeration and variations in the surfactant concentration than those containing Phospholipon 100H/Tween 80 (see **Section 5.4.1**). The BHT content was reduced from 7 mg/g dispersion to 4 mg/g to minimize Ostwald ripening, while the fenofibrate concentration was kept constantly at 7 mg/g dispersion. Using DPPC and DPPG at concentrations of 0.3 mg/g dispersion and 0.01 mg/g dispersion, complete inhibition of crystallization could be extended from ~1 minute for the dispersions without excipients to 1 hour for the coprecipitate (**Figure 73**), thereby widely exceeding the stability target range of 30 min. Even one day after preparation, the dispersions were only partly crystallized, while significant amounts of precipitate remained in its liquid state with particle sizes around 2 μm . Besides crystallization, also Ostwald ripening of the precipitate particles could be importantly slowed down. Again, the onset of crystallization was indicated by a drop in Span values about 60 min after preparation of the dispersion.

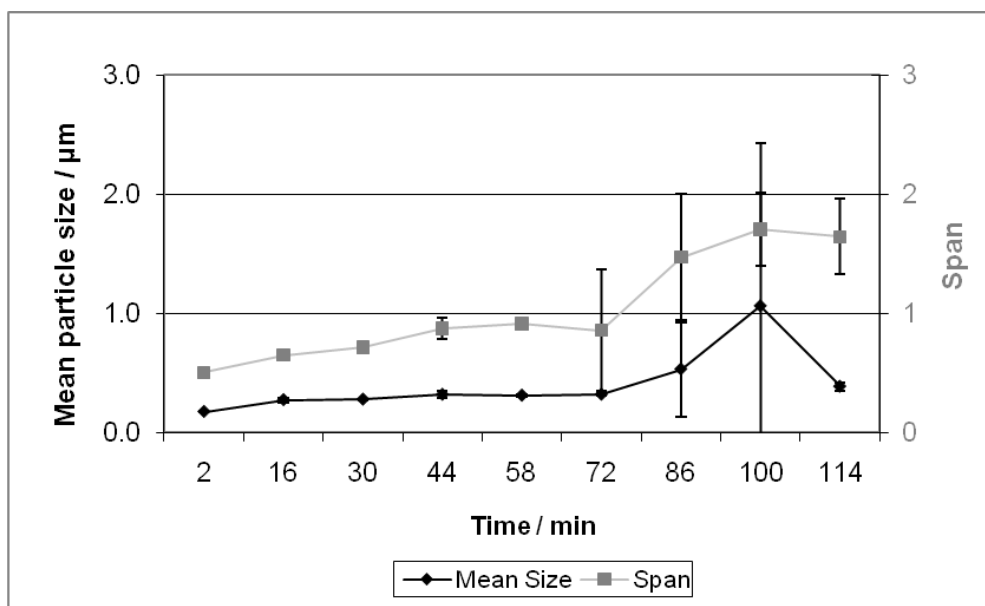


Figure 73: Stabilizing effect observed by the combinatorial stabilization of fenofibrate dispersions with BHT and the surfactants DPPC and DPPG

Also combinations of Tween 80 and Phospholipon 100H as well as DPPC and DPPG in formulations without the additional application of BHT were investigated. They only allowed for a moderate stabilization of the dispersions. **Figure 74** shows the effect of a combination of DPPC (conc. 29 $\mu\text{g/g}$ dispersion) and DPPG (conc. 7 $\mu\text{g/g}$ dispersion). The surfactants obviously adhered to the particle surface, thereby partly inhibiting mass transport between the individual particles and to the emerging crystals seeds. Nevertheless, microscopical observation confirmed the presence of first crystals in the dispersion already 15 min after sample preparation, which subsequently multiplied by seeding other crystals. Due to strong crystal adsorption to the sample container a detectable crystal concentration was not obtained prior to about 40 min after sample preparation.

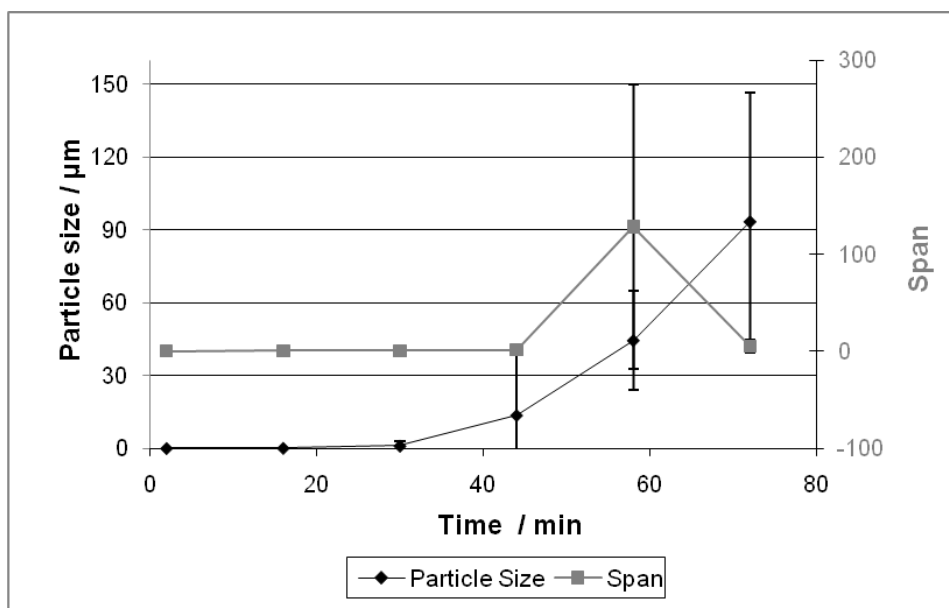


Figure 74: Fenofibrate dispersion stabilized with the phospholipids DPPC and DPPG, without the additional use of BHT

Additional experiments were accomplished by coprecipitation of further potentially stabilizing compounds. However, neither polyvinylpyrrolidone, which is known to strongly adhere to particle surfaces as well as to act as effective crystallization inhibitor [138-140], nor the combination of phospholipids with triacetine, a compound known to stabilize phospholipid layers [175], led to an additional stabilization of the dispersion. Under application of PVP a slow crystal growth rate in the dispersions was maintained, which was in a comparable range as for the PVP free formulations (**Figure 75**). In opposite, the small and comparably well soluble triacetine caused strong Ostwald ripening with particle sizes up to $\sim 8 \mu\text{m}$. Distinguishable crystallization occurred about 20 min after sample preparation. Also the pegylated phospholipid MPEG-2000-DSPE, intended to be used as steric stabilizing agent destabilized the dispersions, rather than stabilizing them.

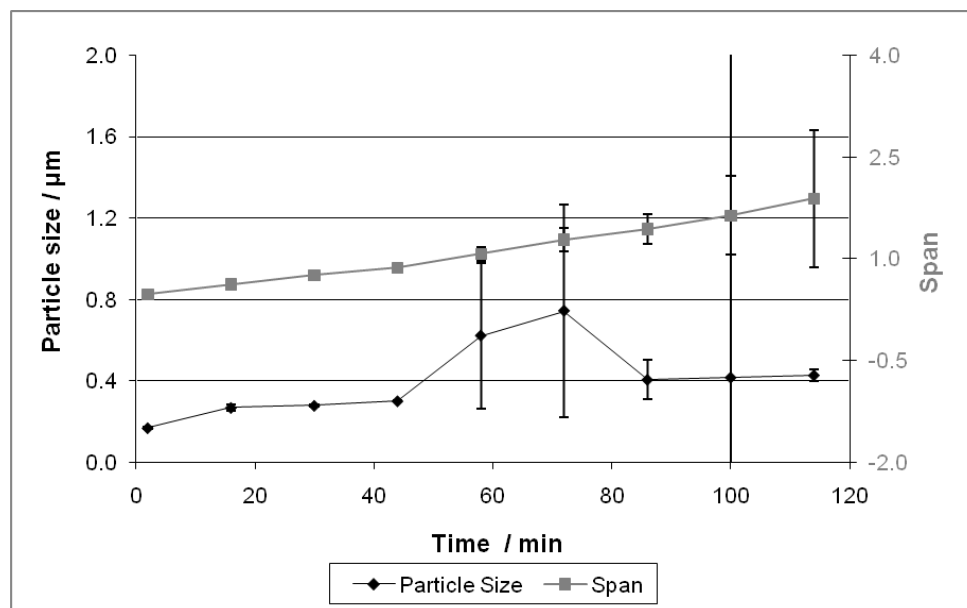


Figure 75: Dispersion of fenofibrate, BHT and the phospholipids DPPC and DPPG additionally stabilized by addition of 0.5% PVP to the aqueous phase

A rather qualitative overview of the experimental results is shown in **Table 16**. The data are interpreted with respect to the kind and relative extent of the individual (de)stabilization mechanism. The experimental setup is characterized by the mixing mode (hand mixing versus the use of the pumping setup) as well as the kind of excipients applied. A quantitative analysis of the results is due to strongly varying analytical data for not completely stabilized dispersions not possible. Due to the difficult analytical differentiation between different particle species outlined in **Chapter 4.2**, a qualitative interpretation of the data with respect to the mechanistical background and the connectivity between the excipient classes and preparation methods applied is most comprehensive.

Table 16: Qualitative overview of the results on the stabilization of fenofibrate dispersions (the time span covered is 1 hour; +++ massive, immediate reaction/rapid proliferation; ++ moderate intensity/slow proliferation; + weak, very slow process)

Composition	Kind of surfactants used	Sample preparation method	Crystallization in the continuous phase	Crystallization on the container wall	Particles > 5 μm directly after sample preparation	Particles > 5 μm formed by Ostwald ripening	Agglomeration of particles	Crystal growth inside the dispersed phase particles	Bursting of particles, followed by immediate crystallization	Coalescence of particles
Only BHT (no fenofibrate used)	-	Hand-mixing	+	+++	+	+				
Only fenofibrate (no excipients used)	-	Pumping setup	++	+++	+	++				
Only fenofibrate (no excipients used)	-	Hand-mixing	+	+++	+	+				
Only Fenofibrate	DPPC, DPPG	Pumping setup	+	++		+				
Only Fenofibrate	Phospholipon 100H, Tween 80	Hand-mixing	+	++	+	+				
BHT to fenofibrate ratio > 1:5	-	Pumping setup	+	++	++	+++				
BHT to fenofibrate ratio > 1:5 + excessive amount of surfactant	Phospholipon 100H	Pumping setup	++	++	+	++	+++	+		
BHT to fenofibrate ratio > 1:5 + excessive amount of surfactant	Phospholipon 100H, Tween 80	Pumping setup	++	+			++			
BHT to fenofibrate ratio > 1:5 + excessive amount of surfactant	DPPC, DPPG	Pumping setup		+						
BHT to fenofibrate ratio > 1:5 + excessive amount of surfactant	DPPC, DPPG, Tween 80	Pumping setup	+	++						
BHT to fenofibrate ratio > 1:5 + excessive amount of surfactant	Phospholipon 100H, Tween 80	Hand-mixing	+	+		+	++			

Composition	Kind of surfactants used	Sample preparation method	Crystallization in the continuous phase	Crystallization on the container wall	Particles > 5 μm directly after sample preparation	Particles > 5 μm formed by Ostwald ripening	Agglomeration of particles	Crystal growth inside the dispersed phase particles	Bursting of particles, followed by immediate crystallization	Coalescence of particles
BHT to fenofibrate ratio $\leq 1:5$ + excessive amount of surfactant	Phospholipon 100H, Tween 80	Hand-mixing	++	+			++			
BHT to fenofibrate ratio $\leq 1:5$ + appropriate amount of surfactant	Phospholipon 100H, Tween 80	Pumping setup		+						
BHT to fenofibrate ratio $> 1:5$ + appropriate amount of surfactant	DPPC, DPPG	Pumping setup								
BHT to fenofibrate ratio $> 1:5$ + appropriate amount of surfactant	Phospholipon 100H, Tween 80	Pumping setup		+		+				
BHT to fenofibrate ratio $> 1:5$ + appropriate amount of surfactant	Phospholipon 100H, Tween 80	Hand-mixing		+		+				
BHT to fenofibrate ratio $> 1:5$ + insufficient amount of surfactant	Phospholipon 100H, Tween 80	Hand-mixing		+	+	+				
BHT to fenofibrate ratio $> 1:5$ + insufficient amount of surfactant	Phospholipon 100H, Tween 80	Pumping setup		+	+	+		+		
BHT to fenofibrate ratio $> 1:5$ + insufficient amount of surfactant	DPPC, DPPG	Pumping setup		++	+	++		+		
BHT to fenofibrate ratio $\leq 1:5$ + excessive amount of surfactant + citric acid	Phospholipon 100H, Tween 80	Hand-mixing		+	+	+	+	++	+	+
BHT to fenofibrate ratio $\leq 1:5$ + excessive amount of surfactant + citric acid	Phospholipon 100H, Tween 80	Pumping setup	+	++		++	++			

Composition	Kind of surfactants used	Sample preparation method	Crystallization in the continuous phase	Crystallization on the container wall	Particles > 5 μm directly after sample preparation	Particles > 5 μm formed by Ostwald ripening	Agglomeration of particles	Crystal growth inside the dispersed phase particles	Bursting of particles, followed by immediate crystallization	Coalescence of particles
BHT to fenofibrate ratio > 1:5 + excessive amount of surfactant + citric acid	Phospholipon 100H, Tween 80	Hand-mixing		+	+	++	+	+		++
BHT to fenofibrate ratio > 1:5 + appropriate amount of surfactant + citric acid	Phospholipon 100H, Tween 80	Hand-mixing		+	+	+		+		++
BHT to fenofibrate ratio > 1:5 + appropriate amount of surfactant + citric acid	Phospholipon 100H, Tween 80	Pumping setup		+		+		+		
BHT to fenofibrate ratio \leq 1:5 + appropriate amount of surfactant + citric acid	Phospholipon 100H, Tween 80	Hand-mixing		++	+	+		++	+	+
BHT to fenofibrate ratio > 1:5 + insufficient amount of surfactant + citric acid	Phospholipon 100H, Tween 80	Hand-mixing		+	++	++		+	+	++
BHT to fenofibrate ratio > 1:5 + insufficient amount of surfactant + citric acid	Phospholipon 100H, Tween 80	Pumping setup		++	++	++		++		
BHT to fenofibrate ratio > 1:5 + surfactant + MPEG-2000-DSPE	DPPC, DPPG, MPEG-2000-DSPE	Pumping setup	+		+	++				
BHT to fenofibrate ratio > 1:5 + surfactant + triacetine	DPPC, DPPG	Pumping setup	++			+++				
BHT to fenofibrate ratio > 1:5 + surfactant + PVP	DPPC, DPPG	Pumping setup	+	+	++	+		+		

5.4.2 LYOPHILIZATION

Lyophilization of the dispersions was accomplished for investigating the downstream processability of the fenofibrate formulations. Aim was not only the removal of the solvents ethanol and water, but also to investigate the possibility to adjust the BHT concentration in the samples subsequently to the actual preparation of the dispersions. An additional target was to gain a deeper insight into the structural habits of the shock frozen dispersions.

5.4.2.1. COMPOSITION OF THE LYOPHILIZATES

It was found that the composition of the dispersions changed within the freeze drying process. Independent from the process conditions applied, a significant decrease in the BHT content was observed for those dispersions primarily containing high amounts of the coprecipitant (**Figure 76**). None of the excipients used showed an inhibitory effect on the sublimation rate of BHT or formed a measurable barrier for the mass transport. Remarkable is the fact that dispersion 6, originally formulated without BHT (see also **Table 9, Section 5.3.2.1**), was found to contain almost 1% (w/w) of BHT in the lyophilized product. Dispersion 6 had been freeze dried simultaneously with dispersions 3-5 and 7. Obviously, partial equilibration between the sublimated BHT in the gas phase of the freeze dryer and the lyophilization products took place. So, within the lyophilization process small amounts of BHT were transferred to the originally BHT-free formulation. Also, for dispersion 4, containing a very low amount of BHT prior to lyophilization; no further reduction in the BHT content could be obtained. This indicates further optimization potential in terms of adjusting the recondensation rate of BHT and facilitating its rapid removal from the system.

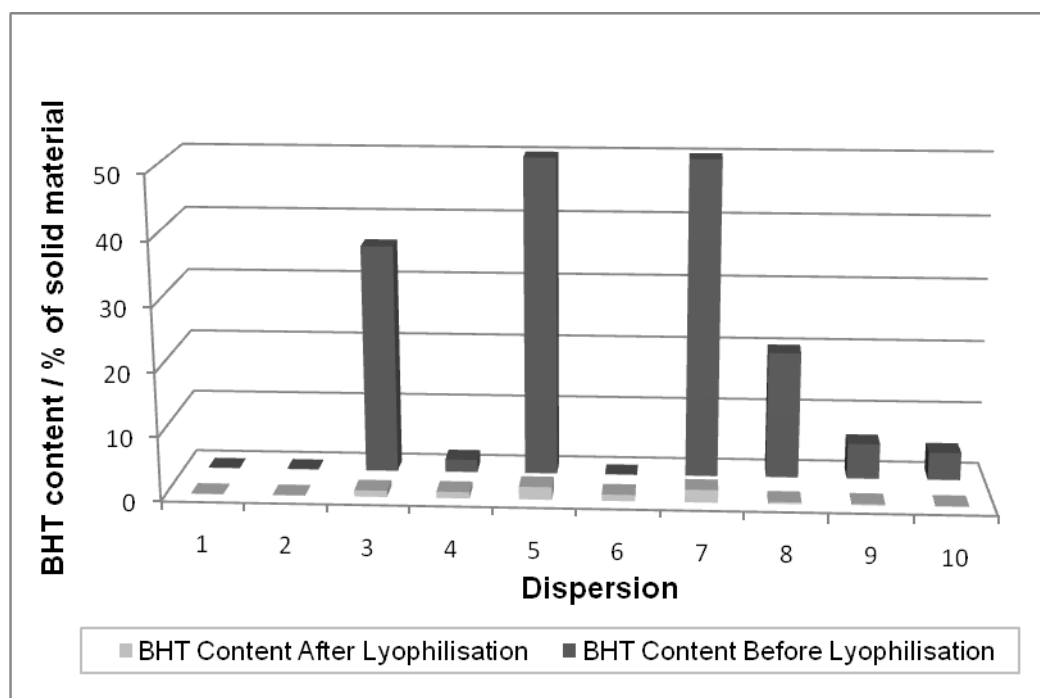


Figure 76: BHT content in the fenofibrate dispersions prior and after the lyophilization process. Data are shown in percent (w/w) of the solid formulation compounds (fenofibrate, BHT, surfactants, citric acid and trehalose)

The residual content of ethanol and water was found to be very low for all of the freeze dried samples. The ethanol concentration was in all cases below 5 ppm, and the water content had been reduced to below 0.1% (w/w). A sufficient stabilization against solvent induced crystallization or degradation of the contained drug during storage was hence given.

5.4.2.2. CAKE STRUCTURE OF THE LYOPHILIZATES

Although the sublimation of BHT was hardly affected by the kind and amount of excipients used, the cake structure of the lyophilizates varied strongly. While the precipitates containing no or low amounts of BHT showed a very nice and fluffy cake structure, those dispersions containing elevated amounts of BHT partly collapsed within the lyophilization process (**Figure 77**). The effect was stronger, the higher the BHT content was prior to lyophilization. Obviously, the removal of the contained BHT prohibited the formation of a stable cake structure. Trehalose was found to countervail this effect, as all samples containing trehalose produced stable lyophilization cakes.

A macroscopically retraceable electrostatic charge of the particles, indicated by the spontaneous condensation of the powder on charged surfaces, e.g. sample containers or spatulas, was found to be remarkably reduced in the presence of surfactants.

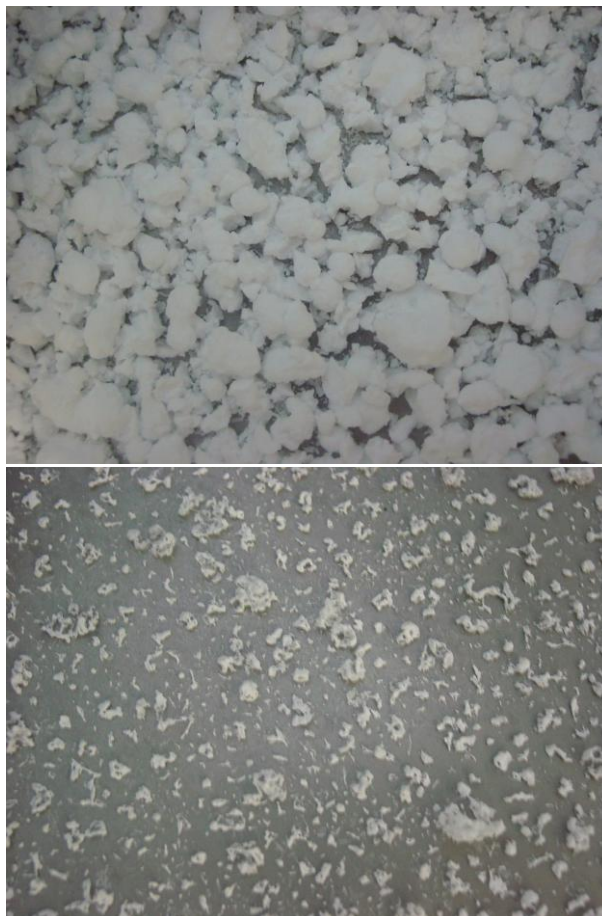


Figure 77: Lyophilization cakes from dispersions 4 (top) and 5 (bottom). Dispersions containing no or low amounts of BHT prior to lyophilization (dispersion 4) showed nice and stable cake structures, while those originally containing high amounts of BHT partly collapsed upon removal of the antioxidant (dispersions 5)

Scanning electron microscopy studies showed that after lyophilization the dispersions still contained clearly distinguishable particles. The size of the particles ranged from ~ 50 nm, which was the lower resolution limit of the scanning electron microscope for the current setup, to ~ 12 μm . A majority of the particles had particle sizes of about ~ 1 - 3 μm . Often these particles were sintered, forming three-dimensional networks in which big pores could be observed (**Figure 78**). The particles had a homogeneous structure without any signs of decomposition. No distinguishable difference concerning the morphology of the individual

particles could be identified with respect to kind and amount of excipients used. Most of the particles were found to be round or oblong, reflecting the original precipitational state. Some also had sharp edges and flat surfaces, which was considered to be an indication for the crystallinity of the material. No impact of the changes in sample viscosity or impaired particle integrity previously observed in the presence of certain excipients could be identified (see also **Section 5.4.1.2**).

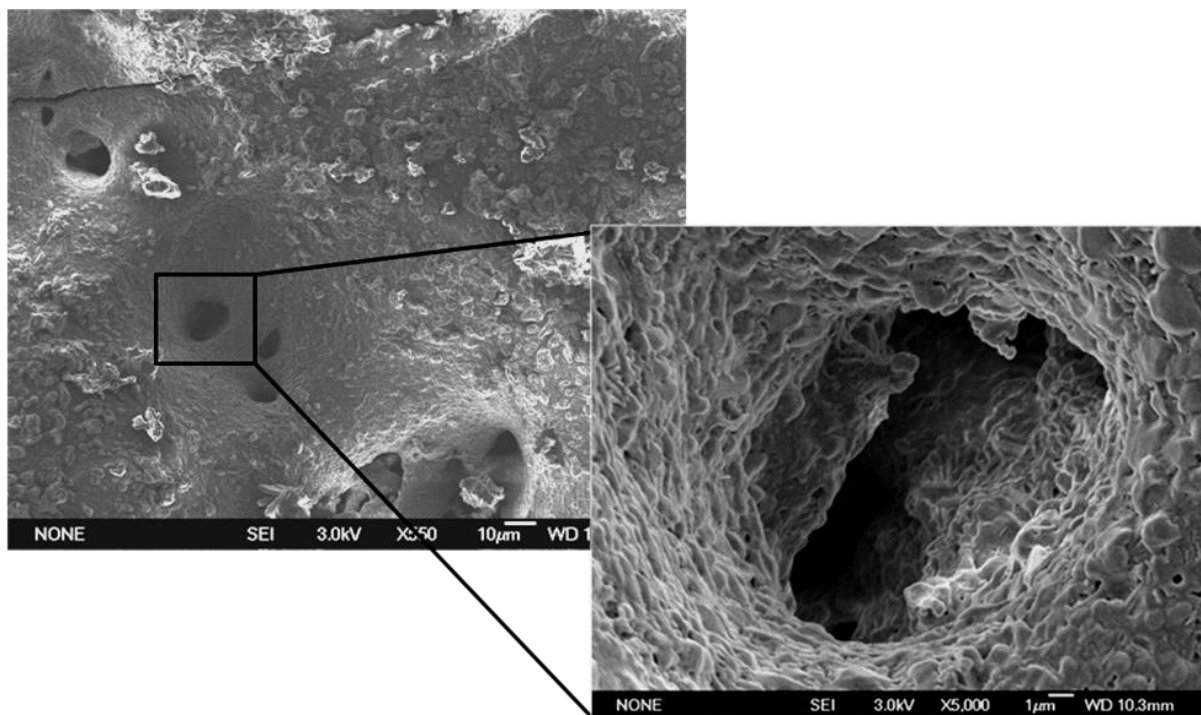


Figure 78: Scanning electron microscopy image of the lyophilized dispersion 2. Wide pores aligned by partly sintered particles can be identified at the surface of the lyophilizate

In those samples containing trehalose, the drug particles were nicely embedded into the sugar matrix (**Figure 79**, top). After redispersion in water and dissolution of the hydrophilic compounds, a clear birefringence of the samples could be observed. The shape of the crystalline remnants remained comparable to that observed within electron microscopy, independently of the excipients used (**Figure 79**, top). Particle size measurements of the redispersed samples showed a bad reproducibility, as the lipophilic and fluffy powder was hardly dispersible. Overall, after redispersion mean particle sizes between 20 μm and 640 μm were recorded (**Table 17**). After exposing the samples to the field of an ultrasonic bath, distinct reductions in particle size were obtained, indicating a breakup of the sintered particle agglomerates into smaller substructures. The size reduction appears to be stronger for

samples containing the cryoprotectant trehalose, what might be attributed to the stronger spatial separation of the particles within the freeze drying process.

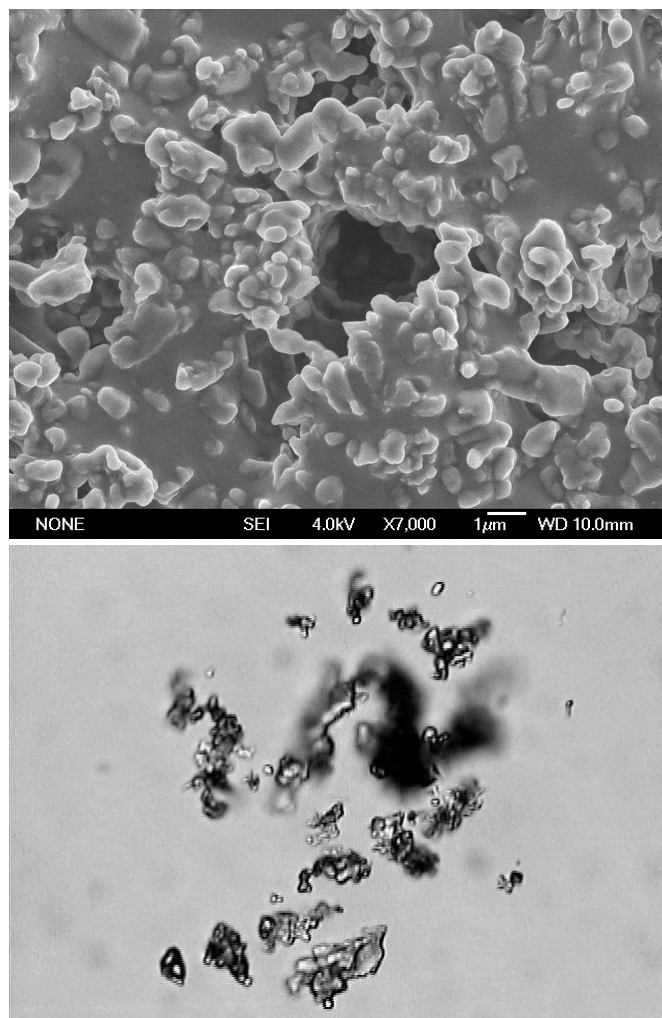


Figure 79: Particles from dispersion 8 being embedded into a trehalose matrix (top) and redispersed agglomerate complexes of dispersion 9 (bottom)

Table 17: Particle sizes measured after redispersion of selected lyophilized dispersions, prior and after application of ultrasound

	Redispersed sample		Sample after application of ultrasound	
	Mean size / μm	Span	Mean size / μm	Span
Dispersion 1	20.974	1.430	-	-
Dispersion 5	640.522	3.924	516.480	13.737
Dispersion 8	188.137	2.650	103.834	2.267
Dispersion 9	395.916	7.928	29.491	2.447
Dispersion 10	88.436	1.786	9.493	3.470

5.4.2.3. THE INFLUENCE OF FREEZE DRYING ON THE PHYSICAL STATE OF FENOFIBRATE

DSC and XRD measurements of the lyophilizates derived from dispersions 1 and 2 (containing fenofibrate as only solute) confirmed the optical impression of the samples' crystallinity. Like the fenofibrate bulk material, the lyophilized products showed a melting peak at 81°C by DSC. Neither the glass transition at -20°C, nor the crystallization peak at 40°C described in the literature for fenofibrate [176] could be observed, indicating a predominantly crystalline lyophilization product (**Figure 80**). Also the XRD diffractogram showed a very comparable pattern for both, lyophilized and bulk fenofibrate (**Figure 81**). Differences in the individual heights of the sample peaks might be attributed to different forms of the crystallites as well as an alternate orientation of the particles during sample preparation, both leading to a varying sample exposure within the measurements.

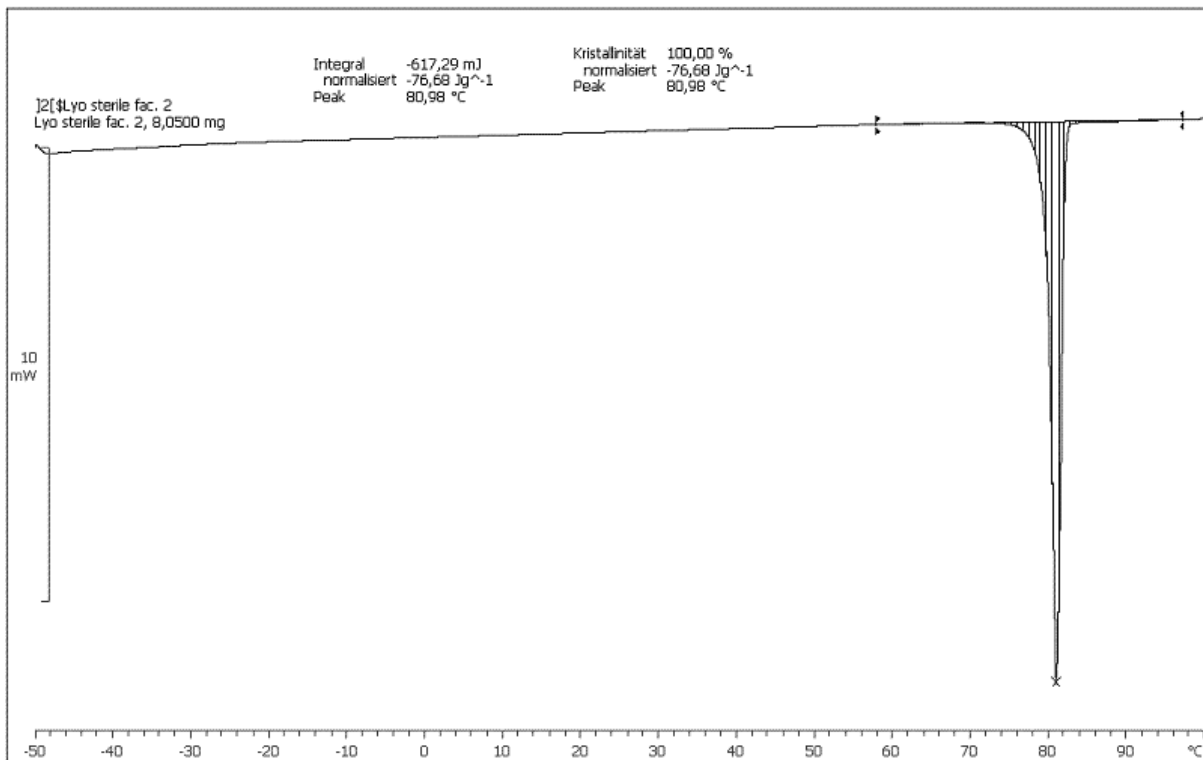


Figure 80: DSC diagram of the lyophilizate of dispersion 1, containing only fenofibrate as solute

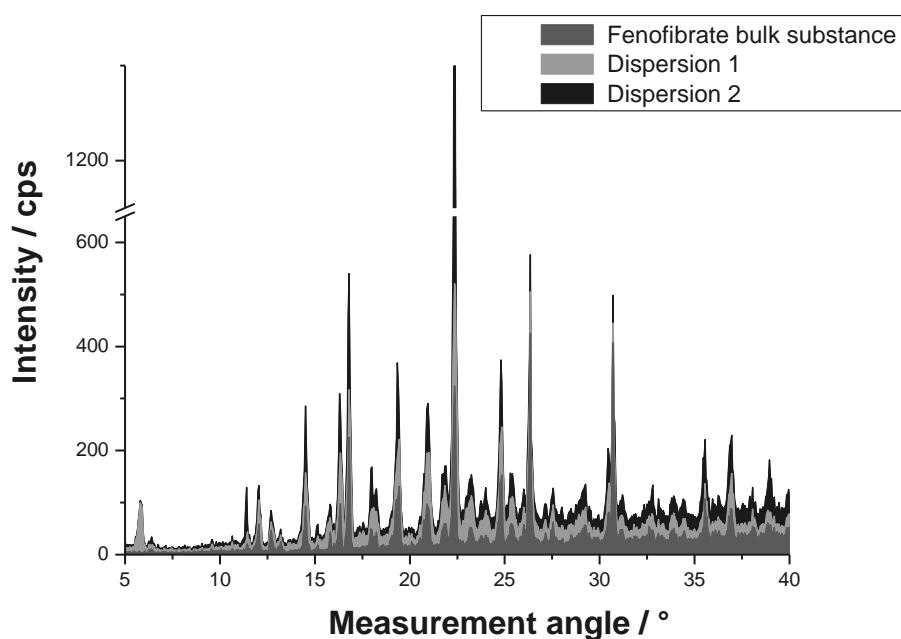


Figure 81: Diffractogram of the fenofibrate bulk substance and the lyophilization products of dispersions 1 and 2

Within electron and light microscopical observation it was clearly found that, independent of the excipients applied, lyophilized dispersions did not contain relevant amounts of amorphous fenofibrate. The crystallization process during lyophilization hence appeared to be a general phenomenon associated to fenofibrate. This outcome finds good confirmation by the results obtained by Waard et al. [177], who found comparable results for the lyophilization of fenofibrate dispersions containing butyl alcohol as organic solvent.

The following reasons can be discussed for the crystallization of fenofibrate within the lyophilization processes:

- Phase separation during freezing
- Thawing of the samples during processing
- The existence of precrystalline structures inside the liquid precipitate particles

Due to the extreme temperature of -196°C and the complete and instantaneous immersion of the dispersion droplets into liquid nitrogen, demixing and crystallization of the dispersion within sample preparation seems to be unlikely. At least some part of the liquid precipitate would be expected to remain in an amorphous state, being detectable by DSC. More likely is the partial thawing of the samples within the freeze drying process. A bad thermal conductivity of the samples might have led to superficial thawing of the frozen dispersion particles, especially considering the round shape of the dispersion particles and hence limited contact area to the lyophilization plates. On the other hand, the freeze drying equipment was run at its limit in terms of temperature and vacuum for assuring a constant freeze chain within sample processing. By applying a cryoscopic constant of 1.86 [154], the freezing point depression for the formulations can be calculated to range from $6-7^{\circ}\text{C}$ for all dispersions. As for the flash freezing, it appears to be unlikely that the dispersions quantitatively reached a temperature exceeding a critical level.

The third explanation concerning the crystallization mechanism therefore provides the most likely explanation. It is provided by the idea that already in the liquid precipitate intermolecular interactions between the fenofibrate molecules exist. Thereby the high molecular mobility of the drug molecules in the liquid state prevents the establishment of an extended periodic arrangement. A lyotropic state and microscopically observable birefringence were not detectable, while the interaction pattern is strong enough for forming a coherent liquid phase. However, the fact that comparable fluorescence patterns had been found by confocal fluorescence microscopy for both, crystalline fenofibrate as well as its liquid precipitate, indicates an analogous molecular interaction in both kinds of samples (see also **Chapter 4, Section 4.4.4**). Fenofibrate molecules might already in the liquid state temporarily arrange loosely head-to-head and tail-to-tail, producing aliphatic and aromatic arrangements as was shown for its crystalline polymorph [136]. In the frozen state, the molecular mobility is decreased strong enough to allow for the establishment of a permanent three-dimensional structure in the precipitate.

5.5. CONCLUSIONS

Excipients with different functionality were investigated for their effects on the stability of the fenofibrate dispersions. By the use of BHT, a new approach for stabilizing and modifying the physical state of liquid-liquid phase separating substances was established, the coprecipitation with a second liquid-liquid phase separating compound. Strong evidence indicates an unspecific interaction between the coprecipitants, which leads to a liquefaction of the sample, impaired surface integrity and slowed down crystallization. In combination with surfactants, a highly potent solubilizing drug delivery system is obtained, which was capable to delay the onset of crystallization from 1 min to 1 hour, and to prevent complete crystallization of the dispersions for more than 1 day. The unspecificity of the underlying stabilization mechanism and the transferability of the mechanical effects to the drugs lopinavir and loratadine thereby raise expectations towards a broad applicability to further poorly soluble compounds. Freeze dried fenofibrate dispersions were found to be completely crystalline. Considering the comparable fluorescence pattern for crystalline fenofibrate as well as the precipitate, a loose periodic arrangement of fenofibrate in the liquid state can be considered, that upon freezing and solvent removal solidifies in a crystal lattice. BHT could to a large extent be removed within the applied freeze drying processes, providing the chance to adjust the excipient concentration to a desired range within the downstream processing of the formulations. However, the freeze drying technology seems to be an inappropriate mean for the long term stabilization of fenofibrate dispersions, as the fact that the amorphous state of fenofibrate gets lost within the lyophilization process, as well as the accompanying increase in particle size, most likely abolish the solubility advantage of the liquid precipitate. In how far the sensitivity of the fenofibrate dispersions to freeze drying is substance related, or correspondingly applies to other liquid-liquid phase separating substances, needs to be further evaluated.

Based on the promising results obtained on the stabilization of the liquid precipitates not only a broad array of API become accessible to be further developed towards a marketable liquid dosage form, but also fundamental properties required for the successful selection of potential coprecipitants were identified. These are namely a comparable lipophilicity and solubility of the coprecipitant and the API, as well as comparable structural characteristics allowing for a weak, but sustainable interaction with the drug. The case of the model-compound BHT showed nicely, that liquid-liquid phase separation of the individual compounds (the drug and

the coprecipitant) correlates very well with a good miscibility of the compounds under application of comparable conditions for the coprecipitation process.

Chapter 6. General Summary of the Thesis

Precipitation products determine everyday life, often without being recognized for their interesting structural properties and potential applications of the underlying “technology”. A nice example for this is the beverage Ouzo, forming liquid precipitates that are stable for weeks or months without the addition of surfactants or other excipients [110, 178-180]. Nobody so far provided a concluding explanation for this fascinating phenomenon [180], which, without doubt, would also be of great interest for the pharmaceutical field, considering the immense pressure to develop new formulation approaches for the ever increasing amount of poorly soluble compounds [15, 16].

The current work not only helps to better understand phase separation phenomena for poorly soluble drugs, but also provides unprecedented insights in the structural properties of the precipitates. In addition, a new formulation approach was developed, allowing for the stabilization of the amorphous state of the dispersions and to purposefully direct the mechanical properties of the contained particles.

6.1. UNDERSTANDING PARTICLE FORMATION

A first objective of the thesis was to use antisolvent precipitation for the preparation of amorphous dispersions of poorly soluble drugs. While this target might seem to be trivial to those skilled in the field, within the accomplishment of the thesis, it turned out to be the most challenging task. Indeed, using first class equipment and defined mixing conditions for the preparation of the dispersions, supersaturations high enough for reproducibly obtaining a defined amorphous precipitate could be attained (**Chapter 2**). Nevertheless, the identification of the kind and properties of the particles turned out to be challenging, as they in many ways did not correspond to the expectations formulated in anticipation of solid-amorphous precipitation products. Unexpectedly, the precipitate formed within antisolvent precipitation did not consist of solid material, but of a liquid precipitate containing significant amounts of complexed solvent and antisolvent (**Chapter 1, Chapter 1**).

To better understand the mechanisms defining phase separation, a simulation model previously used for inorganic materials was further developed to retrace the phase separation

process of fenofibrate (**Chapter 2**). As the rapidity of the process prohibited direct visual observation of the drug's phase separation, the simulation model was found to be very useful to draw conclusions about the ongoing processes within demulsification of the drug. Designed to reproduce and predict phase separation processes based on homogeneous nucleation, the model is well suited to describe nucleation and growth of both liquid-liquid as well as liquid-solid phase separation, as both phenomena generally follow the same mechanisms [148, 181, 182]. It was found to be especially useful to distinguish in how far the phase separation subprocesses uncovered for fenofibrate are in accordance with the model based expectations and in how far further phase separation phenomena need to be considered (**Chapter 3**). Conclusions based on the particle size distribution and the structural properties of the precipitate allowed to portrait the exceptional complexity of the precipitation process and to avoid costly experimental evaluations on the micro-mixing time scale as were accomplished for other systems [6]. The final particle size distribution was found to be primarily defined by the volume of the precipitate formed, which could be influenced by e.g. increasing the drug load (**Section 3.4.4**). In contrast, sample temperature was found to have no impact on the particle size distribution, which was attributed to countervailing effects of drug solubility and solvent complexation in the precipitate (**Sections 3.4.3 and 4.4.6**). The identification of the liquid state of the precipitate was hence fundamental for understanding the phase separation of fenofibrate, as such important degrees of compositional variations of the precipitate would not have been expected for solid particles. Particle size reductions could be achieved by intensifying the mixing conditions (**Sections 2.4.4.1 and 3.4.5**). Elevated flow rates and decreased diameters of the mixing devices used also led to a narrowing of the particle size distribution. Both measures apply simultaneously to nucleation controlled phase separation, as anticipated by the mathematical model, as well as to spinodal decomposition, the spontaneous demulsification from solution without the actual event of nucleation. Only comparison between the experimental and the theoretical results revealed that it was indeed, other than preliminarily anticipated, spinodal decomposition that governs the phase separation process of fenofibrate. Thereby, the final particle size distribution was found to be dominated by mixing controlled breakdown and shaping of the emerging precipitate. The spatial density distribution of the precipitate was identified to be the second factor determining particle size. Decomposition as spatially extended precipitate is typical for spinodal phase separation, and seems to be favored by the interplay between drug and semipolar organic solvents, a phenomenon also regularly encountered in literature in the

context of liquid-liquid phase separation [8, 116-121]. It is the effectiveness of mixing to break these large scale structures which was found to be critical for the product characteristics. As was anticipated, also the use of excipients affected the phase separation process. This was especially the case for surface active compounds, which influence the establishment of an interface between the forming precipitate and the surrounding continuous phase. Latter was exemplarily shown for Tween 80, which was capable to distinctly decrease particles size in dispersions prepared under defined mixing conditions (**Section 3.4.2**). Wide-field fluorescence microscopy proved that the fenofibrate precipitate was not homogeneous in structure, but that particles at least down to particle sizes of 0.8 μm contained fenofibrate rich subparticles (**Section 4.4.3**). In how far below the microscopically observable size additional cluster formation occurs, cannot be evaluated within the scope of this work, as the particles' temperature sensitivity prevented further evaluation by transmission electron microscopy. Also the mechanisms by which the subparticles of the emerging multiple emulsion systems form, remain matter of speculation. Potential explanations are nucleation phenomena inside the particles or, more likely, the constriction of subparticles within the spinodal decomposition process.

The obtained results concerning the size dependency of the precipitate on the initial solute concentration, mixing conditions as well as the observation of particles comprising incorporated small scale colloids are in good consistency with results reported in the limited amount of publications dealing with the rapid precipitation of organic compounds in antisolvent precipitation processes [55, 68, 70, 183]. This indicates, that for organic molecules often other mechanisms govern the particle formation mechanism than would be expected based on those being valid for inorganic materials. In many cases the consideration of liquid-liquid phase separation and spinodal decomposition might help to better understand the observed phenomena and to select appropriate measures for obtaining the desired product characteristics.

Other than anticipated by the start of the thesis, the mathematical model applied failed in predicting the suitability of a drug to be used in antisolvent precipitation. Despite the systematical investigation of the process parameters, the identification of spinodal decomposition as phase separation mechanism limits the simulations to be used as a tool which allows for the differentiation from other phase separation mechanisms, rather than allowing to draw prospective conclusions. Based on the results obtained within this work, the

prediction of the applicability of a compound to anti-solvent precipitation is only possible based on the physico-mechanical characteristics of its precipitate. In the case of spinodal decomposition, these are namely the viscosity of the dispersed phase, the ability to form complexes with solvent and antisolvent as well as the degree to which this complexation is affected by adjustments of the process parameters. As summarized in **Figure 82**, it is mainly the interplay between the volume of the precipitate, its mechanical stability and the effectiveness of the mixing conditions applied, that govern the final particle size distribution.

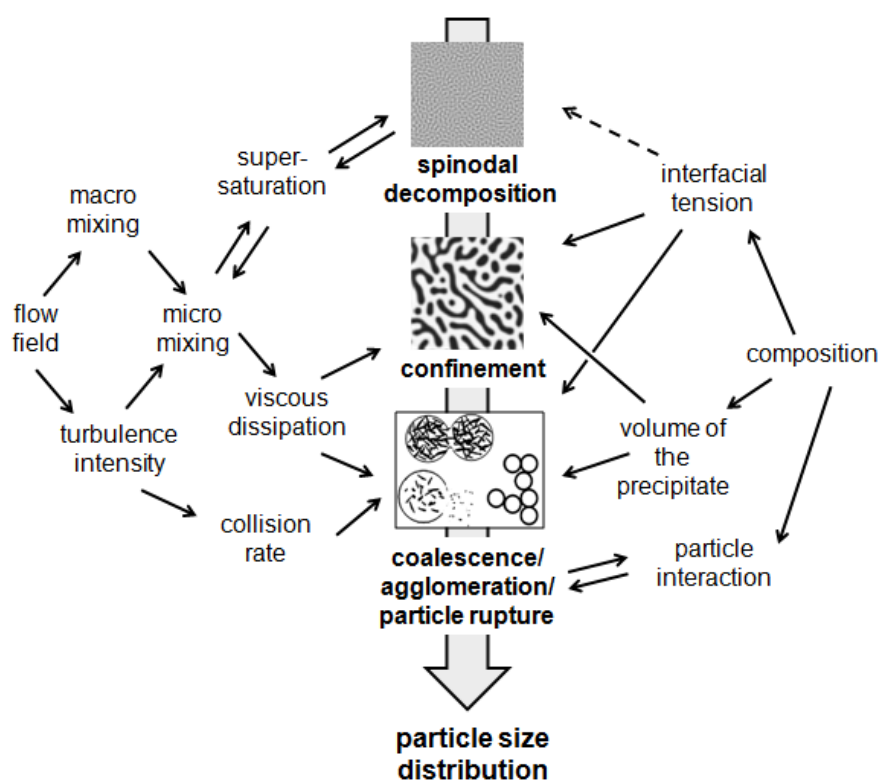


Figure 82: Schematic illustration of the processes affecting the particles size distribution in antisolvent precipitation (adopted from [88])

6.2. DISPERSION STABILITY

Commercial relevance for amorphous drug dispersions can only be gained by assuring sufficient stability of the formulations. As was outlined under **Sections 5.2.1** and **5.2.2**, the development of formulations with the purpose of increasing drug solubility unavoidably threatens the drugs' stability against crystallization and Ostwald ripening. In addition, for many dispersions it is poorly understood how or why certain stabilization approaches apply, while others do not [128]. Indeed, within a rapid screening of a variety of excipients, it was

found that commonly used stabilization approaches were insufficient to effectively improve the stability of fenofibrate dispersions (**Section 5.4.1.1**). It was a main target of the present work, to develop new approaches for the stabilization of amorphous drug dispersions, that allow to combine high solubility and morphological stability. More importantly, the work was focused on gaining a better insight into the underlying mechanisms, for facilitating the transfer of the achievements to alternative compounds.

6.2.1 STRUCTURE BASED STABILIZATION APPROACHES

6.2.1.1. CONTROLLING FENOFIBRATE CRYSTALLIZATION

In the excipient free formulations, the crystallization of fenofibrate was found to exclusively occur in the continuous phase. This is surprising, as one could expect the high solvent and solute concentrations in the precipitate to favor nucleation inside the dispersed phase. Obviously, the liquid state of the precipitate provides an environment impairing agglomeration of drug molecules to form a thermodynamically stable nucleus. Based on the idea of Bonnett et al. [114] that the chemical potential of fenofibrate is the same in the continuous and the dispersed phase, it was found that crystallization kinetics could indeed be triggered to occur in either of these phases. Upon addition of citric acid and the resulting increase in ionic strength, nucleation was shifted to occur exclusively inside the precipitate particles (**Section 5.4.1.2**). In opposite, by application of high amounts of surfactants the drug's solubility was increased to an extent favoring crystallization in the continuous phase (**Section 5.4.1.3**). Highest stability was obtained by adjusting crystallization to a boarderlining point, at which the likelihood of nucleation inside and outside the precipitate was equivalent.

This simple observation provides a first step in understanding liquid precipitates. Citric acid provokes a salting out effect on the drug which is more pronounced in the lipophilic environment of the dispersed phase than in the hydrophilic continuous phase. The high density of fenofibrate molecules inside the precipitate facilitates the formation of clusters reaching the critical nucleus size, so that, in the presence of citric acid, the likelihood of crystal nucleation increases. In addition, citric acid also caused a distinct decrease in the particles' structural integrity, which was attributed to the impaired molecular mobility of the

drug, and prohibited the compensation of structural inhomogeneities at the particle surface. The unique correlation of the functionality of the excipients and the dispersion structure can be expected to apply to the liquid precipitates more than for any other physical state, and was subsequently used for effectively improving dispersion stability. Indeed, only the addition of defined amounts of surfactants allowed to stabilize the particles and to prevent coalescence, providing a first structure based stabilization approach for fenofibrate.

6.2.1.2. COPRECIPIATION AS A TOOL TO MODIFY THE MOLECULAR INTERACTION

Precipitates of liquid-liquid phase separating substances are known to often complex significant amounts of impurities, indicating their potential to assume unspecific molecular interactions [111]. The underlying structural disorder and variability of the precipitates provides a point of action addressed in this work to further improve dispersion stability. Coprecipitates of fenofibrate were prepared by addition of butylated hydroxytoluene, a compound showing a comparable phase separation behavior and (in)stability as the drug. Both substances were found to form apparently homogeneous coprecipitates in a wide concentration range.

Interestingly, the addition of BHT succeeded to postpone the crystallization of fenofibrate from 1 min to about 1 hour after sample preparation. Complete crystallization of the drug could be delayed for even more than 1 day (**Section 5.4.1.3**). Neglecting the functionality of the compounds, the stabilizing effect can be considered to be even more pronounced, as no crystallization could be observed for BHT within the scope of the measurements.

This success was attributed to the interaction potential between fenofibrate and BHT on the expense of the homogeneous interaction between fenofibrate molecules or, respectively, between BHT molecules. The inhibition of fenofibrate nucleation was positively correlated to the BHT concentration applied and found to be not saturable. This indicates a very transient nature of the interaction. The crystallization inhibiting effect was hence attributed to a statistically decreased collision rate of drug molecules in the presence of BHT.

Side effect was a decrease in particle integrity, which was amplified and hence easily detectable in the presence of citric acid. BHT however did not decrease the drug's molecular

mobility, but rather increased it, as it prevented the establishment of fenofibrate-fenofibrate complexes. Observable particle coalescence in the presence of BHT was hence attributed to discontinuities in the interfacial layer caused by the presence of the excipient. Again, surface active reagents were found to be very effective in counteracting this effect, and were capable to not only inhibit coalescence of the particles, but also to prevent mass transfer and crystal growth in the continuous phase.

BHT not only had an impact on the molecular mobility of fenofibrate, but also on the lipophilic drugs lopinavir and loratadine, as was nicely shown by force-distance measurements accomplished on their coprecipitates (**Section 5.4.1.2, Figure 38**). The elasticity of the coprecipitate particles thereby decreased even below the value for the individual compounds. These results give a clear indication for the general applicability of the coprecipitation technique. Thereby the miscibility of BHT and the drugs does not necessarily need to be complete on a molecular level, as was shown by the fact that by addition of BHT to fenofibrate dispersions Ostwald ripening could not be inhibited, which might have been expected based on the result obtained by Lindfors et al. [34].

The use of a coprecipitant as stabilizing agent in combination with the application of surface active reagents represents a new formulation approach for poorly soluble drugs. It maintains the liquid state of the precipitate, and hence its solubility advantage compared to its crystalline polymorphs. More importantly, it is based on a detailed understanding of the molecular dynamics in the system, and hence clearly applicable to a wide variety of (not only) liquid-liquid phase separating compounds. The amount of the coprecipitant needed depends on the interaction potential between the excipient and the drug as well as the solvent/antisolvent system applied. For the substances under investigation within this work, BHT to fenofibrate ratios of 3:5 (w/w) in combination with total surfactant concentrations of ~15 to 300 µg per g/dispersion were found to be most appropriate for the stabilization of the dispersions.

6.2.1.3. DOWNSTREAM PROCESSING

Lyophilization was found to be a valuable tool for solvent removal from the fenofibrate dispersions. Even more importantly, also the BHT content in the dispersions could be varied by the freeze drying process (**Section 5.4.2.1**). This is important, as BHT was found to fully

exhibit its stabilizing effects at concentrations which were significantly increased compared to those at which the antioxidant is commonly applied. By the application of freeze drying as downstream processing technology, toxicity issues connected to the use of the excipient can thereby be avoided.

Surprisingly, but confirmed by the results of de Waard et al. [177], the fenofibrate dispersions were found to crystallize within the lyophilization process (**Section 5.4.2.3**). This fact as well as the comparable fluorescence patterns of liquid and crystalline fenofibrate polymorphs (**Section 4.4.4**) indicates that already in the liquid phase an oriented arrangement of the fenofibrate molecules exists, which solidifies upon solvent removal. Concerning the aim of maintaining the solubility advantage of the liquid precipitate, lyophilization was found to be rather inappropriate, as the crystalline state of the drug as well as the observed increase in particle size counteract this purpose. Further analysis will need to be accomplished to investigate whether the crystallization from the liquid phase during freeze drying is specific for fenofibrate or endemic for liquid-liquid phase separating substances. Also other long term stabilization techniques that involve solvent removal from the liquid dispersions, need to be undertaken a critical review, as they should not affect the amorphous state of the drug, and, in the best case, allow for complete rehydration of the precipitate to its original liquid state.

6.3. OUTLOOK

6.3.1 THE SIMULATION AND THE ACCOMPLISHMENT OF ANTISOLVENT PRECIPITATION

Mathematical models proved to be very useful in identifying the phase separation mechanisms of fenofibrate. In how far such models can be further developed to efficiently support decision makers in the development of drug dispersion technologies is still poorly predictable. Spinodal decomposition, within this work identified as prevalent phase separation mechanism in antisolvent precipitation, still appears hardly accessible by mathematical description. Even without considering the impact of mixing or varying solvent composition, theoretical approaches developed mainly since the 1990s just recently succeed to effectively simulate the structural evolution in spinodal phase separation processes [102, 184, 185]. The formation of complex emulsion systems as were observed for fenofibrate are

not yet included in such simulations. Models especially addressing liquid-liquid phase separation [186, 187] do exist, as well as such mapping coalescence [188, 189] or the hydrodynamical breakdown and of a dispersed liquid phase [75, 190, 191]. Kiesow et al. [192] provided a first approach for simulating the phase separation behavior for organic molecules and presented promising results concerning the predictability of liquid-liquid phase separation in a given solute-solvent system. However, all these models only mirror snapshots of individual subprocesses in phase separation. Nevertheless, the recognition of the importance of such models steadily increases, as they, also beyond this work, proved to be of great help in identifying the measures required for the tailor made particle preparation.

Concerning the practical applicability of the experiences made with fenofibrate to other compounds, it becomes clear, that the mechanical properties of the precipitate must have a distinct impact on sample preparation as well as on dispersion stability. Under intense mixing conditions, the adjustment of sample viscosity by the addition of a suitable coprecipitate can help to control the hydrodynamical impact on the precipitate. It can hence assist to control particle size and size distribution. While the impinging jet reactors used within this work provide good control of the process conditions, other mixing devices might be more effective in reducing particle size. Exemplarily mentioned are cavitation mixing devices such as high pressure homogenizers, which are known to very effectively disrupt liquid phases [193, 194].

6.3.2 THE POTENTIAL USE OF GENERATING AND APPLYING LIQUID-LIQUID PHASE SEPARATION

The structural unspecificity characterizing liquid precipitates reveals a wide applicability of techniques such as the above described coprecipitation with BHT. Besides the solubilizing effect exhibited on the drug itself, it also facilitates the solubilization of potential co-substrates in the dispersed phase, thereby opening up additional formulation pathways.

Liquid-liquid phase separation is not limited to a certain category of compounds, but is observed for a wide variety of structural and functional characteristics. It hence has the potential to be developed in additional fields exceeding the solubilization of poorly soluble drugs. Liquid phase separating substances include small organic molecules which can be neutral, acids or bases [55, 68, 70, 183, 195], proteins [135, 142, 196, 197] polymers [198,

199], inorganic compounds [200] or even colloids [201-203]. Key to the successful stabilization of the liquid phase is in each case to control the interaction potential between the solute molecules in the precipitate. Given the fact that just recently scientific interest recovers the prevalence and industrial applicability of liquid-liquid phase separation [111, 112, 204], it is not surprising that comparable data as obtained by accomplishment of this work are hardly described in the scientific literature. Based on the results described above and on an intense screening of the available publications, two classes of excipients can be identified who account promising for the induction and stabilization of liquid phase separation:

First, these are substances that induce or stabilize the formation of a liquid precipitate by direct molecular interactions (e.g. Van-der-Waals forces or (induced) dipole-dipole) with the solute of interest. Such intrinsically working excipients typically are molecules that have a higher affinity to the solute than to the solvent, forming coprecipitates on a molecular level or by the formation a viscous matrix. BHT falls in this category of substances as do adsorbing or nonadsorbing polymers, which were used for inducing liquid phase separation in colloidal and macromolecular dispersions [142, 205].

Secondly, excipients can be applied that predominantly affect the solubilizing properties of the continuous phase. These include reagents as citric acid, which are capable to change the ionic strength, the pH, or the polarity of a solvent. Examples are acids/bases as well as antisolvents showing a certain miscibility with the solute's solvent, but having poor solubilizing properties for the solute itself. They increase the interactions between the solute molecules on the expense of solute-solvent interactions (salting out). These stimuli extrinsically affecting the physical state of the precipitate can be extended to physical factors such as changes in temperature [117], application of electrical fields [206], as well as other physical parameters which can modify intermolecular interactions.

It can be anticipated, that the prevalence of liquid-liquid phase separation is still underestimated. Reasons therefore are the facts that the liquid phase is often very transient, or that the optical and mechanical properties of the precipitates falsely suggest the prevalence of solid amorphous particles. In consequence, the recognition, analysis and understanding of liquid-liquid phase separation is in most cases limited to macroscopically observable precipitates, as are often described and expected to occur for proteins or polymer blends.

In thematic relation to the stabilization techniques developed for fenofibrate, the use of coprecipitants not only provides the experimental freedom for downstream processing of the dispersions. Knowing that many of the substances in the development pipelines of pharmaceutical companies intrinsically show distinct difficulties to be crystallized, the knowledge gained with the above described experiments is capable to allow for many of these compounds to be further developed towards a marketable dosage form. Imaginable are in situ forming drug delivery systems being composed of a solvent and an antisolvent that are mixed to form the precipitate prior to the intake of the formulation.

Also dosage forms such as capsules containing the pure liquid precipitate appear to be an attractive option when considering the remarkable stability of many liquid-liquid phase separating substances in comparison to fenofibrate [110, 111]. By adjusting the molecular interaction in the precipitates, shelf lives of such products of up to 2 years appear realistic. Such systems would not necessarily need to consist of a dispersed system, but might just comprise one homogeneous phase of the liquid drug/coprecipitation product. Such drug delivery systems have not yet been reported in the scientific field, and might offer an attractive niche in the drug delivery world. Within the life cycle management of a drug, they offer an interesting option for prolonging the exclusivity rights of the license holder.

Considering the wide prevalence of liquid-liquid phase separation in aqueous systems, even solid dosage forms, creating a liquid precipitate upon in-vivo dissolution appear possible. A good example of a yet poorly understood dosage form that might exhibit liquid-liquid phase separation is Kaletra[®], an antiretroviral medication currently marketed by Abbott Laboratories. Recent investigations show, that upon dissolution of the dosage form, particle formation mechanism and composition, drug solubility as well as the robustness against food intake are very comparable to what would have been expected for liquid-liquid phase separating substances [207, 208]. As for the combination of BHT and fenofibrate, also Kaletra[®] is composed of a system comprising two lipophilic compounds, ritonavir and lopinavir.

References

1. Marty, J.J., R.C. Oppenheim, and P. Speiser, *Nanoparticles - a new colloidal drug delivery system*. Pharmaceutica Acta Helvetiae, 1978. **53**(1): p. 17-23.
2. Couvreur, P., et al., *Nanocapsules: a new type of lysosomotropic carrier*. FEBS Lett., 1977. **84**(2): p. 323-6.
3. Kocbek, P., S. Baumgartner, and J. Kristl, *Preparation and evaluation of nanosuspensions for enhancing the dissolution of poorly soluble drugs*. International Journal of Pharmaceutics, 2006. **312**(1-2): p. 179-186.
4. Rabinow, B.E., *Nanosuspensions in drug delivery*. Nature Reviews Drug Discovery, 2004. **3**(9): p. 785-796.
5. Horn, D. and J. Rieger, *Organic nanoparticles in the aqueous phase - theory, experiment and use*. Angewandte Chemie, International Edition, 2001. **40**(23): p. 4330-4361.
6. Haberkorn, H., et al., *Early stages of particle formation in precipitation reactions. Quinacridone and boehmite as generic examples*. Journal of Colloid and Interface Science, 2003. **259**(1): p. 112-126.
7. Mersmann, A. and M. Löffelmann, *Crystallization and Precipitation: The Optimal Supersaturation*. Chemie Ingenieur Technik - CIT, 1999. **71**(11): p. 1240-1244.
8. Bonnett, P.E., et al., *Solution crystallization via a submerged liquid-liquid phase boundary: oiling out*. Chemical Communications (Cambridge, United Kingdom), 2003(6): p. 698-699.
9. Gassmann, P., et al., *Hydrosols - alternatives for the parenteral application of poorly water-soluble drugs*. European Journal of Pharmaceutics and Biopharmaceutics, 1994. **40**(2): p. 64-72.
10. FDA, F.a.D.A. *ANDAs: Pharmaceutical Solid Polymorphism*. Chemistry, Manufacturing, and Controls Information 2007 [cited 2007 August 28th].
11. Brouwer, N.W., M.; van Riet-Nales, D.; de Kaste, D., *Nanopharmaceuticals: Implications for the European Pharmacopoeia*. Pharmeuropa, 2010. **22**(1): p. 5-7.
12. Patel, D.V. and E.M. Gordon, *Applications of small-molecule combinatorial chemistry to drug discovery*. Drug Discovery Today, 1996. **1**(4): p. 134-144.
13. Moos, W.H., G.D. Green, and M.R. Pavia, *Recent advances in the generation of molecular diversity*. Annu. Rep. Med. Chem., 1993. **28**: p. 315-24.
14. Kubinyi, H., *Strategies and recent technologies in drug discovery*. Pharmazie, 1995. **50**(10): p. 647-62.
15. Benet, L. in *Annual European Drug Absorption Network (EDAN) Meeting*. 2007. Katholieke Universiteit Leuven, Belgium.
16. Keck, C.M.K., Szymon; Mauludin, Rachmat; Müller, Rainer H., *Second Generation of Drug Nanocrystals for Delivery of Poorly Soluble Drugs: Smartcrystals Technology*. Dosis, 2008. **24**(2): p. 124-128.
17. Lian, T. and R.J.Y. Ho, *Trends and developments in liposome drug delivery systems*. J. Pharm. Sci., 2001. **90**(6): p. 667-680.
18. Augustijns, P.B., Marcus E., *Solvent Systems and Their Selection in Pharmaceutics and Biopharmaceutics*. Biotechnol.: Pharm. Aspects. Vol. 6. 2007. 457 pp.
19. Rasenack, N., H. Steckel, and B.W. Mueller, *Preparation of microcrystals by in situ micronization*. Powder Technology, 2004. **143-144**: p. 291-296.

20. Keck, C.M. and R.H. Müller, *Drug nanocrystals of poorly soluble drugs produced by high pressure homogenisation*. European Journal of Pharmaceutics and Biopharmaceutics, 2006. **62**(1): p. 3-16.
21. Davis, M.E. and M.E. Brewster, *Cyclodextrin-based pharmaceuticals: past, present and future*. Nat. Rev. Drug Discovery, 2004. **3**(12): p. 1023-1035.
22. Chen, Y., et al., *Enhanced bioavailability of the poorly water-soluble drug fenofibrate by using liposomes containing a bile salt*. Int. J. Pharm., 2009. **376**(1-2): p. 153-160.
23. Tiwari, S.B., D.B. Shenoy, and M.M. Amiji, *Nanoemulsion formulations for improved oral delivery of poorly soluble drugs*. NSTI Nanotech 2006, NSTI Nanotechnol. Conf. Trade Show, 2006. **1**: p. 475-478.
24. Leuner, C. and J. Dressman, *Improving drug solubility for oral delivery using solid dispersions*. Eur. J. Pharm. Biopharm., 2000. **50**(1): p. 47-60.
25. Serajuddin, A.T.M., *Solid Dispersion of Poorly Water-Soluble Drugs: Early Promises, Subsequent Problems, and Recent Breakthroughs*. J. Pharm. Sci., 1999. **88**(10): p. 1058-1066.
26. Gao, P., et al., *Development of a supersaturable SEDDS (S-SEDDS) formulation of paclitaxel with improved oral bioavailability*. J. Pharm. Sci., 2003. **92**(12): p. 2386-2398.
27. Francis, M., *Engineering polymeric micelles for solubilization of poorly-water soluble drugs: A novel approach for oral drug delivery*. 2005. p. 327 pp.
28. Florence, A.T. and E.G. Salole, *Changes in crystallinity and solubility on comminution of digoxin and observations on spironolactone and estradiol*. J. Pharm. Pharmacol., 1976. **28**(8): p. 637-42.
29. Voigt, R., *Pharmazeutische Technologie: Für Studium und Beruf*. Vol. 9. 2000, Stuttgart: Deutscher Apothekerverlag.
30. Noyes, A.A. and W.R. Whitney, *The rate of solution of solid substances in their own solutions*. Journal of the American Chemical Society, 1897. **19**(12): p. 930-4.
31. Stricker, H.S., Cammarata, *Physikalische Pharmazie - Pharmazeutisch angewandte physikalisch-chemische Grundlagen*. 1987 Wiss. Verlagsges.: Stuttgart.
32. Bisrat, M. and C. Nystroem, *Physicochemical aspects of drug release. VIII. The relation between particle size and surface specific dissolution rate in agitated suspensions*. International Journal of Pharmaceutics, 1988. **47**(1-3): p. 223-31.
33. Thomson, W.L., *On the equilibrium of vapour at a curved surface of liquid*. Philosophical Magazine, 1871. **4,42**(282): p. 448-452.
34. Lindfors, L., et al., *Amorphous Drug Nanosuspensions. 1. Inhibition of Ostwald Ripening*. Langmuir, 2006. **22**(3): p. 906-910.
35. Storey, R., et al., *Automation of solid form screening procedures in the pharmaceutical industry - How to avoid the bottlenecks*. Crystallogr. Rev., 2004. **10**(1): p. 45-56.
36. Seitz, F.E., Henry; Turnbull, David, ed. *Solid State Physics: Advances in Research and Applications*. 1970, Academic Press, Inc: New York. 420.
37. Buchanan, R.C., ed. *Materials crystal chemistry*. 1997, Marcel Dekker, Inc.: New York. 462.
38. Byrn, S.R., *Polymorphism and Pharmaceuticals*, in AAPS Webinar. 2009.
39. Hancock, B.C. and M. Parks, *What is the true solubility advantage for amorphous pharmaceuticals?* Pharmaceutical Research, 2000. **17**(4): p. 397-404.

40. Hintz, R.J. and K.C. Johnson, *The effect of particle size distribution on dissolution rate and oral absorption*. International Journal of Pharmaceutics, 1989. **51**(1): p. 9-17.
41. Dai, W.-G., L.C. Dong, and Y.-Q. Song, *Nanosizing of a drug/carrageenan complex to increase solubility and dissolution rate*. International Journal of Pharmaceutics, 2007. **342**(1-2): p. 201-207.
42. Deng, Z., S. Xu, and S. Li, *Understanding a relaxation behavior in a nanoparticle suspension for drug delivery applications*. International Journal of Pharmaceutics, 2008. **351**(1-2): p. 236-243.
43. Liversidge, G.G., *Surface-modified anticancer nanoparticles*. 1992, Sterling Winthrop Inc.: EP. p. 15.
44. Sommer, M., *Mechanical production of nanoparticles in stirred media mills*, in *Institute of Particle Technology of Munich/Erlangen*. 2006, University Erlangen-Nuremberg: Erlangen. p. 1-179.
45. Peters, K., et al., *Preparation of a clofazimine nanosuspension for intravenous use and evaluation of its therapeutic efficacy in murine Mycobacterium avium infection*. Journal of Antimicrobial Chemotherapy, 2000. **45**(1): p. 77-83.
46. Hecq, J., et al., *Preparation and in vitro/in vivo evaluation of nano-sized crystals for dissolution rate enhancement of ucb-35440-3, a highly dosed poorly water-soluble weak base*. European Journal of Pharmaceutics and Biopharmaceutics, 2006. **64**(3): p. 360-368.
47. Zhang, D., et al., *Preparation of Azithromycin Nanosuspensions by High Pressure Homogenization and its Physicochemical Characteristics Studies*. Drug Development and Industrial Pharmacy, 2007. **33**(5): p. 569-575.
48. Midler, M., Jr., et al., *Crystallization method to improve crystal structure and size*. 1994, Merck and Co., Inc., USA: US. p. 11.
49. Sugiyama, M.G., David; Derby, Jeffrey J.; Barocas, Victor H. , *Protein-Salt-Water Solution Phase Diagram Determination by a Combined Experimental-Computational Scheme*. Crystal Growth & Design, 2008. **8**(12): p. 1021.
50. Chen, X., *Nanoparticle engineering processes: Evaporative precipitation into aqueous solution (EPAS) and antisolvent precipitation to enhance the dissolution rates of poorly water soluble drugs*. Dissertation, 2004: p. 190.
51. Ostwald, W., *Vapour pressure of reciprocally soluble liquids*. Annalen der Physik, 1897. **63**(ii): p. 336-41.
52. Schwarzer, H.C. and W. Peukert, *Combined experimental/numerical study on the precipitation of nanoparticles*. AIChE Journal, 2004. **50**(12): p. 3234-3247.
53. Chen, J.-F., et al., *Preparation and Characterization of Amorphous Cefuroxime Axetil Drug Nanoparticles with Novel Technology; High-Gravity Antisolvent Precipitation*. Industrial & Engineering Chemistry Research, 2006. **45**(25): p. 8723-8727.
54. Zhang, J.-Y., et al., *Preparation of amorphous cefuroxime axetil nanoparticles by controlled nanoprecipitation method without surfactants*. International Journal of Pharmaceutics, 2006. **323**(1-2): p. 153-160.
55. Brick, M.C., H.J. Palmer, and T.H. Whitesides, *Formation of Colloidal Dispersions of Organic Materials in Aqueous Media by Solvent Shifting*. Langmuir, 2003. **19**(16): p. 6367-6380.
56. Ali, H.S.M., P. York, and N. Blagden, *Preparation of hydrocortisone nanosuspension through a bottom-up nanoprecipitation technique using microfluidic reactors*. International Journal of Pharmaceutics, 2009. **375**(1-2): p. 107-113.

57. Woo, X.Y., et al., *Adaptive Concentration Control of Cooling and Antisolvent Crystallization with Laser Backscattering Measurement*. *Crystal Growth & Design*, 2009. **9**(1): p. 182-191.
58. Gradl, J., et al., *Precipitation of nanoparticles in a T-mixer: Coupling the particle population dynamics with hydrodynamics through direct numerical simulation*. *Chemical Engineering and Processing*, 2006. **45**(10): p. 908-916.
59. Violante, M.B. and H.W. Fischer, *Method for making uniformly-sized particles from insoluble compounds*. 1991, University of Rochester, USA: USA.
60. Plasari, E., P. Grisoni, and J. Villiermaux, *Influence of process parameters on the precipitation of organic nanoparticles by drowning-out*. *Chem. Eng. Res. Des.*, 1997. **75**(A2): p. 237-244.
61. End, L., D. Horn, and E. Lueddecke, *Method for preparing finely-divided suspensions of pharmaceuticals such as b-carotene and fenofibrate*. 1995, BASF Aktiengesellschaft: DE. p. 6.
62. Robeson, L.M., ed. *Polymer blends: a comprehensive review*. 2007, Hanser Gardner Publication, Inc.: Cincinnati. 459.
63. Stephan, K.M., Franz ed. *Thermodynamik: Grundlagen und technische Anwendungen*. Vol. 14. 1999, Springer-Verlag: Berlin/Heidelberg. 442.
64. Stephan, P.S., Karlheinz; Stephan, Karl; Mayinger, Franz, *Thermodynamik. Grundlagen und technische Anwendungen 2* Vol. 15. 2010, Heidelberg: Springer-Verlag Berlin Heidelberg. 680.
65. Myerson, A.S. and Editor, *Molecular Modeling Applications in Crystallization*. 1999. 354 pp.
66. Schwarzer, H.C. and W. Peukert, *Prediction of aggregation kinetics based on surface properties of nanoparticles*. *Chemical Engineering Science*, 2004. **60**(1): p. 11-25.
67. Garside, J., J.W. Mullin, and S.N. Das, *Growth and dissolution kinetics of potassium sulfate crystals in an agitated vessel*. *Industrial & Engineering Chemistry Fundamentals*, 1974. **13**(4): p. 299-305.
68. Lince, F., D.L. Marchisio, and A.A. Barresi, *Strategies to control the particle size distribution of poly-e-caprolactone nanoparticles for pharmaceutical applications*. *Journal of Colloid and Interface Science*, 2008. **322**(2): p. 505-515.
69. Schoell, J., et al., *Antisolvent Precipitation of PDI 747: Kinetics of Particle Formation and Growth*. *Crystal Growth & Design*, 2007. **7**(9): p. 1653-1661.
70. Woo, X.Y., R.B.H. Tan, and R.D. Braatz, *Modeling and Computational Fluid Dynamics-Population Balance Equation-Micromixing Simulation of Impinging Jet Crystallizers*. *Crystal Growth & Design*, 2009. **9**(1): p. 156-164.
71. *SciFinder Scholar*, American Chemical Society.
72. Kinoshita, T., *The method to determine the optimum refractive index parameter in laser diffraction and scattering methods*. *Funtai Kogaku Kaishi*, 2000. **37**(5): p. 354-361.
73. Rzoska, S.J., V.A. Mazur, and Editors. *Soft Matter Under Exogenic Impacts*. in *NATO Advanced Research Workshop*. 2007. Odessa, Ukraine.
74. Schwarzer, H.-C., et al., *Predictive simulation of nanoparticle precipitation based on the population balance equation*. *Chemical Engineering Science*, 2005. **61**(1): p. 167-181.
75. Vankova, N., et al., *Emulsification in turbulent flow I. Mean and maximum drop diameters in inertial and viscous regimes*. *J Colloid Interface Sci*, 2007. **312**(2): p. 363-80.

76. Anon, *CRC Handbook of Chemistry and Physics*, 88th edited by David R. Lide. Journal of the American Chemical Society. Vol. 130. 2008. 382.
77. Gradl, J., et al., *Predictive simulation of nanoparticles-precipitation in a T-mixer by coupling direct numerical simulation with population balance equations*. AIChE Spring National Meeting, Conference Proceedings, Orlando, FL, United States, Apr. 23-27, 2006, 2006: p. 908-916.
78. Baldyga, J.B., John R., *Turbulent Mixing and Chemical Reactions*. Vol. 1. 1999: Wiley, J 868.
79. Schwarzer, H., Christoph, ed. *Nanoparticle precipitation - An experimental and numerical investigation including mixing*. Vol. 1. 2005, Logos Verlag Berlin GmbH, Berlin. 200.
80. Rodriguez-Hornedo, N. and D. Murphy, *Significance of Controlling Crystallization Mechanisms and Kinetics in Pharmaceutical Systems*. Journal of Pharmaceutical Sciences, 1999. **88**(7): p. 651-660.
81. Schoell, J., et al., *Precipitation of α -L-glutamic acid: determination of growth kinetics*. Faraday Discussions, 2007. **136**: p. 247-264.
82. Anderson, V.J. and H.N.W. Lekkerkerker, *Insights into phase transition kinetics from colloid science*. Nature (London, United Kingdom), 2002. **416**(6883): p. 811-815.
83. Young, T., *An Essay on the Cohesion of Fluids*. Philos. Trans. R. Soc., 1805. **95**: p. 23.
84. Sutjiadi-Sia, Y., P. Jaeger, and R. Eggers, *Interfacial tension of solid materials against dense carbon dioxide*. Journal of Colloid and Interface Science, 2008. **320**(1): p. 268-274.
85. Planinsek, O., et al., *The utilization of surface free-energy parameters for the selection of a suitable binder in fluidized bed granulation*. International Journal of Pharmaceutics, 2000. **207**(1-2): p. 77-88.
86. Chudej, J.G., A., Capek, I. *Dispersion Copolymerization of Styrene with Vinylbenzyl-Terminated Polyoxyethylene Macromonomer*. in *Macromol. Symp.* 2002.
87. Marinova, K.G., et al., *Charging of Oil-Water Interfaces Due to Spontaneous Adsorption of Hydroxyl Ions*. Langmuir, 1996. **12**(8): p. 2045-51.
88. Schwarzer, H.C. and W. Peukert, *Tailoring particle size through nanoparticle precipitation*. Chemical Engineering Communications, 2004. **191**(4): p. 580-606.
89. Walters, D.A., *A stable transitional flow pattern in the surface tension driven spreading of ethanol-water solutions*. Langmuir, 1990. **6**(5): p. 991-994.
90. Wakisaka, A. and K. Matsuura, *Microheterogeneity of ethanol-water binary mixtures observed at the cluster level*. Journal of Molecular Liquids, 2006. **129**(1-2): p. 25-32.
91. *IUPAC Compendium of Analytical Nomenclature*. September 12th 2010]; Available from: <http://goldbook.iupac.org/G02641.html>.
92. Broze, G. and Editor, *Handbook of Detergents, Part A: Properties*. 1999. 797 pp.
93. Rulison, C., *Characterization of Ethanol/Water Solutions*. 1998, Krüss GmbH, Application note
94. Bollen, A.M. and J.A. Wesselingh, *The behaviour of the binodal and spinodal curves for near-binary compositions*. Fluid Phase Equilibria, 1998. **149**(1-2): p. 17-25.
95. Blaß, E., *Transport Mechanisms across Fluid Interfaces. (Papers of the Final Meeting of a Priority Program of the Deutsche Forschungsgemeinschaft, held 29*

- November-1 December 1999, in Munchen, Germany.) [In: *DECHEMA Monogr.*, 2000; 136]. 2000. 390 pp.
96. Wan, L.S.C. and P.F.S. Lee, *CMC of polysorbates*. *Journal of Pharmaceutical Sciences*, 1974. **63**(1): p. 136-137.
 97. Kawakami, K., et al., *Solubilization behavior of a poorly soluble drug under combined use of surfactants and cosolvents*. *European Journal of Pharmaceutical Sciences*, 2006. **28**(1-2): p. 7-14.
 98. Jamzad, S. and R. Fassihi, *Role of surfactant and pH on dissolution properties of fenofibrate and glipizide--a technical note*. *AAPS PharmSciTech*, 2006. **7**(2): p. E33.
 99. Çengel, Y.A., ed. *Heat transfer: a practical approach*. Vol. 2. 2003, The McGraw-Hill Companies, Inc.: New York. 932.
 100. Btawdziewicz, J., et al., *Direct numerical simulation of three-dimensional drop breakup in isotropic turbulence*. *FED (American Society of Mechanical Engineers)*, 1998. **245**: p. 1/9-1/14.
 101. Dekany, I., *The Encyclopedic Handbook of Emulsion Technology Edited by Johan Sjoblom*. *Reaction Kinetics and Catalysis Letters*. Vol. 74. 2001. 397-399.
 102. Sofonea, V. and K.R. Mecke, *Morphological characterization of spinodal decomposition kinetics*. *Eur. Phys. J. B*, 1999. **8**(1): p. 99-112.
 103. Zhang, H.-X., et al., *Micronization of atorvastatin calcium by antisolvent precipitation process*. *International Journal of Pharmaceutics*, 2009. **374**(1-2): p. 106-113.
 104. Wang, X. and D.J. Kirwan, *Quasi-Emulsion Precipitation of Pharmaceuticals. 2. Application to Control of Polymorphism*. *Crystal Growth & Design*, 2006. **6**(10): p. 2228-2240.
 105. Murnane, D., C. Marriott, and G.P. Martin, *Comparison of salmeterol xinafoate microparticle production by conventional and novel antisolvent crystallization*. *European Journal of Pharmaceutics and Biopharmaceutics*, 2008. **69**(1): p. 94-105.
 106. Nocent, M.B., L.; Espitalier, F.; Baron, M.; Couarraze, G. , *Definition of a solvent system for spherical crystallization of salbutamol sulfate by quasi-emulsion solvent diffusion (QESD) method*. *Journal of Pharmaceutical Sciences*, 2001. **90**(10): p. 1620-1627.
 107. Wang, X., J.M. Gillian, and D.J. Kirwan, *Quasi-Emulsion Precipitation of Pharmaceuticals. 1. Conditions for Formation and Crystal Nucleation and Growth Behavior*. *Crystal Growth & Design*, 2006. **6**(10): p. 2214-2227.
 108. Ostwald, W., *The formation and changes of solids*. *Zeitschrift für Physikalische Chemie, Stöchiometrie und Verwandtschaftslehre*, 1897. **22**: p. 289-330.
 109. Threlfall, T., *Structural and Thermodynamic Explanations of Ostwald's Rule*. *Organic Process Research & Development*, 2003. **7**(6): p. 1017-1027.
 110. Sitnikova, N.L., et al., *Spontaneously Formed trans-Anethol/Water/Alcohol Emulsions: Mechanism of Formation and Stability*. *Langmuir*, 2005. **21**(16): p. 7083-7089.
 111. Tung, H.-H.P., Edward L.; Midler, Michael ; McCauley, James Andrew *Crystallization of Organic Compounds - An Industrial Perspective*. 2009: Wiley. 289.
 112. Carpenter, K.J. and W.M.L. Wood, *Industrial crystallization for fine chemicals*. *Advanced Powder Technology*, 2004. **15**(6): p. 657-672.
 113. *Particle size analysis by laser light diffraction*, in *Ph. Eur.* . 2007, Council of Europe: Strasbourg.

114. Bonnett, P.C., K.J.; Davey, R.J. . *A study into the phenomenon of oiling out.* in *15th International Symposium On Industrial Crystallization*. 2002. Sorrento, Italy.
115. Hancock, B.C. and G. Zografi, *Characteristics and significance of the amorphous state in pharmaceutical systems*. *Journal of Pharmaceutical Sciences*, 1997. **86**(1): p. 1-12.
116. Kim, S., C. Wei, and S. Kiang, *Crystallization Process Development of an Active Pharmaceutical Ingredient and Particle Engineering via the Use of Ultrasonics and Temperature Cycling*. *Organic Process Research & Development*, 2003. **7**(6): p. 997-1001.
117. Lafferrere, L., C. Hoff, and S. Veessler, *Study of liquid-liquid demixing from drug solution*. *Journal of Crystal Growth*, 2004. **269**(2-4): p. 550-557.
118. Veessler, S., et al., *Phase Transitions in Supersaturated Drug Solution*. *Organic Process Research & Development*, 2003. **7**(6): p. 983-989.
119. Deneau, E. and G. Steele, *Some physicochemical studies on the oiling out of a pharmaceutical compound*. *World Congress of Chemical Engineering*, 7th, Glasgow, United Kingdom, July 10-14, 2005, 2005: p. 83440/1-83440/10.
120. Deneau, E. and G. Steele, *An In-Line Study of Oiling Out and Crystallization*. *Organic Process Research & Development*, 2005. **9**(6): p. 943-950.
121. Lafferrere, L., C. Hoff, and S. Veessler, *In Situ Monitoring of the Impact of Liquid-Liquid Phase Separation on Drug Crystallization by Seeding*. *Crystal Growth & Design*, 2004. **4**(6): p. 1175-1180.
122. Jung, C., et al., *Simultaneous Measurement of Orientational and Spectral Dynamics of Single Molecules in Nanostructured Host-Guest Materials*. *J. Am. Chem. Soc.*, 2007. **129**(17): p. 5570-5579.
123. Laplace, P.S., *Traité de Mécanique Céleste*. Gauthier-Villars, 1806. **Supplement to Book 10**.
124. Schramm, L.L., ed. *Emulsions, foams, and suspensions: fundamentals and applications*. 2005, Wiley-VCH Verlag GmbH & Co. KGaA: Weinheim. 448.
125. Espitalier, F., B. Biscans, and C. Laguérie, *Particle design Part B: batch quasi-emulsion process and mechanism of grain formation of ketoprofen*. *Chemical Engineering Journal*, 1997. **68**(2-3): p. 103-114.
126. Aksimentiev, A., et al., *Kinetics of the droplet formation at the early and intermediate stages of the spinodal decomposition in homopolymer blends*. *Macromolecular Theory and Simulations*, 2000. **9**(8): p. 661-674.
127. Rosenberg, J., et al., *Pharmaceutical compositions of fenofibrate with enhanced oral bioavailability*. 2007, Abbott Laboratories: USA. p. 30.
128. Bunjes, H., *An overview on nano-particulate systems*. 2008, Arbeitsgemeinschaft für Pharmazeutische Verfahrenstechnik e.v.: Basel, Switzerland.
129. Lindfors, L., et al., *Amorphous Drug Nanosuspensions. 3. Particle Dissolution and Crystal Growth*. *Langmuir*, 2007. **23**(19): p. 9866-9874.
130. Jolley, J.E., *Microstructure of photographic gelatin binders*. *Photogr. Sci. Eng.*, 1970. **14**(3): p. 169-77.
131. Attili, A., *Study of the glass transition of a supercooled liquid mixture in bulk and confined phases*, in *Dispartimento di Fisica "Edoardo Amaldi"*. 2003, Universita Degli Studi Roma Tre: Rome. p. 171.
132. Derdour, L., *A method to crystallize substances that oil out*. *Chemical Engineering Research and Design*, 2010. **88**(9): p. 1174-1181.
133. Espitalier, F., B. Biscans, and C. Laguérie, *Particle design Part A: Nucleation kinetics of ketoprofen*. *Chemical Engineering Journal*, 1997. **68**(2-3): p. 95-102.

References

134. Ray, W.J., Jr. and C.E. Bracker, *Polyethylene glycol: catalytic effect on the crystallization of phosphoglucosylase at high salt concentration*. J. Cryst. Growth, 1986. **76**(3): p. 562-76.
135. Kuznetsov, Y.G., A.J. Malkin, and A. McPherson, *The liquid protein phase in crystallization: a case study-intact immunoglobulins*. Journal of Crystal Growth, 2001. **232**(1-4): p. 30-39.
136. Henry, R.F., et al., *Fenofibrate*. Acta Crystallographica, Section E: Structure Reports Online, 2003. **E59**(5): p. o699-o700.
137. Lee, H.C., Robert, D.; Cody, Anita M.; Spry Paul G., *Reduction of Concrete Expansion by Ettringite Using Crystallization Inhibition Techniques*. Environmental & Engineering Geoscience, 2003. **9**(4): p. 313-326.
138. Foltmann, H. and A. Quadir, *Polyvinylpyrrolidone (PVP) - one of the most widely used excipients in pharmaceuticals: an overview*. Drug Delivery Technol., 2008. **8**(6): p. 22, 24, 26-27.
139. Qiu, Y.L., Lirong; Chen, Yisheng; Zhang, Geoff G. Z.; Porter, William *Developing Solid Oral Dosage Forms: Pharmaceutical Theory & Practice*. 2009, Burlington USA: Academic Press. 943.
140. Lindfors, L., et al., *Nucleation and crystal growth in supersaturated solutions of a model drug*. Journal of Colloid and Interface Science, 2008. **325**(2): p. 404-413.
141. Flaschner, O. and I.G. Rankin, *Die Schmelz- und Sättigungskurven der binären Systeme: Substituierte Benzoesäuren und Wasser*. Monatshefte fuer Chemie, 1910. **31**: p. 23-50.
142. Galkin, O. and P.G. Vekilov, *Control of protein crystal nucleation around the metastable liquid-liquid phase boundary*. Proceedings of the National Academy of Sciences of the United States of America, 2000. **97**(12): p. 6277-6281.
143. Flink, J. and M. Karel, *Effects of process variables on retention of volatiles in freeze-drying*. Journal of Food Science, 1970. **35**(4): p. 444-7.
144. *BHT (butylated hydroxy toluene) - Preservative / Use*. 2010, SmartBodyz Nutrition.
145. *Inactive Ingredient List*. [cited 2010 Sept. 19th]; Available from: <http://www.accessdata.fda.gov/scripts/cder/iig/index.cfm>.
146. *Generally Recognized As Safe (GRAS) List*. Available from: <http://www.access.gpo.gov/cgi-bin/cfrassemble.cgi?title=200321>.
147. Ostwald, W., *Lehrbuch der allgemeinen Chemie. Second edition*. Vol. II, 2; Part I. 1896. Large octavo, 208 pages.
148. McClements, D.J., *Food emulsions: principles, practice, and techniques*. Vol. 2. 1999: CRC Press LLC. 378.
149. Kabal'nov, A.S., et al., *Influence of the nature and the composition of the disperse phase on the stability of direct emulsions to recondensation*. Kolloidnyi Zhurnal, 1985. **47**(6): p. 1048-1053.
150. Kabal'nov, A.S., A.V. Pertsov, and E.D. Shchukin, *Application of the Lifshits-Slezov theory to recondensation of direct emulsions*. Kolloidnyi Zhurnal, 1984. **46**(6): p. 1108-1111.
151. Kabal'nov, A.S., A.V. Pertsov, and E.D. Shchukin, *Ostwald ripening in two-component disperse phase systems: application to emulsion stability*. Colloids and Surfaces, 1987. **24**(1): p. 19-32.
152. Lindfors, L., et al., *Amorphous Drug Nanosuspensions. 2. Experimental Determination of Bulk Monomer Concentrations*. Langmuir, 2006. **22**(3): p. 911-916.

153. Reichman, D., and Garti, N, *Foods Polymers, Gels and Colloids*, ed. E. Dickinson. 1991, Cambridge: Royal Soc. Chem. 588.
154. Leuenberger, H.E., Ottheinrich, Lanz; Michael; Martin, Alfred N., *Physikalische Pharmazie: Pharmazeutisch angewandte und physikalisch-chemische Grundlagen*. Vol. 4. 2002, Stuttgart: Wissenschaftliche Verlagsgesellschaft Stuttgart. 785.
155. Teagarden, D.L. and D.S. Baker, *Practical aspects of lyophilization using non-aqueous co-solvent systems*. European Journal of Pharmaceutical Sciences, 2002. **15**(2): p. 115-133.
156. Zacharis, E., P.J. Halling, and D.G. Rees, *Volatile buffers can override the "pH memory" of subtilisin catalysis in organic media*. Proceedings of the National Academy of Sciences of the United States of America, 1999. **96**(4): p. 1201-1205.
157. Hui, Y.H. and Editor, *Handbook of Food Products Manufacturing*. 2007. 1221 pp.
158. Wittaya-Areekul, S., *Freeze-drying from nonaqueous solution*. Warasan Pheasatchasat, 1999. **26**(1-4): p. 33-43.
159. Costantino, H., R.; Pikal, Michael, J., ed. *Lyophilization of biopharmaceuticals*. Biotechnology: Pharmaceutical Aspects. 2004, American Association of Pharmaceutical Scientists. 686.
160. Dawson, P.J. and D.J. Hockley, *Scanning electron microscopy of freeze-dried preparations: relationship of morphology to freeze-drying parameters*. Dev. Biol. Stand., 1992. **74**(Biol. Prod. Freeze-Drying Formulation): p. 185-92.
161. Khan, S., I. Parikh, and H. Loughrey, *Method of preparing stable suspensions of insoluble microparticles*. 2000, RTP Pharma Inc.,USA: WO. p. 26.
162. Lindfors, L. *Nanoparticle formulations of poorly soluble drugs*. in *6th World Meeting on Pharmaceutics, Biopharmaceutics and Pharmaceutical Technology*. 2008. Barcelona.
163. Bassil, N.C., et al., *Nanoparticulate formulations of fenofibrate*. 2003, Jagotec AG,Switz.: World. p. 34.
164. Gustavsson, N.O., et al., *Pharmaceutically acceptable starch*. 2002, Bioglan AB, Sweden: WO. p. 43.
165. Krill, S.K., *Inhibitors of crystallization in a solid dispersion*. 2001, Abbott Laboratories,USA: WO. p. 50.
166. Broman, E., C. Khoo, and L.S. Taylor, *A comparison of alternative polymer excipients and processing methods for making solid dispersions of a poorly water soluble drug*. International Journal of Pharmaceutics, 2001. **222**(1): p. 139-151.
167. Yoshioka, M., B.C. Hancock, and G. Zografi, *Inhibition of indomethacin crystallization in poly(vinylpyrrolidone) coprecipitates*. Journal of Pharmaceutical Sciences, 1995. **84**(8): p. 983-986.
168. Parikh, I., *Fenofibrate microparticles containing a surface modifier*. 2002, Jagotec AG, Switzerland: US. p. 5.
169. Jumaa, M. and B.W. Müller, *The stabilization of parenteral fat emulsion using non-ionic ABA copolymer surfactant*. International Journal of Pharmaceutics, 1998. **174**(1-2): p. 29-37.
170. Auweter, H., et al., *Formulations of curcumine containing stable crystalline curcumine A*. 2001, BASF Aktiengesellschaft: EP. p. 10.
171. Mu, L. and S.S. Feng, *A novel controlled release formulation for the anticancer drug paclitaxel (Taxol®): PLGA nanoparticles containing vitamin E TPGS*. Journal of Controlled Release, 2003. **86**(1): p. 33-48.

172. Mokhtari, T., et al., *The effect of shear on colloidal aggregation and gelation studied using small-angle light scattering*. J. Colloid Interface Sci., 2008. **327**(1): p. 216-223.
173. Manley, S., et al., *Limits to Gelation in Colloidal Aggregation*. Physical Review Letters, 2004. **93**(10): p. 108302/1-108302/4.
174. Berli, C.L.A., D. Quemada, and A. Parker, *Gel transition of depletion flocculated emulsions*. Colloids and Surfaces, A: Physicochemical and Engineering Aspects, 2003. **215**(1-3): p. 201-204.
175. Tinkov, S., *Development of Ultrasound Contrast Agents for Targeted Drug and Gene Delivery* 2009. p. No pp.
176. Zhou, D., et al., *Physical stability of amorphous pharmaceuticals: importance of configurational thermodynamic quantities and molecular mobility*. Journal of Pharmaceutical Sciences, 2002. **91**(8): p. 1863-1872.
177. de Waard, H., W.L.J. Hinrichs, and H.W. Frijlink, *A novel bottom-up process to produce drug nanocrystals: Controlled crystallization during freeze-drying*. Journal of Controlled Release, 2008. **128**(2): p. 179-183.
178. Ganachaud, F. and J.L. Katz, *Nanoparticles and nanocapsules created using the Ouzo effect: spontaneous emulsification as an alternative to ultrasonic and high-shear devices*. ChemPhysChem, 2005. **6**(2): p. 209-216.
179. Vitale, S.A. and J.L. Katz, *Liquid Droplet Dispersions Formed by Homogeneous Liquid-Liquid Nucleation: "The Ouzo Effect"*. Langmuir, 2003. **19**(10): p. 4105-4110.
180. Scholten, E., E. van der Linden, and H. This, *The life of an anise-flavored alcoholic beverage: Does its stability cloud or confirm theory?* Langmuir, 2008. **24**(5): p. 1701-1706.
181. Colombani, J. and J. Bert, *Toward a complete description of nucleation and growth in liquid-liquid phase separation*. J. Non-Equilib. Thermodyn., 2004. **29**(4): p. 389-395.
182. Vekilov, P.G., *Two-step mechanism for the nucleation of crystals from solution*. Journal of Crystal Growth, 2005. **275**(1-2): p. 65-76.
183. Johnson, B.K. and R.K. Prud'homme, *Mechanism for Rapid Self-Assembly of Block Copolymer Nanoparticles*. Physical Review Letters, 2003. **91**(11): p. 118302/1-118302/4.
184. Kendon, V.M., et al., *Inertial effects in three-dimensional spinodal decomposition of a symmetric binary fluid mixture: a lattice Boltzmann study*. Journal of Fluid Mechanics, 2001. **440**: p. 147-203.
185. Mischaikow, K.W., Thomas, *Probabilistic validation of homology computations for nodal domains*. The Annals of Applied Probability, 2007. **17**(3): p. 980-1018.
186. Tegze, G., T. Pusztai, and L. Granasy, *Phase field simulation of liquid phase separation with fluid flow*. Materials Science & Engineering, A Structural Materials Properties, Microstructure and Processing, 2005. **A413-A414**: p. 418-422.
187. Anwar, J. and P.K. Boateng, *Computer Simulation of Crystallization from Solution*. Journal of the American Chemical Society, 1998. **120**(37): p. 9600-9604.
188. Simon, M., *Koaleszenz von Tropfen und Tropfenschwärmen*. 2004: p. 127.
189. Korobko, A.V., et al., *Coalescence in semiconcentrated emulsions in simple shear flow*. J. Chem. Phys., 2005. **123**(20): p. 204908/1-204908/11.
190. Vankova, N., et al., *Emulsification in turbulent flow 2. Breakage rate constants*. J Colloid Interface Sci, 2007. **313**(2): p. 612-29.

191. Steiner, H., et al., *Numerical simulation and experimental study of emulsification in a narrow-gap homogenizer*. Chem. Eng. Sci., 2006. **61**(17): p. 5841-5855.
192. Kiesow, K., F. Tumakaka, and G. Sadowski, *Experimental investigation and prediction of oiling out during crystallization process*. Journal of Crystal Growth, 2008. **310**(18): p. 4163-4168.
193. Chevalier-Lucia, D., et al., *Submicron emulsions processed by ultra-high pressure homogenization*. High Pressure Research: An International Journal, 2009. **29**(4): p. 732-738.
194. Leal-Calderon, F., V. Schmitt, and J. Bibette, *Emulsion science: basic principles*. 2 ed. 2007, New York: Springer Science+Business Media, LLC. 227.
195. Svaerd, M., S. Gracin, and A.C. Rasmuson, *Oiling out or molten hydrate-liquid-liquid phase separation in the system vanillin-water*. Journal of Pharmaceutical Sciences, 2007. **96**(9): p. 2390-2398.
196. Broide, M.L., et al., *Binary-liquid phase separation of lens protein solutions*. Proceedings of the National Academy of Sciences of the United States of America, 1991. **88**(13): p. 5660-4.
197. Slotta, U.K., et al., *An engineered spider silk protein forms microspheres*. Angewandte Chemie, International Edition, 2008. **47**(24): p. 4592-4594.
198. Chen, H.-L., et al., *Simultaneous liquid-liquid demixing and crystallization and its effect on the spherulite growth in poly(ethylene terephthalate)/poly(ether imide) blends*. Polymer, 1998. **39**(26): p. 6983-6989.
199. Soh, Y.S., J.H. Kim, and C.C. Gryte, *Phase behavior of polymer/solvent/non-solvent systems*. Polymer, 1995. **36**(19): p. 3711-17.
200. Bemmelen, J., M., *Die Absorption. II. Abhandlung: Die Bildung der Gels und ihre Struktur*. Zeitschrift für Anorganische Chemie, 1898. **18**(1): p. 14-18.
201. Asherie, N., A. Lomakin, and G.B. Benedek, *Phase diagram of colloidal solutions*. Physical Review Letters, 1996. **77**(23): p. 4832-4835.
202. De Hek, H. and A. Vrij, *Interactions in mixtures of colloidal silica spheres and polystyrene molecules in cyclohexane : I. Phase separations*. Journal of Colloid and Interface Science, 1981. **84**(2): p. 409-422.
203. Gast, A.P., C.K. Hall, and W.B. Russel, *Polymer-induced phase separations in nonaqueous colloidal suspensions*. Journal of Colloid and Interface Science, 1983. **96**(1): p. 251-67.
204. Smith, K.W., et al., *Liquid-liquid phase separation in acetone solutions of palm olein: implications for solvent fractionation*. European Journal of Lipid Science and Technology, 2007. **109**(4): p. 350-358.
205. Ilett, S.M., et al., *Phase behavior of a model colloid-polymer mixture*. Phys. Rev. E Stat. Phys., Plasmas, Fluids, Relat. Interdiscip. Top., 1995. **51**(2): p. 1344-52.
206. Shah, M., O. Galkin, and P.G. Vekilov, *Localized Generation of Attoliter Protein Solution Droplets by Electrofocused Liquid-Liquid Separation*. Journal of Physical Chemistry B, 2009. **113**(20): p. 7340-7346.
207. Tho, I., et al., *Formation of nano/micro-dispersions with improved dissolution properties upon dispersion of ritonavir melt extrudate in aqueous media*. European Journal of Pharmaceutical Sciences, 2010. **40**(1): p. 25-32.
208. Kanzer, J., et al., *In situ formation of nanoparticles upon dispersion of melt extrudate formulations in aqueous medium assessed by asymmetrical flow field-flow fractionation*. Journal of Pharmaceutical and Biomedical Analysis, 2010. **53**(3): p. 359-365.

Curriculum Vitae

Name: Klaus Freitag
Date of birth: April 12th 1980
Place of birth: Frankenberg (Eder)

Education and Work Experience

Since June 10: Laboratory head Galenics, SwissCo Services AG, Sisseln, Switzerland

Nov. 09 - Mai 10: Project manager Galenics, SwissCo Services AG, Sisseln, Switzerland

March 06 - July 09: Ph.D. candidate at the Department of Pharmacy, Pharmaceutical Technology and Biopharmaceutics, Ludwig-Maximilian University Munich, Germany; research group of Prof. Dr. Gerhard Winter

Feb. 09 - April 09: Internship at the University of Colorado, Denver, USA; research group of Prof. Dr. Thomas Anchordoquy

Dec. 05: Registration as a pharmacist

May 05 - Oct. 05: 2. part of the preregistration year: Practical training in the public pharmacy "Apotheke am Obermarkt" in Frankenberg, Germany

Nov. 04 - April 05: 1. part of the preregistration year: Internship at the University of British Columbia, Vancouver, Canada; research groups of Prof. Dr. Urs Hafeli and Prof. Dr. Brian Rodrigues

Oct. 00 - Dec. 05: Study of pharmacy

- Oct. 2000 - Sept. 2004 at the Philipps-University in Marburg, Germany (1st – 6th and 8th semester)
- Sept. 2003 - Feb. 2004 at the Université Paris Sud 11, Paris, France (7th semester)

Sept. 99 - June 00: Military service in Frankenberg, Germany

Sept. 90 - June 99: Gymnasium "Edertalschule" in Frankenberg, Germany